Department of Physics
Indian Institute of Technology Guwahati
Ph.D. Thesis

Supernova Neutrino Oscillations : Beyond Two Flavors

Madhurima Chakraborty

Supervisor: Dr. Sovan Chakraborty
July, 2022.

Supernova Neutrino Oscillations : Beyond Two Flavors

A thesis submitted by

Madhurima Chakraborty

to

Indian Institute of Technology Guwahati
in partial fulfillment of the requirements
for the award of the degree of
Doctor of Philosophy in Physics

Department of Physics
Indian Institute of Technology Guwahati
Guwahati - 781039, Assam, India

Statement

The work contained in the thesis entitled **"Supernova Neutrino Oscillations : Beyond Two Flavors"** has been carried out at the Department of Physics, Indian Institute of Technology Guwahati, India by me under the supervision of Dr. Sovan Chakraborty. The material of this thesis has not been submitted elsewhere for any other degree. Works presented in the thesis are all my own unless referenced to the contrary in the text.

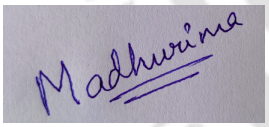

(Madhurima Chakraborty)
Department of Physics
Indian Institute of Technology Guwahati
Guwahati - 781039, India

Date: 25.11.2022

Disclaimer

The bibliography included in this thesis is, by no means complete but contains the ones which are consulted thoroughly by me. I apologize for inadvertently missing out some of the research papers, review articles and other scientific documents pertaining to the focus of this thesis which should also have been cited.

Certificate

It is certified that the work contained in the thesis entitled "*Supernova Neutrino Oscillations : Beyond Two Flavors*" by Ms. Madhurima Chakraborty, a Ph.D. student of the Department of Physics, Indian Institute of Technology Guwahati is carried out under my supervision and has not been submitted elsewhere for the award of any other degree.

Sovan Chakraborty

(Dr. Sovan Chakraborty)
Department of Physics
Indian Institute of Technology Guwahati
Guwahati - 781039, India

Date: 29/11/2022

To

My Parents (Prithwish Chakraborty and Chaina Chakraborty)

and

in memory of my boro jethu (Late Jyotirmoy Chakraborty)

Acknowledgement

As I conclude this wonderful journey, I feel grateful to a lot of people who have been associated with me during these five years.

First of all, I would like to express my sincerest gratitude to my thesis supervisor Dr. Sovan Chakraborty for his continuous support during my Ph.D tenure. It has been an amazing journey and a very good learning experience for me to work with him. His vast knowledge in every aspect of life has always motivated me to expand the horizon of my knowledge. He has always encouraged me to explore more in the subject and take up new projects. I am also thankful to him for giving me the opportunity to be involved in different types of problems and collaborations that helped me a lot to increase my experience and knowledge.

I would like to acknowledge my doctoral committee members - Dr. Arunansu Sil, Dr. Debasish Borah and Dr. Sayan Chakrabarti (in alphabetical order) for their useful suggestions during the yearly assessments of my research work. Also, I have learned many things from them during the discussions in the high energy physics journal club. I am really grateful to them as they were intended to support me whenever required.

Thanks to the instructors, who taught us during the Ph.D course work. Thank you Dr. Girish Sampath Setlur, Dr. Meduri C Kumar, Dr. Padma K Padmanabhan and Dr. Pravat Kumar Giri (in alphabetical order) for teaching us so wonderfully.

I thank to all HODs (Prof. Poulose Poulose, Prof. Subhradip Ghosh, Prof. Perumal Alagarsamy) during my Ph.D study. I would like to thank all the technical assistants, academic and non-academic staff of the department who helped me in various ways during my research period.

I would like to thank my collaborators Dr. Francesco Capozzi and Dr. Manibrata Sen. It has been a very pleasant and a great learning experience for me working with them.

I thank all my seniors in the Physics Department of IIT Guwahati with whom I have shared cordial relationships. I have learnt a lot from them during the various

discussions.

Thanks to all my batchmates and friends in IIT Guwahati for all the wonderful memories during these five years. Thank you Ipsita, my roommate and my all time companion, without whom my stay in this campus would not have been so wonderful. Thank you for always being with me and supporting me in all situations. Thank you for always solving my silliest of doubts with great patience. Thank you Manisha for helping me at various occasions, especially during course work. Thank you for all the wonderful hostel memories that we have created together. Thanks to Devabrat, Arghyajit and Devender for helping me clear my doubts at various times. All the physics discussions, especially the tutorial solving ones were very exciting and a great learning experience. Thanks to Santa, my hostel mate for all the beautiful moments that we spent together. Thanks to my other friends Poulomi and Pritam for the amazing memories at the SERB school including the physics discussions. I would like to thank my friend Mamta who has been with me and supported me throughout my journey starting from the MSc days.

I would like to thank my beloved juniors Prantik and Esha. I have discussed several things with them, which helped me to clarify my understanding. Also, thanks to many other juniors, with whom I have shared cordial relationships.

Most importantly, I would like to thank my parents. This thesis is dedicated to them. I owe everything to them. It is because of their determination and sacrifices that I have been able to reach to this point in my life.

I would like to thank all my relatives for their love and blessings for me. I miss my boro jethu who have passed away two years ago but have left a vivid memory of his affection and blessings for me. This thesis is dedicated to his memory as well. He has always encouraged me in all my endeavours since my childhood days. Thanks to him for his unconditional love for me. At last I would like to thank Krishnakanta (my would be husband) for his immense love and care for me. Thanks for all the valuable advices and being a constant source of encouragement for me. Thanks for always being with me and supporting me through all the ups and downs of my life.

List of Publications

(1) **"Three flavor neutrino conversions in supernovae: slow & fast instabilities"**,
Madhurima Chakraborty, Sovan Chakraborty,
eprint : arXiv : 1909.10420 (hep-ph)
Published in : JCAP **01**(2020)005

(2) **"Mu-Tau Neutrinos: Influencing Fast Flavor Conversions in Supernovae"**,
Francesco Capozzi, **Madhurima Chakraborty**, Sovan Chakraborty and Manibrata Sen,
eprint : arXiv : 2005.14204 (hep-ph)
Published in : Phys. Rev. Lett. **125**, 251801 (2020)

(3) **"Supernova Fast Flavor Conversions in 1+1 D : Influence of Mu-tau neutrinos"**,
Francesco Capozzi, **Madhurima Chakraborty**, Sovan Chakraborty and Manibrata Sen,
eprint : arXiv : 2205.06272 (hep-ph)
Published in : Phys. Rev. D **106**, 083011 (2022)

"In the world's broad field of battle,
In the bivouac of Life,
Be not like dumb, driven cattle
Be a hero in the strife

Trust no Future, howe'er pleasant
Let the dead Past bury its dead
Act,—act in the living Present
Heart within, and God o'erhead

.
.
.

Let us, then, be up and doing,
With a heart for any fate;
Still achieving, still pursuing,
Learn to labor and to wait."

—- *Henry Wadsworth Longfellow*

Abstract

The discovery of the neutrino oscillations by the various neutrino experiments from the Sun, atmosphere, reactors and accelerators has been one of the important developments in the field of particle physics. It is a proof of the fact that the neutrinos are not massless as predicted by the Standard Model of particle physics. It is a quantum mechanical phenomenon where the neutrinos can change their flavor from one to another due to the different flavor and mass eigenstates. The neutrino oscillations are enhanced while passing through a medium which is known as the Mikheyev-Smirnov-Wolfenstein (MSW) resonance. The neutrinos from a core-collapse supernova can be an interesting probe of the nuclear processes and the dynamics of a supernova explosion. In a dense medium like a core-collapse supernova, in addition to the MSW resonance, the neutrinos also undergo flavor conversions known as collective oscillations. This arises due to the neutrino-neutrino interactions in the dense medium.

In this thesis, we focus on the self induced neutrino flavor conversions in the context of both slow and fast regime. The fast conversions are independent of the neutrino mass and they grow at the scale of the large neutrino-neutrino interaction strength (10^5 km^{-1}) of the dense core. The slow collective modes, on the other hand grow at a slower rate as they are driven by the smaller vacuum oscillation frequencies (10^0 km^{-1}). In the literature, these flavor conversions have been exclusively studied in the standard two flavor scenario. Here, we discuss the aspects of studying these conversions in the three flavor scenario. First we carry out a linearized study of the three flavor slow and fast instabilities. Our slow flavor results are in qualitative agreement with the existing non-linear three flavor studies. For the fast modes, our results show that the inclusion of the third flavor may impact the growth rates of flavor instabilities in comparison to the two flavor scenario. Motivated by this and the supernova simulations with muon production, we perform the first non-linear simulations of fast conversions in the presence of three flavors. The relaxation of the assumption of taking equal fluxes of the non-electron flavors of neutrinos and antineutrinos leads to some interesting results. Our analysis shows the need of the

muon and tau lepton number angular distributions alongwith the electron lepton number to have a complete understanding of the system. Both our only temporal and the 1+1 D analysis are qualitatively same. Overall, our study emphasizes the need to go beyond the simplistic approximation of the three species while studying fast flavor oscillations. Finally, we investigate the phenomenological implication of the fast oscillations on the diffuse supernova neutrino background.

Contents

1 Neutrino oscillations **1**

1.1 Vacuum oscillations . . . 3

1.1.1 Two flavor case . . . 4

1.1.2 Three flavor case . . . 6

1.2 Oscillation in matter . . . 8

1.2.1 Constant matter density . . . 9

1.2.2 Varying matter density . . . 11

1.3 Current status of three flavor neutrino oscillations . . . 12

2 Supernova neutrino oscillations **15**

2.1 Core-collapse supernova . . . 15

2.1.1 Explosion mechanism . . . 15

2.1.2 Neutrino emission . . . 17

2.1.3 Neutrino spectrum . . . 19

2.2 Oscillations of supernova neutrinos . . . 21

2.2.1 MSW conversions . . . 23

2.2.2 Collective oscillations . . . 25

2.2.2.1 Slow oscillations . . . 28

2.2.2.2 Fast oscillations . . . 29

3 Linear stability analysis **33**

3.1 Linearization . . . 33

3.1.1 Three flavor neutrino system . . . 36

3.2 Stability analysis . . . 39

3.2.1 Slow modes . . . 39

3.2.2 Fast modes . . . 46

3.3 Discussion . . . 55

4 Non-linear analysis of fast oscillations **59**
4.1 Fast oscillations : Three flavor . . . 59
4.2 Evolution equation . . . 61
4.2.1 Angular distributions . . . 62
4.3 Non-linear analysis : Time evolution . . . 66
4.3.1 Two flavor . . . 67
4.3.2 Three flavor . . . 67
4.4 Non-linear analysis : Space and time evolution . . . 70
4.5 Discussion . . . 75

5 Diffuse supernova neutrino background **77**
5.1 Introduction . . . 77
5.2 Calculation of the DSNB flux . . . 79
5.3 Model uncertainties . . . 80
5.3.1 Black hole fractions . . . 82
5.3.2 Oscillation scenarios . . . 83
5.3.3 Dependence on SN simulations . . . 85
5.4 Detector configurations . . . 86
5.4.1 Water Cherenkov detectors . . . 87
5.4.2 Gadolinium doped water Cherenkov detectors . . . 88
5.4.3 Liquid argon detectors . . . 88
5.5 Results . . . 89
5.5.1 Black hole fractions . . . 89
5.5.2 Oscillation scenarios . . . 91
5.5.3 Dependence on SN simulations . . . 91
5.6 Number of events . . . 93
5.7 Discussion . . . 94
5.8 Observable effects . . . 97

6 Conclusion **99**
6.1 Future outlook . . . 104

Chapter 1

Neutrino oscillations

The development of the theory of beta decay was one of the milestones in the theory of weak interactions. The discovery of beta decay can be traced back to the discovery of phenomenon of radioactivity in uranium by Henri Becquerel in 1896. In addition to this, there were two more types of radioactive decay, namely alpha and gamma decay. The phenomenon of beta decay caught the attention of the scientists due to its unusual behaviour. James Chadwick in 1914 measured the β-spectrum and found it to be continuous. Moreover, the laws of conservation of energy and angular momentum were found to be violated. If the β decay was a two body decay similar to α and γ decay, then it would have shown discrete spectra. One of the proposed solutions to this puzzle was that this missing energy could be explained by the existence of a new particle which eventually led to the birth of the 'neutrino'. The neutrino was first postulated by Wolfgang Pauli in 1930 [1, 2] to explain the energy-momentum conservation in radioactive beta decays which was then discovered experimentally by Cowan and Reines in 1956 [3].

The neutrino is a very light neutral lepton and is one of the most abundant particles in the universe. It can interact only via the weak interaction and gravity. Hence, it is very hard to detect. The Standard Model of particle physics predicts three flavors of neutrinos corresponding to the three charged leptons i.e., electron neutrino (ν_e), muon neutrino (ν_μ) and tau neutrino (ν_τ). Similarly there are three antineutrinos ($\bar{\nu}_e$, $\bar{\nu}_\mu$, $\bar{\nu}_\tau$) [4]. There are a large number of sources of neutrinos like from nuclear reactions inside the Sun, collisions of cosmic rays with nuclei in the upper atmosphere, Type II supernovae, neutrino background leftover from the big bang, particle accelerators, nuclear reactors, etc.

Over the years, a large number of evidence regarding the existence of neutrino oscillations have been provided by the different experiments from the Sun [5–10],

atmosphere [11–14], reactors [8, 15–17] and accelerators [18–20]. The idea of neutrino oscillations was first suggested by Pontecorvo (1957) [21] and later by Maki, Nakagawa and Sakata (1962) [22]. It is a quantum mechanical phenomenon where the neutrinos can change their flavor from one to another and the reason being their different flavor and mass eigenstates. Neutrinos are produced in one of the three flavor eigenstates whereas they propagate as linear combinations of the mass eigenstates. During propagation, the mass eigenstates develop nontrivial relative phases which leads to the phenomenon of neutrino oscillations and this is an indication of the fact that neutrinos are not massless as considered in the Standard Model of particle physics. When neutrinos pass through a medium, they interact with the electrons and nucleons present there through weak interactions. This creates an effective potential for the neutrinos which leads to the matter enhanced flavor oscillations known as the MSW (Mikheyev-Smirnov-Wolfenstein) resonance [23–26]. The effect on the neutrino oscillations due to the MSW resonance has been studied using the data from the different solar neutrino experiments [27–30]. In addition to this, the potential of the long baseline experiments in testing the MSW effect has also been investigated [31–33]. Besides Sun, nuclear reactors, accelerators etc., neutrinos are also produced inside the core of a supernova as a result of the nuclear and particle processes happening there. The SN neutrinos play a crucial role in the collapse and explosion of massive stars.

Massive stars whose masses are greater than $8M_{\odot}$ undergo Type II supernova explosion at the end of their lifetimes. During this explosion, most (99 %) of the gravitational energy is carried away by the neutrinos. Thus these neutrinos carry information from the heart of the explosion and, due to their weakly interacting nature, offer the only direct probe of the dynamics and thermodynamics at the center of a supernova [34, 35]. SN1987A [36] was the first supernova whose observations provided a great opportunity for the modern astronomers to study the development of supernova in great detail and it also provided much insight into core-collapse supernovae. The high density of neutrinos in a core-collapse supernova provides an opportunity to study the flavor oscillations due to interaction of neutrinos among themselves. As a result, in addition to MSW resonance, another phenomenon occurs which is known as the collective oscillations [35]. As the name suggests, collective oscillation of neutrinos is a phenomenon in which neutrinos of different energies collectively undergo flavor conversion in a coherent manner. The neutrino spectra observed from a galactic SN can carry the signatures of neutrino flavor conversions deep inside a star. These signatures can be further utilised to infer the unknown

neutrino properties, as well as to understand stellar dynamics.

In this thesis, we focus on the neutrino oscillations in a supernova. To introduce the formalism in supernova neutrino oscillation, we first discuss the vacuum oscillations and the MSW resonance. This chapter also states the current status of the understanding of the three flavor oscillations.

1.1 Vacuum oscillations

The flavor eigenstates of the neutrinos (ν_e, ν_μ and ν_τ) are different from the mass eigenstates (ν_1, ν_2 and ν_3). Thus, the probability that a neutrino created in a particular flavor state will be found at a later time in the same state or any other flavor state oscillates with time.

The flavor eigenstates (ν_α) can be written as a linear combination of the mass eigenstates (ν_j) in the form [37]:

$$|\nu_\alpha\rangle = \sum_j U^*_{\alpha j} |\nu_j\rangle \tag{1.1}$$

where, the unitary matrix 'U' is the neutrino mixing matrix. Note that for antineutrinos, the relation between the mass and flavor eigenstates is $|\bar{\nu}_\alpha\rangle = \sum_j U_{\alpha j} |\bar{\nu}_j\rangle$. Suppose initially at time $t = 0$, the neutrino is produced in flavor eigenstate $|\nu_\alpha\rangle$. Now we are interested to find the probability of finding this neutrino in some other state $|\nu_\beta\rangle$ at a later time 't'. So, if the initial state is $|\nu(0)\rangle = |\nu_\alpha\rangle = \sum_j U^*_{\alpha j} |\nu_j\rangle$. Then, at a later time 't' it becomes

$$|\nu(t)\rangle = \sum_j U^*_{\alpha j} e^{-iE_j t} |\nu_j\rangle \tag{1.2}$$

The probability of finding the neutrino in the state $|\nu_\beta\rangle$ is given by

$$P(\nu_\alpha \to \nu_\beta; t) = |\langle \nu_\beta | \nu(t) \rangle|^2 = \left| \sum_j U_{\beta j} U^*_{\alpha j} e^{-iE_j t} \right|^2 \tag{1.3}$$

For relativistic neutrinos ($|\mathbf{p}_i| >> m_i$),

$$E_i = \sqrt{|\mathbf{p}_i|^2 + m_i^2} \simeq |\mathbf{p}_i| + \frac{m_i^2}{2|\mathbf{p}_i|} \tag{1.4}$$

Here, the terms of $\mathcal{O}(\frac{m_i^4}{|\mathbf{p}_i|^3})$ and higher have been neglected. Further we expand the

second term of equation 1.4 as follows :

$$\begin{aligned}\frac{m_i^2}{2|\mathbf{p}_i|} &= \frac{m_i^2}{2(E_i - m_i^2)^{1/2}} \\ &\simeq \frac{m_i^2}{2E_i}\left(1 + \frac{m_i^2}{2E_i^2}\right) \\ &\simeq \frac{m_i^2}{2E_i}\end{aligned} \tag{1.5}$$

Here also the further higher order terms are neglected. Now, we substitute equations 1.4 and 1.5 in equation 1.3. Also we consider that all the mass eigenstates have same energy ($E_i \simeq E$). So the transition probability can be written as

$$\begin{aligned}P(\nu_\alpha \to \nu_\beta; t) = \Big|\sum_i U_{\beta i}U_{\alpha i}\Big|^2 &- 4\sum_{i>j} Re(U^*_{\alpha i}U_{\beta i}U_{\alpha j}U^*_{\beta j})\sin^2\left(\frac{\Delta m^2_{ij}}{4E}t\right) \\ &+ 2\sum_{i>j} Im(U^*_{\alpha i}U_{\beta i}U_{\alpha j}U^*_{\beta j})\sin\left(\frac{\Delta m^2_{ij}}{4E}t\right)\end{aligned} \tag{1.6}$$

Using the unitarity property of U, the above equation becomes

$$\begin{aligned}P(\nu_\alpha \to \nu_\beta; t) = \delta_{\alpha\beta} &- 4\sum_{i>j} Re(U^*_{\alpha i}U_{\beta i}U_{\alpha j}U^*_{\beta j})\sin^2\left(\frac{\Delta m^2_{ij}}{4E}t\right) \\ &+ 2\sum_{i>j} Im(U^*_{\alpha i}U_{\beta i}U_{\alpha j}U^*_{\beta j})\sin\left(\frac{\Delta m^2_{ij}}{4E}t\right)\end{aligned} \tag{1.7}$$

where, $\Delta m^2_{ij} = m_i^2 - m_j^2$ is the mass squared difference. Moreover, when $\alpha = \beta$, equation 1.7 represents the survival probability and when $\alpha \neq \beta$, it denotes the conversion probability. Now we discuss the two flavor and three flavor scenarios in detail.

1.1.1 Two flavor case

First we consider the simple case of two neutrino mixing. Here, two species of neutrinos ν_e and ν_μ, i.e. $\alpha = e, \mu$ and $j = 1, 2$ are considered. In this scenario, the mixing matrix 'U' takes the form [38] :

$$U = \begin{pmatrix} c & s \\ -s & c \end{pmatrix} \tag{1.8}$$

So, the flavor eigenstates can be written as a linear combination of the mass eigenstates as follows:

$$\begin{aligned} |\nu_e\rangle &= c\,|\nu_1\rangle + s\,|\nu_2\rangle \\ |\nu_\mu\rangle &= -s\,|\nu_1\rangle + c\,|\nu_2\rangle \end{aligned} \tag{1.9}$$

where, $c = \cos\theta_0$, $s = \sin\theta_0$ and θ_0 denotes the vacuum mixing angle whose value lies in the interval $[0, \pi/2]$. Let us suppose that at time $t = 0$, the neutrino is in flavor state $|\nu_e\rangle$. So the transition probability to $|\nu_\mu\rangle$, given by the equation 1.7 takes the form :

$$P(\nu_e \to \nu_\mu; t) = P(\nu_\mu \to \nu_e; t) = \sin^2(2\theta_0)\sin^2\left(\frac{\Delta m^2_{21}}{4E}t\right) \tag{1.10}$$

For relativistic neutrinos, $L \simeq t$ and thus equation 1.10 can also be written as

$$P(\nu_e \to \nu_\mu; L) = P(\nu_\mu \to \nu_e; L) = \sin^2(2\theta_0)\sin^2\left(\frac{\Delta m^2_{21}}{4E}L\right) \tag{1.11}$$

where $\Delta m^2_{21} = m^2_2 - m^2_1$ and L is the distance between the source and the detector. Note that we will identify Δm^2_{21} as the solar mass squared difference later. Focussing on equation 1.11, there are two terms which govern the neutrino oscillation. They are as follows:

(1) The first term ($\sin^2(2\theta_0)$) depends on the mixing angle and it describes the amplitude or depth of the neutrino oscillations. The maximum value of the amplitude is 1 and it occurs when mixing is maximal i.e. $\theta_0 = 45°$. The mixing is small when θ_0 is close to zero or 90°. This is the case when the flavor and mass eigenstates are almost coinciding.

(2) The second term determines the frequency of the oscillation. It is a function of the mass squared difference ($\frac{\Delta m^2_{21}}{4E}$) and the distance ($L$). Not only the mixing needs to be large, the phase should also not be very small in order to have a substantial amount of transition probability.

The reactor oscillation experiments have $E \sim 1$ MeV while for the accelerator oscillation experiments $E \sim 1$ GeV. So the transition probability can be expressed as :

$$P(\nu_e \to \nu_\mu; L) = P(\nu_\mu \to \nu_e; L) = \sin^2(2\theta_0)\sin^2\left(\pi\frac{L}{l_{osc}}\right) \tag{1.12}$$

where l_{osc} is the oscillation length which is equal to the distance between any two closest maxima or minima of the transition probability. It is given as

$$l_{osc} = \frac{4\pi E}{\Delta m^2_{21}} \simeq 2.48\, m\, \frac{E\,(MeV)}{\Delta m^2_{21}\,(eV^2)} \simeq 2.48\, km\, \frac{E\,(GeV)}{\Delta m^2_{21}\,(eV^2)} \tag{1.13}$$

In order to measure the transition between different flavors in different neutrino oscillation experiments, one important quantity is $\frac{\Delta m^2_{21} L}{2E}$. So if $\frac{\Delta m^2_{21} L}{2E} \ll 1$, then the transition cannot be measured or in other words, if $L \ll l_{osc}$, then the phase factor in the second term of equation 1.12 is very small and thus oscillations fail to develop. On the other hand, if $\frac{\Delta m^2_{21} L}{2E} \gg 1$ or $L \gg l_{osc}$, then the transition probability undergoes fast oscillations. As a result, it gets averaged out at the detector and the probability of transition becomes $\bar{P} = \frac{1}{2} sin^2 2\theta_0$. Therefore, the only information which can be obtained from such experiments is that about the mixing angle θ_0. So to obtain the complete information about the oscillations, the various experiments are designed by choosing suitable values of $\frac{L}{E}$ so as to make them sensitive to different Δm^2_{21} values. In other words, the ratio $\frac{L}{E}$ is chosen in such a way so that $\frac{\Delta m^2_{21} L}{2E} \sim 1$. Based on this factor, the different oscillation experiments are classified into Short Baseline, Long Baseline and Very Long Baseline experiments.

1.1.2 Three flavor case

Now we consider the case of three flavors of neutrinos ν_e, ν_μ and ν_τ. In this scenario, according to equation 1.1, $\alpha = e, \mu, \tau$ and $j = 1, 2, 3$. The mixing matrix 'U' is known as the Pontecorvo-Maki-Nakagawa-Sakata (PMNS) matrix [21, 22] which can be parametrized as [4]:

$$U = \begin{pmatrix} c_{12}c_{13} & s_{12}c_{13} & s_{13}e^{-i\delta} \\ -s_{12}c_{23} - c_{12}s_{23}s_{13}e^{i\delta} & c_{12}c_{23} - s_{12}s_{23}s_{13}e^{i\delta} & s_{23}c_{13} \\ s_{12}s_{23} - c_{12}c_{23}s_{13}e^{i\delta} & -c_{12}s_{23} - s_{12}c_{23}s_{13}e^{i\delta} & c_{23}c_{13} \end{pmatrix} \times \begin{pmatrix} 1 & 0 & 0 \\ 0 & e^{i\frac{\alpha_{21}}{2}} & 0 \\ 0 & 0 & e^{i\frac{\alpha_{31}}{2}} \end{pmatrix} \tag{1.14}$$

So, the flavor eigenstates can be written as a linear combination of the mass eigenstates as follows:

$$\begin{pmatrix} \nu_e \\ \nu_\mu \\ \nu_\tau \end{pmatrix} = \begin{pmatrix} U_{e1} & U_{e2} & U_{e3} \\ U_{\mu 1} & U_{\mu 2} & U_{\mu 3} \\ U_{\tau 1} & U_{\tau 2} & U_{\tau 3} \end{pmatrix} \begin{pmatrix} \nu_1 \\ \nu_2 \\ \nu_3 \end{pmatrix} \tag{1.15}$$

where, $c_{ij} = \cos\theta_{ij}$ and $s_{ij} = \sin\theta_{ij}$ and θ_{ij} lies in the interval $[0,\ \pi/2]$. So, there are three mixing angles $\theta_{12}, \theta_{13}, \theta_{23}$, one Dirac C-P violating phase ($\delta = [0,\ 2\pi]$) and two Majorana C-P violating phases α_{21} and α_{31}. The Majorana phases do not affect the neutrino oscillations and thus we will not consider them further. In the three flavor case, the oscillation probabilities are given by the general expression 1.7, where now there are three mass squared differences ($\Delta m^2_{21}, \Delta m^2_{31}$ and Δm^2_{32}). The three mass eigenstates have a hierarchy between them on which the sign of the three mass squared differences depend. If $m_1 \ll m_2 \ll m_3$, the mass ordering is considered to be normal and it is inverted if $m_3 \ll m_1 \simeq m_2$. The solar neutrino data indicates the presence of a small mass squared difference while the atmospheric data requires a larger mass squared difference for its explanation. So the smaller one is termed as the solar mass squared difference, i.e., $\Delta m^2_{\odot} \approx \Delta m^2_{21}$ and the larger one is the atmospheric mass squared difference, i.e., $\Delta m^2_{atm} \approx \Delta m^2_{31} \approx \Delta m^2_{32}$. In addition to the above two mass orderings, it is also possible that the neutrinos are quasi-degenerate in mass and only their mass differences follow an ordering. However, several studies have been carried out to investigate the validity of this scheme [39–43]. In the quasi-degenerate case, $m_i > 0.2$ eV. The current limit on the kinematical mass for beta decay from the KATRIN experiment is $m_\beta < 0.8$ eV (90 % CL) and the sensitivity goal is 0.2 eV [44]. On the other hand, the current cosmological bound on the sum of the neutrino masses is $\sum m_\nu < 0.12$ eV [45]. So, the current limit and sensitivity from KATRIN would correspond to $\sum m_\nu \approx 2.4$ eV and 0.6 eV. In [44], it is reported that the latest upper limit from KATRIN have narrowed down the allowed range of quasi-degenerate neutrino-mass models and have provided model-independent information about the neutrino mass. It further allows the testing of non-standard cosmological models. In contrast to the two flavor case, here it is difficult to obtain a simple form of the probability. However, it can be simplified under some limiting cases two of which have been discussed below.

Let us first consider the case of atmospheric, reactor and accelerator experiments for which $\frac{\Delta m^2_{21} L}{2E} << 1$. Effectively there are no oscillations in this case and it can

be considered that $\Delta m^2_{21} \to 0$. So the oscillation probability becomes :

$$P(\nu_\alpha \to \nu_\beta; L) = 4\,|U_{\alpha 3}|^2\,|U_{\beta 3}|^2\,\sin^2\left(\frac{\Delta m^2_{31}\,L}{4E}\right) \tag{1.16}$$

For instance, the survival probability of the electron neutrinos can be written as :

$$P(\nu_e \to \nu_e; L) = 1 - \sin^2(2\theta_{13})\,\sin^2\left(\frac{\Delta m^2_{31}\,L}{4E}\right) \tag{1.17}$$

which is similar to that of two flavor case with mixing angle as θ_{13} and mass squared difference as Δm^2_{31}.

Now we consider another limiting case which is applicable for the solar neutrino experiments and the very long baseline experiments. We have $\frac{\Delta m^2_{31}\,L}{2E} \simeq \frac{\Delta m^2_{32}\,L}{2E} \gg 1$ and thus the oscillation probability due to Δm^2_{31} and Δm^2_{32} get averaged out. So the survival probability of ν_e becomes :

$$P(\nu_e \to \nu_e; L) = c^4_{13}\,P + s^4_{13} \tag{1.18}$$

where, P is again the two flavor ν_e survival probability with the mixing angle as θ_{12} and the mass squared difference as Δm^2_{21}. The expression for P in case of vacuum neutrino oscillations is given by :

$$P = 1 - \sin^2(2\theta_{12})\,\sin^2\left(\frac{\Delta m^2_{21}\,L}{4E}\right) \tag{1.19}$$

1.2 Oscillation in matter

Till now, we focussed on the vacuum neutrino oscillations. But in all realistic situations, like neutrino propagation in Sun, neutrino propagation through the Earth before detection, neutrino oscillation in dense objects like supernovae etc., the neutrinos interact with the background matter. As a result, they undergo a refractive effect due to which the oscillation probability is enhanced. This is known as the Mikheyev-Smirnov-Wolfenstein (MSW) effect.

Ordinary matter consists of electrons, protons and neutrons. So, when neutrinos pass through it, they interact with the constituents through the Standard Model weak interactions (as shown in figure 1.1). The neutrinos undergo both elastic and inelastic scattering with the electrons and nucleons [23]. The dominant contribu-

tions are from the elastic processes which are proportional to G_F as compared to the G_F^2 dependent inelastic processes. All the flavors of neutrinos (ν_e, ν_μ and ν_τ) interact through neutral current interactions with the electrons and the nucleons. Additionally, ν_e undergo charged current interactions with electrons. However, due to the absence of muons and tauons, the non-electron flavors (ν_μ and ν_τ) do not have similar interactions. As a result, an effective potential is created which is proportional to the number density of the matter constituents. Due to charge neutrality, the contribution from electrons and protons to the neutral current interactions cancel each other. So, the form of the potential due to charged current and neutral current interactions is given by [38]:

$$\begin{aligned} V_{cc} &= \sqrt{2} G_F n_e(r) \\ V_{nc} &= -\sqrt{2} G_F \frac{n_n(r)}{2} \end{aligned} \tag{1.20}$$

where, $n_e(r)$ and $n_n(r)$ are the local electron and neutron densities respectively. The equation of motion for the evolution of neutrinos in matter background is given as:

$$i\frac{d}{dt}\begin{pmatrix} \nu_e \\ \nu_\mu \end{pmatrix} = \begin{pmatrix} -\frac{\Delta m^2}{4E}\cos 2\theta_0 + V_{cc} & \frac{\Delta m^2}{4E}\sin 2\theta_0 \\ \frac{\Delta m^2}{4E}\sin 2\theta_0 & \frac{\Delta m^2}{4E}\cos 2\theta_0 \end{pmatrix}\begin{pmatrix} \nu_e \\ \nu_\mu \end{pmatrix} \tag{1.21}$$

Here, there is a common term in the diagonal elements due to neutral current interactions (V_{nc}) which can be written as proportional to an identity matrix. This will only appear as an overall phase factor which can be eliminated by the redefinition of fields. Thus, it will not affect the oscillation probability. This equation of motion (in flavor basis) is valid when the matter density is constant as well as when it varies with distance. This equation is not easy to solve analytically in general but it can be done so under certain conditions.

1.2.1 Constant matter density

First, we consider the case of constant matter density, i.e., n_e is constant. This makes the problem analytically solvable. Here, we consider the basis of instantanteous matter eigenstates, in which the Hamiltonian is diagonalizable. The transformation relation between the flavor states and matter states in the two flavor scenario is given by [46],

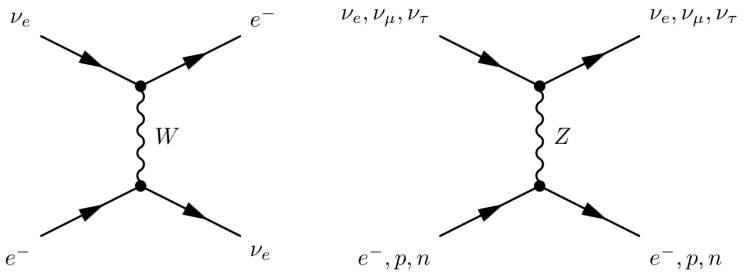

Figure 1.1: The Feynmann diagrams for the charged current and neutral current interactions of the neutrinos with background matter. Left panel : Charged current interaction of electron neutrino with the electron. Right panel : Neutral current interactions of all the flavors of neutrinos with electron, proton and neutron. This figure is taken from [37].

$$\begin{pmatrix} \nu_e \\ \nu_\mu \end{pmatrix} = \begin{pmatrix} \cos\tilde{\theta} & \sin\tilde{\theta} \\ -\sin\tilde{\theta} & \cos\tilde{\theta} \end{pmatrix} \begin{pmatrix} \tilde{\nu}_1 \\ \tilde{\nu}_2 \end{pmatrix} \tag{1.22}$$

where the mixing angle in matter $\tilde{\theta}$ in terms of the vacuum mixing angle θ_0 is given by :

$$\tan 2\tilde{\theta} = \frac{\frac{\Delta m^2}{2E}\sin 2\theta_0}{\frac{\Delta m^2}{2E}\sin 2\theta_0 - \sqrt{2}G_F n_e} \tag{1.23}$$

The effective mass squared difference and the effective squared masses in matter are given by the following two equations respectively.

$$\Delta\tilde{m}^2 = \sqrt{(\Delta m^2 \cos 2\theta_0 - 2EV_{cc})^2 + (\Delta m^2 \sin 2\theta_0)} \tag{1.24}$$

$$\tilde{m}^2_{1,2} = \frac{1}{2}(m_1^2 + m_2^2 + 2EV_{cc} \pm \Delta\tilde{m}^2) \tag{1.25}$$

So, now the oscillation probability in matter with constant density can be written similar to that of vacuum. Here the difference is that the vacuum parameters are replaced by their corresponding ones in matter. The expression for oscillation probability is given by [46]

$$P(\nu_e \to \mu_\mu) = \sin^2 2\tilde{\theta}\, \sin^2\left(\frac{\Delta\tilde{m}^2}{4E}L\right) \tag{1.26}$$

and the amplitude of the oscillation is

$$\sin^2 2\tilde{\theta} = \frac{\left(\frac{\Delta m^2}{2E}\right)^2 \sin^2 2\theta_0}{\left(\frac{\Delta m^2}{2E}\cos 2\theta_0 - \sqrt{2}G_F n_e\right)^2 + \left(\frac{\Delta m^2}{2E}\right)^2 \sin^2 2\theta_0} \tag{1.27}$$

Note that from equation 1.27, the maximum value of l.h.s is reached, i.e., $\sin^2 2\tilde{\theta} = 1$ when the following condition is satisfied

$$\frac{\Delta m^2}{2E}\cos 2\theta_0 = \sqrt{2}G_F n_e \tag{1.28}$$

This is known as the Mikheyev Smirnov Wolfenstein (MSW) resonance condition. It is evident from equations 1.23 and 1.27 that the mixing in matter is maximal ($\tilde{\theta} = 45°$) on the fulfillment of the MSW resonance condition. Moreover, it is independent of the vacuum mixing angle (θ_0) which means that even for a very small value of θ_0, the oscillation probability of neutrino in matter can be enhanced. In case of antineutrinos, the effective potential V_{cc} has an opposite sign and thus the resonance cannot occur simutaneously for both neutrinos and antineutrinos. It occurs for one at a time for a particular value of Δm^2.

1.2.2 Varying matter density

We now consider the realistic case where the matter density varies with distance or time. In this scenario, the transformation matrix between the flavor and matter basis also becomes time dependent. Thus, the evolution equation now becomes

$$i\frac{d}{dt}\begin{pmatrix}\tilde{\nu}_1\\ \\ \tilde{\nu}_2\end{pmatrix} = \begin{pmatrix}\frac{\Delta\tilde{m}^2}{2E} & -i\frac{d\tilde{\theta}}{dt}\\ \\ i\frac{d\tilde{\theta}}{dt} & -\frac{\Delta\tilde{m}^2}{2E}\end{pmatrix}\begin{pmatrix}\tilde{\nu}_1\\ \\ \tilde{\nu}_2\end{pmatrix} \tag{1.29}$$

It can be clearly seen from the above equation that the Hamiltonian is not diagonal in this basis. Depending on the size of the off-diagonal elements, we can classify the variation to be adiabatic or non adiabatic. This can be quantified by a parameter called as adiabaticity parameter given by

$$\gamma \equiv \frac{|\frac{\Delta\tilde{m}^2}{2E}|}{|\frac{d\tilde{\theta}}{dt}|} = \left|\frac{4(\Delta\tilde{m}^2)^3}{\Delta m^2 \sin 2\theta_0}\left(\frac{dV_{cc}}{dt}\right)^{-1}\right| \tag{1.30}$$

If the variation of the off-diagonal $|\frac{d\tilde{\theta}}{dt}| << \frac{\Delta\tilde{m}^2}{2E}$, then $\gamma >> 1$ (adiabatic) and thus the transition between $\tilde{\nu}_1$ and $\tilde{\nu}_2$ are suppressed. However, the situation is non-

adiabatic for $\gamma << 1$ where there are substantial transitions. So, the transition probability from one matter eigenstate to another is given by

$$P_r = \frac{exp\Big(-\frac{\pi}{2}\gamma_r F\Big) - exp\Big(-\frac{\pi}{2\sin^2\theta_0}\gamma_r F\Big)}{1 - exp\Big(-\frac{\pi}{2\sin^2\theta_0}\gamma_r F\Big)} \tag{1.31}$$

where F is a parameter depending on the density profile and γ_r is the adiabaticity parameter at the MSW resonance. The value of γ near the MSW resonance is given by

$$\gamma_r = \frac{\Delta m^2}{2E}\frac{\sin^2 2\theta_0}{\cos 2\theta_0}\Big|\frac{1}{V_{cc}}\frac{dV_{cc}}{dt}\Big|_r^{-1} \tag{1.32}$$

Further details of the matter resonance in the specific scenario of dense medium like supernova will be discussed in the subsequent chapter. Now we move on to the current status of the three flavor neutrino oscillations in the next section.

1.3 Current status of three flavor neutrino oscillations

In the three flavor framework of neutrinos, there are six parameters which govern their oscillations. In order to explain the generalized system completely, all of these parameters need to be determined. The six parameters are the two mass squared differences Δm^2_{21} and Δm^2_{31}, three mixing angles $\theta_{12}, \theta_{23}, \theta_{13}$ and the CP violating phase δ. Depending on the sign of Δm^2_{31}, there are two mass orderings. $\Delta m^2_{31} > 0 (< 0)$ corresponds to normal ordering (inverted ordering).

Currently, five ($\Delta m^2_{21}, |\Delta m^2_{31}|, \theta_{12}, \theta_{23}$ and θ_{13}) out of six of these unknown parameters have been determined with great precision from the various experiments using atmospheric, solar, reactor and accelerator neutrinos. However, the mass ordering (sign of Δm^2_{31}) and δ are still unknown.

The solar neutrino parameters, i.e. solar mass squared difference Δm^2_{21} and the solar mixing angle θ_{12} are mainly constrained by the KamLAND reactor experiment [8], SNO [9, 47], Super-Kamiokande [11, 48], Borexino [49], and Gallex [50]. The bounds on the parameters θ_{23} and Δm^2_{atm} come from the atmospheric neutrino experiments (SK) [11, 12] and the long baseline accelerator experiments (eg. MINOS) [51]. The mixing angle θ_{13} is determined by the reactor experiments [15, 16]. The value of the CP violating phase 'δ' is planned to be determined by the long baseline experiments. The best fit values of the oscillation parameters determined from the global analysis with the error at 1σ are given by [52]. The values corresponding to

both mass orderings are mentioned in table 1.1.

	Normal Ordering	Inverted Ordering
$\sin^2\theta_{12}$	$0.304^{+0.012}_{-0.012}$	$0.304^{+0.013}_{-0.012}$
$\frac{\Delta m^2_{21}}{10^{-5}\,eV^2}$	$7.42^{+0.21}_{-0.20}$	$7.42^{+0.21}_{-0.20}$
$\sin^2\theta_{23}$	$0.573^{+0.016}_{-0.020}$	$0.575^{+0.016}_{-0.019}$
$\frac{\lvert\Delta m^2_l\rvert}{10^{-3}\,eV^2}$	$+2.517^{+0.026}_{-0.028}$	$-2.498^{+0.028}_{-0.028}$
$\sin^2\theta_{13}$	$0.02219^{+0.00062}_{-0.00063}$	$0.02238^{+0.00063}_{-0.00062}$
$\delta/^\circ$	197^{+27}_{-24}	282^{+26}_{-30}

Table 1.1: The best fit values to the global data for the oscillation parameters corresponding to both normal (NO) and inverted ordering (IO) (taken from [52]). The errors at 1 σ are also mentioned. Here $\Delta m^2_{3l} \equiv \Delta m^2_{31} > 0$ for NO and $\Delta m^2_{3l} \equiv \Delta m^2_{32} < 0$ for IO.

In comparison to the previous data, the latest analysis [52] shows that the allowed range of δ is pushed towards the CP conserving value of 180° and it is allowed at 0.6 σ. On the other hand, in case of inverted ordering (IO) the best fit value of δ is close to maximal CP violation which is favoured at around 3σ. All these results are obtained after incorporating the new data from the long baseline accelerator experiments T2K [53] and NOvA [54].

Regarding the mass ordering, the normal ordering (NO) is favoured at 1.6 σ which has also decreased significantly as compared to the previous hints. However, when combined with the χ^2 map provided by the SK experiment for their atmospheric data, the hint for NO is at 2.7 σ.

Besides the oscillation parameters, the other important information about the neutrinos which is not known to us is its absolute mass and nature. The oscillation probability is not affected by the nature of the neutrinos (Dirac or Majorana) and thus it cannot be determined by the neutrino oscillation experiments. The experiments searching for neutrinoless double beta decay [55–57] can be helpful in investigating the Majorana nature of neutrinos. Although the absolute mass of the neutrino is not yet known, there is an upper bound on the sum of the neutrino masses from cosmology, i.e., $\sum m_\nu \lesssim 0.15$ eV [58, 59].

In this chapter, we provided a generalized introduction to the basics of neutrino oscillations. We began the discussion with the vacuum neutrino oscillations. Then we explained the more realistic scenario of MSW resonance which occurs when neutrinos pass through a medium. We elaborated the effects for both cases of

constant and varying density of the medium. As mentioned earlier, in addition to the production of neutrinos from the Sun, nuclear reactors, and accelerators, another major source of MeV neutrinos is the core-collapse supernova. The neutrinos emitted from a supernova can indirectly probe the nuclear processes at a supernova core and is an exciting field of study. In the next chapter, we will particularly focus on neutrino production and oscillations in a supernova.

Chapter 2

Supernova neutrino oscillations

In the previous chapter, we introduced the neutrino oscillations and summarized the current status of the three flavor neutrino oscillations. In this chapter we extend the discussion by focussing on the neutrino oscillation in dense medium, particularly core-collapse supernova.

2.1 Core-collapse supernova

A supernova (SN) occurs at the end of the lifetime of a star. It is the superexplosion pronouncing the death of a massive star. SNe are broadly classified into two types, namely type I and type II. The distinction is based on their light curves and the presence or absence of hydrogen lines in their spectra. Here we are interested in the type II supernova explosion which is also known as the core-collapse supernova. It occurs for the massive stars having mass greater than $(8 - 10)M_{\odot}$. In this section, we present an overview of the mechanism of a core-collapse supernova and the corresponding emission of neutrinos [34].

2.1.1 Explosion mechanism

The whole process of maintaining the stability of a star depends on the interplay between two forces, i.e. the gravitational force acting inwards and the outward pressure due to the material present inside the star. When the gravitational force becomes larger and the star starts moving inwards, the temperature inside the star increases, thereby creating favourable conditions for the nuclear fusion to occur. Nuclear fusion is a process in which lighter elements fuse together to form heavier ones and a large amount of energy is released. The fusion process in low mass stars ends after

helium fusion. However, the stars having mass larger than 8 to 10 $M_\odot$ undergo further fusion processes after the formation of carbon [34, 35, 60–65]. Helium burning is followed by carbon which is further followed by neon, oxygen, silicon. Each of the successive burning process lasts for a shorter period of time than the previous one which finally ends with the production of iron. As a result, an onion shell structure is formed where each successive inner shell represents the heavier element. After the formation of iron, the fusion process stops. This is because iron has the highest average binding energy per nucleon and thus requires energy in order to fuse into heavier elements. So now, the star begins to collapse as the electron degeneracy pressure can no longer hold it against the inward gravitational force (as star reaches Chandrashekhar mass limit of 1.4 $M_\odot$). As it starts to collapse, the temperature in the star's core keeps on increasing and γ rays are released. These high energy γ rays break the iron nuclei up into He nuclei through the process called photo-disintegration. As the contraction continues, electron capture takes place releasing large number of neutrinos. These neutrinos carry considerable amount of energy which further causes the core to cool and contract even further. At $\rho \approx 10^{12} g/cm^3$, neutrinos get trapped in the core as their diffusion time becomes larger than the collapse time. The collapse continues until nuclear densities reach $\rho \approx 10^{14} g/cm^3$. This is when the core stiffens which further slows down the infall of the core. At this point of time, the core bounces back and creates a shock-wave into the outer core. Finally, the shock wave reaches the surface of the star. This is followed by the explosion of the star which blasts off its outer envelope injecting the stellar material and the newly generated elements into the interstellar medium. This ultimately leaves behind a neutron star or a black hole depending on the final mass of the core.

The scenario where the source of the explosion is the shock-wave is known as the "prompt explosion scenario" [34, 66, 67]. This is usually true for low mass stars. However, the simulations suggest that for larger progenitors while moving outwards, a lot of the kinetic energy of the shock-wave is lost in dissociating the heavy nuclei in the surroundings. This causes the shock-wave to stall after about 100 ms. Thus for larger stellar mass objects, explosion fails to take place. It is speculated that for the explosion to be successful, more energy needs to be deposited in the shock-wave while it propagates out. This can be possible if the neutrinos diffuse from their last scattering surface (neutrinosphere) and deposit some of the energy by interacting with the dense matter behind the shock-wave. This is known as the "delayed explosion scenario" [68, 69] where the neutrinos help in reviving the shock-wave leading to a successful explosion. Note that the exact mechanism of

the explosion is still not known and is under active research. It has been found in hydrodynamical simulations [70, 71] that the delayed neutrino heating scenario does not always result in successful explosions without any artificial trigger like in 1D simulations, the heavy mass stars fail to explode which leads to the need of multidimensional simulations. In 2D simulations, including convection process results in successful explosions whereas in 3D the convection alone is not enough to drive the explosion [71–74].

2.1.2 Neutrino emission

The explosion of a star into a type II supernova is accompanied by the emission of a large number of neutrinos, and 99% of the total gravitational energy (10^{53} ergs) of the collapse is released in form of neutrinos ($\approx 10^{58}$). This neutrino emission happens in a time period of $\sim$ 10 seconds and contains neutrinos of all three flavors. The emission of the neutrinos occurs mainly in three phases [60, 65] namely Neutronization Burst Phase, Accretion Phase and Kelvin-Helmholtz Cooling Phase. Figure 2.1 shows the variation of the luminosities (top panel) and average energies of the different neutrino flavors (bottom panel) with the post bounce time in seconds. We discuss these three phases in detail below.

- NEUTRONIZATION BURST : This phase lasts for around 25 ms after the core bounce. Due to the electron capture on the free protons, a large number of electron neutrinos are emitted during this phase as compared to other flavors and thus the name 'neutronization burst'. This phase is shown in the leftmost panel of figure 2.1. It can be seen from the figure that the luminosity of the electron flavor neutrino is highest in this phase as compared to the other flavors.

- ACCRETION PHASE : This phase (middle panel of figure 2.1) can be further divided into the early accretion phase and the later accretion phase. The early phase extends up to ∼100 ms post bounce. During this time, the shock wave propagates out to a distance of ∼200 km before it stalls. The later phase lasts for several hundred milliseconds until the shock is revived. Here, other flavors are also emitted in appreciable amount as can be seen from the luminosities. Also there is a hierarchy in average energies ($\langle E_{\nu_{\mu,\tau}}\rangle > \langle E_{\overline{\nu}_e}\rangle > \langle E_{\nu_e}\rangle$). Note that the y-axis scale for the luminosity in the middle panel is 10 times that of the left one.

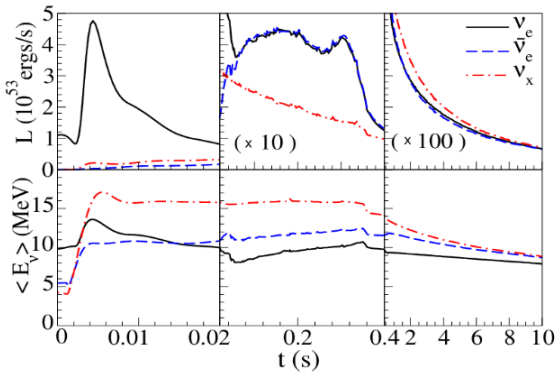

Figure 2.1: The luminosities and average energies of different neutrino flavors vs the post bounce time for the three phases of neutrino emission. These are obtained from the results of Basel/Darmstadt simulation [75] of a 18 $M_\odot$ progenitor. The left, middle and right panels correspond to the neutronization burst phase, accretion phase and cooling phase respectively. In the top middle panel, y-axis scale is 10 times that of left one and it is 100 times for the top right panel. This figure is taken from [76].

- KELVIN-HELMHOLTZ COOLING PHASE: This is the final phase which lasts till a time period of 10-20 s. Here, after the shock is revived and the mantle of the star starts moving outwards, the neutrino emission is simply due to the cooling of the hot proto-neutron star. In this phase shown in the rightmost panel of figure 2.1, the hierarchy of the average energies is milder compared to that of accretion phase. In this panel, the scale of y-axis for luminosity is 100 times of the leftmost panel.

The reason for such a hierarchy in the average energies of the different flavors of neutrinos is the fact that they have different interaction cross-sections with the nucleons. In other words, the non-electron flavors ($\nu_\mu, \nu_\tau, \bar{\nu}_\mu$ and $\bar{\nu}_\tau$) have smaller opacities as compared to ν_e and $\bar{\nu}_e$. The electron neutrino and antineutrino take part in the reactions

$$\begin{aligned} \nu_e + n &\rightarrow p + e^- \\ \bar{\nu}_e + p &\rightarrow n + e^+ \end{aligned} \tag{2.1}$$

However, the non-electron flavor neutrinos and antineutrinos do not undergo such charged current reactions as they do not have enough energy to produce the heavy leptons. As a result, they decouple earlier, i.e. at higher temperatures and also have higher energies. Moreover, since the electron neutrino has a larger cross-section than that of the electron antineutrino, $\bar{\nu}_e$ decouples earlier than ν_e. So, the average energies of the different flavors follows the order as $\langle E_{\nu_e} \rangle < \langle E_{\bar{\nu}_e} \rangle < \langle E_{\nu_{\mu,\tau}} \rangle$. In ad-

dition to this, due to the dependence of cross-section of neutrino-nucleon scattering on energy ($\sigma \propto G_F^2 E_\nu^2$), the last scattering surface of neutrinos called the neutrinosphere is also energy and flavor dependent. The neutrinosphere radius changes with the post bounce time. The typical value ranges from around 10^2 km during the accretion phase to around 30 km at the beginning of the cooling phase [77].

The whole hydrodynamic process of the explosion of a massive star into a supernova is very complex. More detailed information about the neutrino fluxes and the average energies are provided by the numerical simulations. In these simulations, detailed neutrino transport is applied taking into account all the necessary weak interaction processes. As is evident from figure 2.1, the luminosities and the average energies of the emitted neutrinos are a function of time. The delayed neutrino heating mechanism does not always lead to successful explosions in the SN hydrodynamic simulations. Although the lowest mass progenitors ($8M_\odot - 10M_\odot$) with oxygen-neon-magnesium core or small iron cores explode in the 1D simulations (spherically symmetric), the heavier mass ones do not [70, 78–83]. So, for the heavy mass progenitors, one has to implement the multi-dimensional simulations in order to obtain a successful neutrino driven explosion. In 2D (axisymmetric) simulations, inclusion of the convection process inside the PNS just below the neutrinosphere [64, 70] amplify the early neutrino luminosities and thus more amount of energy is deposited behind the shock. This can result in explosion sometimes. In 3D case, the convection alone is not enough to drive the explosion [71–74]. In addition to this, non-radial hydrodynamic instabilities like SASI (Standing Accretion Shock Instability) [84–86] can also aid the neutrino driven explosion in the multi-dimensional models. Recently, 2D simulations have been carried out by including muons [87] whose presence is usually neglected due to their low abundance in supernova matter as compared to electrons. It has been shown that the inclusion of muons leads to the softening of neutron star equation of state and faster contraction of the neutron star. This further leads to higher values of luminosity and average energy of the emitted neutrinos and thus helps in successful neutrino driven explosions.

2.1.3 Neutrino spectrum

The large number of neutrinos reaching the detectors after being emitted from deep inside the core of an exploding star can provide significant information about the inside of the star as well as the masses and mixing of neutrinos [35, 88, 89]. In order to extract this information, measurement of the neutrino signal from a galactic

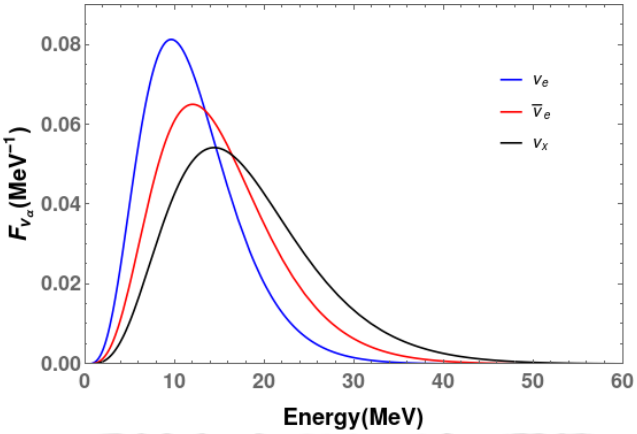

Figure 2.2: Neutrino spectra given by equation 2.2 for typical average energies $\langle E_{\nu_e}\rangle = 12$ MeV, $\langle E_{\bar{\nu}_e}\rangle = 15$ MeV, $\langle E_{\nu_x}\rangle = 18$ MeV. Here, $\beta = 4$. The parameter values has been taken from [91].

SN is required. The emission of the neutrinos from a supernova is similar to that of a blackbody emission. However, their spectrum is somewhat different from the thermal spectrum. This is because of the dependence of the interaction cross-sections of the neutrinos with the background nucleons on energy. So, the neutrinos of different energies are emitted at different radii and at different temperatures. As a result, the spectrum of a SN neutrino signal becomes pinched. So, the neutrino spectra is fitted by the SN simulations with a quasi-thermal spectra also known as the alpha-fit [90, 91]. Note that here we have denoted the spectral parameter by β instead of α (the usual convention). The form of the function used to fit the spectra is as follows:

$$F_{\nu_\alpha}(E) = \frac{(\beta+1)^{(\beta+1)}}{\Gamma(\beta+1)} \frac{E^\beta}{(\langle E_{\nu_\alpha}\rangle)^{\beta+1}} \exp\left[-(\beta+1)\frac{E}{\langle E_{\nu_\alpha}\rangle}\right] \tag{2.2}$$

where, α denotes the flavor of the neutrino and $\int dE F_{\nu_\alpha} = 1$. The average energy of the neutrinos is given by $\langle E_{\nu_\alpha}\rangle$ and $\Gamma(x)$ is the Euler gamma function. β is the spectral parameter which determines the width of the spectra and is given by :

$$\beta = \frac{2\langle E\rangle^2 - \langle E^2\rangle}{\langle E^2\rangle - \langle E\rangle^2} \tag{2.3}$$

The spectral parameter β is also time dependent which means that they can be different for different neutrino emission phases. The typical values of β as given by simulations [91] are in the range $2 \leq \beta \leq 5$, with the lower limit being the broadest and the higher limit the narrowest spectra. The total number of neutrinos emitted

or the total flux is given by

$$\Phi_{\nu_\alpha}(E) = \frac{L_{\nu_\alpha}}{\langle E_{\nu_\alpha} \rangle} F_{\nu_\alpha}(E) \tag{2.4}$$

where L_{ν_α} is the luminosity of the corresponding flavor of neutrino. We have shown an example of the spectra in figure 2.2 for some typical values of the average energies taken from [91]. In figure 2.2, $\nu_x = \bar{\nu}_x$ denotes the non electron flavors $\nu_\mu, \nu_\tau, \bar{\nu}_\mu$ and $\bar{\nu}_{tau}$ or their linear combinations.

While passing through the dense supernova matter, the neutrinos undergo flavor oscillations due to the background matter which will be reflected in their final fluxes reaching the detector. So, we will discuss the various oscillation scenarios undergone by the SN neutrinos in the next section.

2.2 Oscillations of supernova neutrinos

The neutrinos free streaming from the neutrinosphere travel through the supernova envelope where they undergo interactions with the background matter which is then followed by their travel through the vacuum in interstellar space before they reach the detector. In addition to the ordinary matter densities inside the core, these neutrinos also encounter a large background neutrino density. As a result, besides MSW conversion another phenomenon known as collective oscillations take place.

Let us first start with the equation of motion governing the evolution of the neutrinos while they travel from the supernova core to the detector. The formalism of describing the flavor evolution of the neutrino beams through the Schrödinger equation is not adequate when we are dealing with the evolution of a statistical ensemble of neutrinos simultaneously mixing and scattering in a medium. Such scenario arises in a supernova or early universe, where the neutrino density is so high that an ensemble has to be considered rather than single particle states. Here, in addition to the refraction caused by background matter and background neutrinos, collisions have to be taken into consideration [23, 25, 92]. These collisions can destroy the coherence and thus oscillations can be affected. So, in order to model the neutrino flavor conversions, the density matrix formalism is adopted as it can take into consideration both mixed states and possible loss of coherence due to collisions which is explained in detail in [93]. The equations of motion describing the spatial and temporal evolution of the neutrino occupation number matrices $\varrho_{\mathbf{p},\mathbf{x},t}$

for momentum $\mathbf{p}$ at position $\mathbf{x}$ and time t can be written in the form [93]

$$(\partial_t + \mathbf{v_p} \cdot \nabla_\mathbf{x})\, \varrho_{\mathbf{p},\mathbf{x},t} = -i[H_{\mathbf{p},\mathbf{x},t}, \varrho_{\mathbf{p},\mathbf{x},t}] + C[\varrho_{\mathbf{p},\mathbf{x},t}] \tag{2.5}$$

where, $H_{\mathbf{p},\mathbf{x},t}$ is the Hamiltonian of the system and $C[\varrho_{\mathbf{p},\mathbf{x},t}]$ is the collision term. The occupation number matrices for neutrinos and anti-neutrinos are $\varrho_\mathbf{p}$ and $\bar{\varrho}_\mathbf{p}$, respectively and in general has the form

$$\varrho_{\mathbf{p},\mathbf{x},t} = \begin{pmatrix} \varrho^{ee}_{\mathbf{p},\mathbf{x},t} & \varrho^{e\mu}_{\mathbf{p},\mathbf{x},t} & \varrho^{e\tau}_{\mathbf{p},\mathbf{x},t} \\ \varrho^{\mu e}_{\mathbf{p},\mathbf{x},t} & \varrho^{\mu\mu}_{\mathbf{p},\mathbf{x},t} & \varrho^{\mu\tau}_{\mathbf{p},\mathbf{x},t} \\ \varrho^{\tau e}_{\mathbf{p},\mathbf{x},t} & \varrho^{\tau\mu}_{\mathbf{p},\mathbf{x},t} & \varrho^{\tau\tau}_{\mathbf{p},\mathbf{x},t} \end{pmatrix}. \tag{2.6}$$

The elements of $\varrho_{\mathbf{p},\mathbf{x},t}$ denoted by $\varrho^{ll'}_{\mathbf{p},\mathbf{x},t} = \varrho^{\nu_l\nu_{l'}}_{\mathbf{p},\mathbf{x},t}$ with l, $l' = $ e, μ, τ are proportional to the expectation values of the neutrino field bilinears, i.e. $\varrho^{\nu_l\nu_{l'}}_{\mathbf{p},\mathbf{x},t} \propto \langle a^\dagger_{\nu_{l'}}\, a_{\nu_l}\rangle$. Similarly for antineutrinos $\bar{\varrho}^{\nu_l\nu_{l'}}_{\mathbf{p},\mathbf{x},t} \propto \langle \bar{a}^\dagger_{\nu_l}\, \bar{a}_{\nu_{l'}}\rangle$. Here, $a^\dagger_{\nu_l}\,(\bar{a}^\dagger_{\nu_l}), a_{\nu_l}\,(\bar{a}_{\nu_l})$ are the creation and annihilation operators for neutrino (antineutrino) in the flavor eigenstate ν_l respectively. So, the survival probability of a particular flavor of neutrino is given by the diagonal elements of $\varrho_{\mathbf{p},\mathbf{x},t}$, whereas the off-diagonal elements provide encode the phase information, i.e they tell us about the flavor conversion. The collision term is proportional to G_F^2 and in our subsequent dicussions we will neglect it. The Hamiltonian consists of three parts, i.e., vacuum term, MSW potential and the neutrino-neutrino interaction terms.

Focussing on the Hamiltonian, we first begin with the vacuum term which is given by

$$H^{vacuum}_\mathbf{p} = U \frac{M^2}{2\,\mathbf{p}} U^\dagger \tag{2.7}$$

where, U is the transformation matrix given by equation 1.8 for two flavor and equation 1.14 for three flavors. The mass squared matrix in the mass basis for the general three flavor case is $M^2 = \text{diag}\ (m_1^2, m_2^2, m_3^2)$. For studying neutrino oscillations, this can be further parametrised in terms of ω. For example, it can be written as $H^{vacuum}_\mathbf{p} = \text{diag}\ (+\omega/2, -\omega/2)$ in an effective two flavor scenario. Here, $\omega = \pm\frac{\Delta m^2}{2E}$ for relativistic neutrinos of energy E and $\pm$ refers to normal and inverted mass ordering respectively. If solar mass squared difference is used, ω becomes $\omega_L = \frac{\Delta m^2_\odot}{2E}$ while for atmospheric mass squared difference, it is $\omega_H = \frac{\Delta m^2_{atm}}{2E}$.

Now as the neutrinos pass through the medium, they experience a refractive effect due to the constituents of the matter. This results in the MSW resonance

effect as described in the previous chapter. So the matter potential due to the background electrons is

$$\lambda = \sqrt{2} G_F n_e(\mathbf{x}) \tag{2.8}$$

where $n_e(\mathbf{x})$ is the background electron density. In weak interaction basis, the matter contribution to the Hamiltonian can be written as

$$H_{\mathbf{p}}^{matter} = \lambda \, diag(1, 0, 0) \tag{2.9}$$

In addition to this, there is a third term ($H_{\mathbf{p}}^{\nu\nu}$) due to the presence of which the evolution equation 2.5 becomes nonlinear making it difficult to solve, even numerically. This term arises due to the large neutrino density in the supernova environment and is responsible for the so-called collective oscillations. So the neutrino-neutrino interaction contribution to the Hamiltonian is given by

$$H_{\mathbf{p}}^{\nu\nu} = \mu_0 \int d^3\mathbf{q}/(2\pi)^3 (1 - \mathbf{v_p} \cdot \mathbf{v_q})(\varrho_{\mathbf{q},\mathbf{x},t} - \bar{\varrho}_{\mathbf{q},\mathbf{x},t}) \tag{2.10}$$

where the neutrino-neutrino interaction strength is $\mu_0 = \sqrt{2} G_F n_\nu$, n_ν being the background neutrino density, v_p is the velocity of test neutrino, v_q is the velocity of the background neutrino, and G_F is the Fermi constant. The non zero off-diagonal entries of the ϱ give rise to off diagonal refractive indices. Moreover, this term is proportional to $(1 - \mathbf{v_p} \cdot \mathbf{v_q})$ which leads to different potentials due to neutrinos travelling in different paths and this results in flavor decoherence. Under the assumption of isotropic medium, this effect vanishes.

Note that the antineutrinos have a similar equation of motion as equation 2.5, the only difference being that $H_{\mathbf{p}}^{vacuum}$ is replaced by $-H_{\mathbf{p}}^{vacuum}$. We will now move on to the detailed discussion of MSW and collective oscillations in the context of supernova below.

2.2.1 MSW conversions

Initially it was believed that the flavor conversions in a supernova take place only due to the Mikheyev-Smirnov-Wolfenstein (MSW) resonance phenomenon [88, 94]. In the MSW effect as explained before, the neutrino flavor conversion is enhanced when the condition $\Delta m^2 \cos 2\theta / 2E = \pm\sqrt{2} G_F n_e$ is satisfied. Here the plus sign corresponds to neutrinos and the minus sign is for the antineutrinos. In a supernova environment, the whole three flavor system can be categorized into two independent

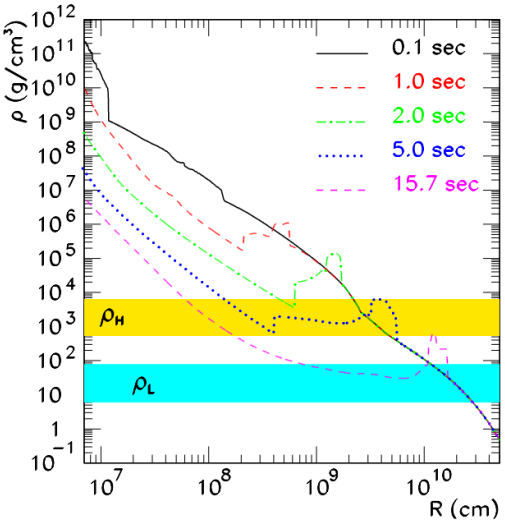

Figure 2.3: Density profile at different post bounce times for a 15 $M_\odot$ progenitor [96]. The yellow and light blue patches show the range of value of ρ_H and ρ_L respectively. This figure is taken from [97].

two flavor systems corresponding to the two different mass squared differences. This is because of the hierarchy between them, i.e., the solar mass squared difference ($\Delta m^2_\odot$) is about two orders smaller than the atmospheric mass squared difference (Δm^2_{atm}). As a result two resonance layers can be defined, one at high density and the other one at low densities corresponding to the two different Δm^2 and the MSW conversions at the two regions can be studied separately [25, 88, 95]. The layer at higher density ($\rho_H \sim 10^3 - 10^4$) g/cc is called the H-resonance layer. The lower density layer ($\rho_L \sim 10 - 100$) g/cc is known as the L-resonance layer. Figure 2.3 shows the density profiles at different post bounce times for a 15 $M_\odot$ progenitor [96, 97]. The yellow and light blue regions in the plot correspond to range of values for ρ_H and ρ_L respectively corresponding to the expected energy ranges of the neutrinos. As mentioned earlier that depending on the sign of the mass squared difference, the resonance takes place either for neutrinos or antineutrinos. The solar mass squared difference $\Delta m^2_\odot$ is always positive and thus the L-resonance occurs only for neutrinos. On the other hand, the H-resonance occurs for neutrinos in normal ordering ($\Delta m^2_{atm} > 0$) and for antineutrinos in the inverted ordering ($\Delta m^2_{atm} < 0$). The final ν_e and $\bar{\nu}_e$ fluxes after MSW resonance are given by [88] :

$$F_{\nu_e} = pF^0_{\nu_e} + (1-p)F^0_{\nu_x} \tag{2.11}$$

$$F_{\bar{\nu}_e} = \bar{p}F^0_{\bar{\nu}_e} + (1-\bar{p})F^0_{\nu_x} \tag{2.12}$$

where p and $\bar{p}$ are the survival probabilities of the electron neutrinos and antineutrinos respectively. $F^0_{\nu_\alpha}$ represent the initial fluxes of the corresponding flavor (α) at the source. So the values of p and $\bar{p}$ for the two mass orderings are given in the table 2.1 [88]. where P_H is the crossing probability at the resonance which signifies the

	NO	IO
ν_e	$\sin^2\theta_{12}\, P_H$	$\sin^2\theta_{12}$
$\bar{\nu}_e$	$\cos^2\theta_{12}$	$\cos^2\theta_{12}\, P_H$

Table 2.1: Survival probability of electron neutrinos and antineutrinos in the two mass orderings after undergoing MSW resonance.

transformation of one mass eigenstate to other. For adiabatic transition, $P_H = 0$ and a specific numerical value for non-adiabatic case. Further, random temporal variations can occur in the MSW resonance due to the presence of turbulence in the matter density [98–105].

2.2.2 Collective oscillations

The above discussion on MSW effect in supernova considers the refractive effect due to neutrinos within a supernova to be negligible. However, this is not true as the neutrino density inside a supernova is very high ($\sim 10^{31}$/cc at $r \sim 30$ km) as a result of which there is a significant contribution of the neutrino-neutrino interactions [106–110]. Here, each neutrino propagates in a background of other neutrinos which makes the problem non-linear as mentioned before. The potential experienced by the neutrinos is proportional to the neutrino density ($\propto \sqrt{2}G_F n_\nu$). The interactions are of the type

$$\begin{aligned} \nu_e(\mathbf{p}) + \nu_x(\mathbf{k}) &\leftrightarrow \nu_x(\mathbf{p}) + \nu_e(\mathbf{k}) \\ \nu_e(\mathbf{p}) + \bar{\nu}_e(\mathbf{k}) &\leftrightarrow \nu_x(\mathbf{p}) + \bar{\nu}_x(\mathbf{k}) \end{aligned} \tag{2.13}$$

where, ν_x, $\bar{\nu}_x$ are $\nu_\mu, \nu_\tau, \bar{\nu}_\mu, \bar{\nu}_\tau$ or a linear combination of them as in a supernova, the non-electron flavors are considered to have the same fluxes. Thus, this potential is not flavor diagonal and the off-diagonal components also have a significant contribution. This leads to the phenomenon known as collective oscillations where the neutrinos having different energies undergo flavor conversion in a coherent manner.

A large number of studies [108, 111–144] have been carried out in the last two

decades in order to investigate both the presence and outcome of collective oscillations. Depending on the time scale required for the development of these self-induced flavor conversions, they are classified as slow or fast. The growth rate of the slow modes is proportional to $\omega_{\rm vac} \sim \mathcal{O}(1)$ km^{-1}, where $\omega_{\rm vac} = \frac{\Delta m^2}{2E}$ is the vacuum oscillation frequency. It usually occurs at a distance of $10^2 - 10^3$ km from the centre. In comparison to this, the growth of fast modes is dependent on the neutrino-neutrino interaction strength μ_0 given by $\mu_0 = \sqrt{2} G_F n_\nu$ which can be as large as $\sim 10^5$ km^{-1} in the dense core [1]. We now introduce the framework to study the slow and fast oscillations.

Framework

In the following we use the framework used in the [119] to describe the quantum kinetic equations for the ultra-relativistic neutrino streams. The equation of motion given in equation 2.5 for flavor oscillations in absence of collisions can be written in a compact form as

$$v^\beta \partial_\beta \varrho_{\mathbf{p}} = -i[H_{\mathbf{p}}, \varrho_{\mathbf{p}}]\,. \tag{2.14}$$

Note that we have dropped the indices 'x' and 't'. The neutrino velocity four-vector is defined as $v^\beta = (1, \mathbf{v})$ with the three velocity vector, $\mathbf{v} = \hat{\mathbf{p}} = \mathbf{p}/\mid \mathbf{p} \mid$ for every $\mathbf{p}$ mode, the usual summation convention over $\beta = 0, 1, 2, 3$ is implied. Thus explicitly, $v^\beta \partial_\beta$ is written as $(\partial_t + \mathbf{v} \cdot \nabla)$. The Hamiltonian matrix $H_{\mathbf{p}}$ includes the three components from vacuum, matter and the neutrino-neutrino interactions and takes the form ($E = \mid \mathbf{p} \mid$)

$$H_{\mathbf{p}} = \frac{M^2}{2E} + \sqrt{2}\, G_F\, v_\beta (F_l^\beta + F_\nu^\beta) \tag{2.15}$$

For the vacuum oscillation term, in the initial conditions we take M^2 to be diagonal. This is because in the extreme densities near the core where the neutrino neutrino interactions are important, the effective matter mixing angles become very small. The mass and flavor eigenstates are identical. Thus, the mass squared matrix can be considered as diagonal. In this way, we are ignoring the flavor mixing but not the masses of neutrinos.

[1] Throughout the thesis, dense core usually refers to the distance near the neutrinosphere $\sim \mathcal{O}(10)$ km unless otherwise stated.

$$H_{\mathbf{p}}^{vacuum} = \frac{M^2}{2E} = \frac{1}{2E}\begin{pmatrix} m_1^2 & 0 & 0 \\ 0 & m_2^2 & 0 \\ 0 & 0 & m_3^2 \end{pmatrix}. \tag{2.16}$$

The matter contribution depends on the charged-current contribution of the charged leptons. In the local four-Fermion current-current description in the weak interaction basis the matter term is $H_{\mathbf{p}}^{matter} = \sqrt{2} G_F \, v_\beta F_l^\beta$, where

$$F_l^\beta = \int 2\, d\mathbf{p} \begin{pmatrix} v_e^\beta (f_{e,\mathbf{p}} - \bar{f}_{e,\mathbf{p}}) & 0 & 0 \\ 0 & v_\mu^\beta (f_{\mu,\mathbf{p}} - \bar{f}_{\mu,\mathbf{p}}) & 0 \\ 0 & 0 & v_\tau^\beta (f_{\tau,\mathbf{p}} - \bar{f}_{\tau,\mathbf{p}}) \end{pmatrix}, \tag{2.17}$$

where $\int d\mathbf{p} = \int d^3\mathbf{p}/(2\pi)^3$. The charged lepton four velocity with momentum $\mathbf{p}$ is $v_l^\beta = (1, \mathbf{v}_l)$ with $\mathbf{v}_l = \mathbf{p}/(\mathbf{p}^2 + m_l^2)^{1/2}$ and the occupation numbers are $f_{l,\mathbf{p}}$ (for the antiparticle $\bar{f}_{l,\mathbf{p}}$), $l = e, \mu, \tau$. Similarly, the neutrino-neutrino interaction contribution to the Hamiltonian $H_{\mathbf{p}}^{\nu\nu} = \sqrt{2} G_F v_\beta F_\nu^\beta$, where the neutrino flux matrix is $F_\nu^\beta = \int d\mathbf{p}\; v^\beta (\varrho_{\mathbf{p}} - \bar{\varrho}_{\mathbf{p}})$ and $v^\beta = (1, \hat{\mathbf{p}})$. Thus one may define the overall matter effect caused by both charged leptons and neutrinos, $H^{matter} = v_\beta \lambda^\beta$, where $\lambda^\beta = (\lambda^0, \boldsymbol{\lambda}) =$ Diagonal of $\sqrt{2}\, G_F \, (F_l^\beta + F_\nu^\beta) = \sqrt{2}\, G_F \int d\mathbf{p} \left[2\, v_l^\beta \, (f_{l,\mathbf{p}} - \bar{f}_{l,\mathbf{p}}) + v^\beta \, (\varrho_{\mathbf{p}}^{ll} - \bar{\varrho}_{\mathbf{p}}^{ll}) \right]$ with $\beta = 0, .., 3$.

Note that the temporal components F_l^0 and F_ν^0 represent the charged lepton and neutrino densities, respectively. The spatial parts ($\beta = 1, 2, 3$) of F_l^β and F_ν^β are the corresponding current terms for charged leptons and the neutrinos. However, the usual dense neutrino systems under considerations are isotropic, hence the current terms can be neglected for most of the examples. In the absence of the current terms only the temporal components, i.e. the ordinary matter term or charged lepton density (F_l^0) and the neutrino density (F_ν^0) are the major contributions from the matter terms [119].

Focussing on the definition of the neutrino flux matrix $F_\nu^\beta = \int d\mathbf{p}\; v^\beta (\varrho_{\mathbf{p}} - \bar{\varrho}_{\mathbf{p}})$, the integral on $\mathbf{p}$ contains integration over neutrino energy and the angular variables. In the case of slow oscillations, the energy spectrum of neutrino plays an important role, i.e., crossing in the difference of ν_e and ν_x fluxes as a function of energy is a requirement for occurrence of flavor conversions. On the other hand, the crossing in

the difference of the angular spectrum of neutrinos and antineutrinos is crucial for the fast flavor conversions to take place.

2.2.2.1 Slow oscillations

The non-linear partial differential equations of motion (7 dimensional) describing the evolution of neutrinos (equation 2.5) are very complex as they are non-linear in nature. Thus, various symmetries are imposed to reduce the degrees of freedom of the problem and make it easier to solve. The evolution of the neutrinos has been extensively studied considering the "bulb model" where it is assumed that the neutrinos are emitted in a uniform and half-isotropic manner from the surface of a neutrinosphere (assumed to be spherical). In addition to this, in some cases azimuthal symmetry is also imposed and the neutrinos are assumed to evolve only radially (stationary evolution). Under these assumptions, the partial differential equations reduce to ordinary ones and become relatively easier to solve numerically [108–112, 145]. In order to understand the problem better, an analogy with the motion of a gyroscopic pendulum in flavor space has also been studied [111, 112, 145] where an equal number of neutrinos and antineutrinos are shown to completely convert from one flavor to another even for a small mixing angle. These oscillations are termed as "Bipolar" where in the inverted mass ordering, the upright position of the pendulum corresponds to the initial flavor and after conversion, the final flavor is denoted by the inverted position and the lepton number is conserved. On the other hand, there is no significant flavor conversion in the normal ordering. The signature of these conversions can be seen in the presence of spectral splits which arises because the $\bar{\nu}_e$ is completely converted to $\bar{\nu}_x$ whereas ν_e conversion happens above a critical value of energy ($E > E_c$) [109, 145–147]. The reason for this is that the initial energy of antineutrinos are smaller than that of neutrinos and also the lepton number conservation has to hold true. Although for a long time this absence of flavor conversions in normal ordering was considered to be the standard case, the later studies [142, 148–150] showed that this is just a result of the various symmetry assumptions. It has been shown in [150] that spectral splits can be present in the case of normal ordering also when the asymmetry among the fluxes of the different flavors of neutrinos is not very large. Moreover, it has been found [151–154] that the multi-angle scenario can have an effect on the spectral splits which can be smeared or completely removed. This would further lead to complete decoherence. In addition to this, the various symmetries used as the initial conditions like stationarity, azimuthal symmetry, spatial homogeneity have

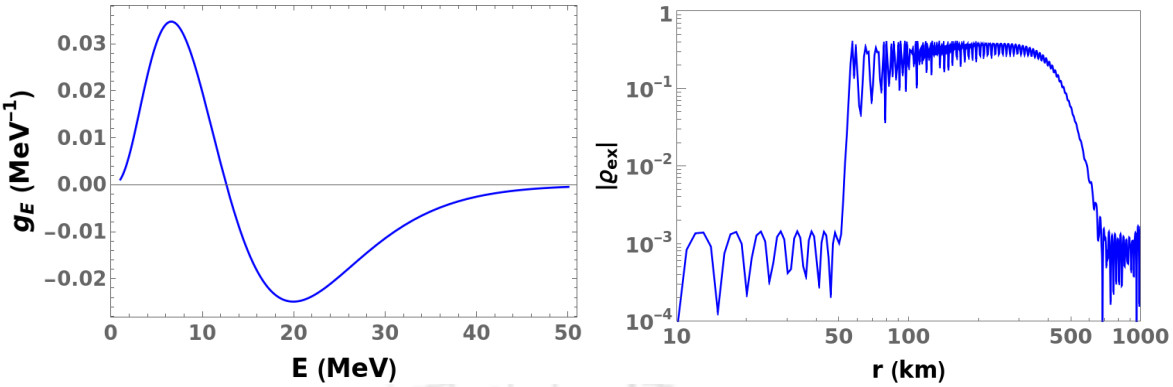

Figure 2.4: Growth of the off-diagonal element of ϱ in the two flavor scenario corresponding to the crossing in g_E. The left panel shows the crossing in g_E which represents the difference in the fluxes of ν_e and ν_x. The right panel corresponds to the growth of the off-diagonal element due to the crossing. The growth has been plotted for energy E= 32 MeV and normal ordering. The parameter values for the ν_e and ν_x spectra are same as used in [169]

.

also been shown to be spontaneously broken [155–168]. It has been found that as a result of this, new instabilities arise which are generally suppressed in the case of a dominating matter potential. But it has also been shown in [167, 168] that a pulsating solution can be generated with a frequency which can compensate the matter effect and lead to collective oscillations. The slow collective oscillations take place at around few hundred kms ($\sim 10^2$) from the neutrinosphere. The left panel of figure 2.4 shows the crossing in the difference spectra 'g_E', i.e. the difference of the fluxes of ν_e and ν_x. The crossing leads to the growth of the off-diagonal element with distance which is shown in the right panel. The off-diagonal growth is shown for energy E= 32 MeV and for normal ordering. It can be seen from the figure that the non-linear regime starts at around 70 km. The onset of the slow oscillations has been studied using the method of 'Linear stability analysis' which will be discussed in the next chapter in detail.

2.2.2.2 Fast oscillations

All the studies mentioned above are based on the assumption that the angular distribution is same for all the flavors. However, the actual scenario is different as we focus on the regions deeper inside the star. The different flavors of neutrinos decouple at different radii and thus have a very different angular distribution near the neutrinosphere. The interaction cross-sections of the non electron flavors (ν_μ, ν_τ) with the background nucleons are smaller than that of the electron flavors. As a result, near the neutrinosphere, the angular distributions of ν_μ, ν_τ are more forward peaked

followed by $\bar{\nu}_e$ and further by ν_e. Thus, on lifting this assumption of same angular distributions, new instabilities can arise. These are called fast flavor conversions or fast oscillations [116, 170, 171]. They occur deeper inside the star on extremely short time scales. The growth rate is proportional to the neutrino-neutrino interaction strength $\mu_0 \sim 10^5$ km^{-1} and thus are faster than the slow oscillations. These conversions can occur even in the absence of neutrino mixing, i.e. for massless neutrinos. The vacuum oscillation frequency acts only as an initial seed for such oscillations to develop. Thus, it is also independent of the mass ordering.

The main requirement for fast flavor conversions to occur is the presence of zero crossing in the difference of the angular distribution of ν_e and $\bar{\nu}_e$ which means that in some directions the flux of ν_e is greater than that of $\bar{\nu}_e$ and vice versa in the other directions. This difference is termed as the electron lepton number (ELN) in the literature. The studies [116–118, 120, 170–186] have shown that the zero crossing in ELN is the necessary and sufficient condition for fast conversions to occur. Figure 2.5 shows the growth of the off-diagonal element of ϱ indicating fast flavor conversions in two flavor scenario. The left panel shows the crossing in ELN and the right panel shows the corresponding growth of the off-diagonal element. Note that the growth occurs at the nanoseconds scale. The method of linear stability analysis has been adopted in many works [119, 120, 172, 187, 188] to provide a detailed description of fast oscillations. These studies [122, 174, 178] too assume spatial homogeneity and azimuthal symmetry. The flavor pendulum analogy [122] also holds in this case, but unlike slow conversions, here the real part of the pulsation of flavor wave represents the spin of the pendulum and is a determining factor for the final amount of conversion.

Focussing on the simulations, the angular distributions of the neutrino fluxes are not usually provided by them. Rather the simulations provide the angular moments. Based on this, a few methods have been proposed [134–136, 175, 189] which exploit these moments to study the instabilities in the system through stability analysis. Some of the first explorations [190, 191] of this topic did not result in any instabilities because of certain limitations like they were 1D or restricted to specific locations of supernova. However, recent studies have reported the locations of supernova where crossings can be found. In addition to the presence of the crossings near the neutrinosphere due to different cross-sections of the various flavors, another possibility can be the presence of the asymmetric emission of lepton number (LESA) [84, 192–194]. Moreover, it has been shown in [195–197] that the crossings can be generated in the backward directions due to the coherent neutrino-nucleus scattering

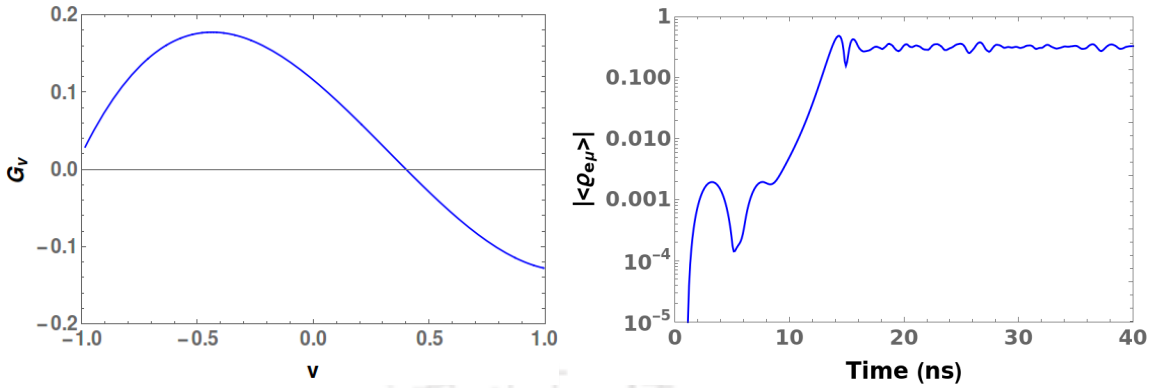

Figure 2.5: Growth of the angle averaged off-diagonal element of ϱ in the two flavor picture showing fast conversions. The left panel shows the ELN crossing and the right panel shows the growth of the off-diagonal element corresponding to it. The angular spectra of the ν_e and $\bar{\nu}_e$ are taken from [118]

.

in the pre-shock as well as post shock region. The recent work [180] has shown that the propagation of neutrinos in space and time can cancel the crossing which was initially present and thus the instability also vanishes. The works [123, 126–128, 181, 182] have aimed to study the final fate of the fast oscillations. They have shown that during the evolution, the power of a fast instability is transferred from large scales to small scales which further leads to the decoherence of the system. An analytical formula has been derived in [182] to calculate this amount of decoherence. Some other studies [198] show the dependence of the outcome of the fast conversions on the size of the mass squared differences and on their ordering. Besides this, the role of collisions in this context, dependence of fast flavor conversions on the number of crossings and the effect of new physics such as non-standard interactions on fast conversions have also been pointed out in [173, 183, 199].

Some of the initial studies [116, 118, 170, 171] concluded that the fast oscillations lead to flavor equilibrium among all the flavors of neutrinos upto the conservation of lepton number. This was found to hold for all energies of the neutrino as well as for both mass orderings. But according to some recent studies [139, 200, 201], this may not be the actual case. In addition to this, some implications of the fast flavor oscillations on the neutrino driven winds and their nucleosynthesis have been investigated in [202] under the assumption of fast flavor conversions leading to flavor equilibration. It has been found that the total mass loss can be increased by around order of 1.5 resulting in more proton rich conditions inside the star. Further, this can lead to the increase in the production of ^{64}Zn and light p-nuclei like ^{74}Se, ^{78}Kr and ^{84}Sr. Some effects on the abundances of the metal poor stars, galactic chemical

evolution and isotopic anomalies in meteorites have also been discussed.

In this chapter, we looked into the mechanism of a supernova explosion and the creation of neutrinos in it. These neutrinos, being weakly interacting act as an essential probe of the dynamics of the inside of a star. As the neutrinos pass through the dense supernova matter, in addition to the usual MSW resonance, they also undergo self-interactions due to the large density of neutrinos. This results in a phenomenon known as collective oscillations. We have discussed the development of this topic over the years through the various studies which have been carried out to solve the complex system of evolution of neutrinos in a supernova. In the subsequent chapters, our main focus will be on the treatment of this problem in the six species scenario in both the linear and nonlinear regimes.

Chapter 3

Linear stability analysis

The problem of neutrino evolution in a supernova is nonlinear in nature due to the presence of the neutrino-neutrino interactions which makes it difficult to solve, even numerically. Therefore, a semi-analytical approach has been adopted in the literature known as the linearized stability analysis, where exponential growths of the flavor off-diagonal elements in the linearized regime signify flavor instabilities. In this chapter, we study the phenomena of self induced flavor conversions in supernova using the method of linear stability analysis. Here we consider the evolution of the system considering all the three flavors of the neutrinos.

3.1 Linearization

In compact astrophysical objects, the neutrino population are considered to be produced in flavor eigenstates making the ϱ matrices diagonal in the flavor basis. Thus the flavor mixings are denoted by the growth of the off-diagonal elements. One of the techniques used to understand the phenomena of collective oscillations is the 'Linear Stability Analysis' [155, 166, 203, 204], where exponential growths of the flavor off-diagonal elements in the linearized regime signify flavor instabilities. In this approach, the equations of motion are reduced to a linear set of equations (upto the linear order of the off-diagonals of occupation number matrix ϱ). Here, the off-diagonal terms are considered to remain small and any subsequent growth will imply the presence of self-induced flavor conversion caused by neutrino-neutrino interactions. In this regard, the focus is on the off-diagonal terms and they being small, it is reasonable to look into the linearized equations of motion of the off-diagonal elements ($l \neq l'$) for both the neutrinos ($\varrho^{ll'}_{\mathbf{p}}$) and antineutrinos ($\bar{\varrho}^{ll'}_{\mathbf{p}}$) (equation 2.6). Many linear stability analysis studies have been carried out in the

literature [119, 120, 122, 155, 166, 171, 172, 174, 187, 188, 203–206] in the context of both slow and fast oscillations. However, combining the fast oscillations together with the nonstationary (evolution in time) and inhomogeneous (evolution in space) flavor evolution require different techniques. Since it involves both the time and spatial evolution and the related Fourier modes, it is reasonable to use the dispersion picture [119, 120, 126, 187, 188]. In the dispersion picture, the imaginary Fourier modes of the disturbances in time and space signify the instabilities, giving the most general description of the fast oscillations.

However, all these developments in the understanding of fast oscillations, non stationarity and inhomogeneities are developed in the framework of a 2 flavor system of neutrinos. This is indeed a reasonable approximation as per many SN simulations showing an effective 2 flavor description i.e, 'similar' fluxes of the mu and tau neutrinos and anti-neutrinos. This similar flux is approximated to 'same' and denoted as the 'ν_x'. It has always remained an interesting aspect to check the validity of the 'similar' flux arguments, i.e. if the differences in the x flavors are not neglected requiring a three flavor study [207]. Indeed, most of the three flavor studies [207, 208] pointed out that the effective two flavor analysis is a reasonable approximation due to the 'similar' flux argument. However, a three flavor study is needed to understand topics like including inhomogeneities, non-stationarity and fast oscillation. In the three flavor scenario, radiative corrections to the neutrino-neutrino interaction term becomes important [209] which breaks the degeneracy between ν_μ and ν_τ. In [210], it has been shown that these corrections are proportional to $\mathcal{O}(10^{-6})$. Due to weak magnetism corrections, the cross-section for neutral current scattering with nucleons is larger for neutrinos than antineutrinos [211]. As a result, there is already a small difference ($\sim 0.5\%$) between the number of neutrinos and antineutrinos of heavy flavors (ν_μ and ν_τ). However, as shown in [87], taking into account the presence of muons in the accretion phase (till ~ 0.6 s), the difference between ν_μ and $\bar{\nu}_\mu$ increases. In the accretion phase, the peak temperatures are very high (30 MeV) and the thermal distribution of photons and neutrinos extends beyond 100 MeV and thus the creation of muons becomes favourable. The difference between the maximum number of the muon neutrinos and antineutrinos become $\sim 5\%$ after including muons in the simulation. Motivated from this, in this chapter, we carry out the analysis taking into account the deviation from the 'similar flux' argument. Here we extend the techniques of the linear stability analysis and the dispersion picture of fast oscillations to a three flavor analysis. We study the impact of adding one extra flavour for both the slow and fast oscillations.

For the slow oscillations the past three flavor analysis results [169, 208] were based on numerically solving the non linear evolution. In our analysis we check if we can reproduce the same from the linearized stability analysis picture. The main result of the 'slow' three flavor nonlinear analysis is that the flavor conversions due to the atmospheric and solar sector are not completely de-coupled. Thus the late onset of the solar mass squared difference which governed the flavor conversion in otherwise two flavor analysis can speed up when another extra flavor is added. Indeed, our linearized study successfully reproduce these results from the past non-linear three flavor analysis. In the following, we also analyze the 'fast' flavor conversion in both time and space using the dispersion relation technique. In the linearized regime, the three flavor evolution decouples into three, two flavor evolutions. These two flavor evolutions are dependent on the fluxes and densities of the different species of neutrinos. In the dispersion picture, we focus on a two beam case to realize how the addition of the extra flavor may affect the evolution. We find that these three effective two flavor evolutions are sensitive to the flux differences of the $\mu(\tau)$ neutrinos and anti-neutrinos. Thus the similar to same approximation for the x flavor fluxes may not reveal the true picture of the fast conversions. These small differences can still act as a seed to influence the growth of the flavor instabilities, in turn 'speeding up' or 'slowing down' the fast flavor conversion in a non-linear picture.

Expanding the equations of motion 2.14 upto the linear order of the off-diagonals of ϱ, we obtain

$$
\begin{aligned}
i\, v^\beta \partial_\beta \varrho^{e\mu}_{\mathbf{p}} \;=\; & \left[\frac{m_1^2 - m_2^2}{2E} + v_\beta(\lambda_e^\beta - \lambda_\mu^\beta)\right] \varrho^{e\mu}_{\mathbf{p}} \\
& - \sqrt{2}\, G_F\, (\varrho^{ee}_{\mathbf{p}} - \varrho^{\mu\mu}_{\mathbf{p}}) v^\beta \int d\mathbf{p}' v'_\beta\, (\varrho^{e\mu}_{\mathbf{p}'} - \bar{\varrho}^{e\mu}_{\mathbf{p}'}) \qquad (3.1)
\end{aligned}
$$

$$
\begin{aligned}
i\, v^\beta \partial_\beta \varrho^{e\tau}_{\mathbf{p}} \;=\; & \left[\frac{m_1^2 - m_3^2}{2E} + v_\beta(\lambda_e^\beta - \lambda_\tau^\beta)\right] \varrho^{e\tau}_{\mathbf{p}} \\
& - \sqrt{2}\, G_F\, (\varrho^{ee}_{\mathbf{p}} - \varrho^{\tau\tau}_{\mathbf{p}}) v^\beta \int d\mathbf{p}' v'_\beta\, (\varrho^{e\tau}_{\mathbf{p}'} - \bar{\varrho}^{e\tau}_{\mathbf{p}'}) \qquad (3.2)
\end{aligned}
$$

$$i\,v^{\beta}\partial_{\beta}\varrho^{\mu\tau}_{\mathbf{p}} = \left[\frac{m_2^2-m_3^2}{2E}+v_{\beta}(\lambda^{\beta}_{\mu}-\lambda^{\beta}_{\tau})\right]\varrho^{\mu\tau}_{\mathbf{p}} - \sqrt{2}\,G_F\,(\varrho^{\mu\mu}_{\mathbf{p}}-\varrho^{\tau\tau}_{\mathbf{p}})v^{\beta}\int d\mathbf{p}'v'_{\beta}\,(\varrho^{\mu\tau}_{\mathbf{p}'}-\bar{\varrho}^{\mu\tau}_{\mathbf{p}'}) \quad (3.3)$$

Note that here the index β is being summed over. In this linearized picture, the three flavor system corresponds to the three independent two flavor cases. The off-diagonal elements evolve independent of one another. Note that in principle, the evolution EOMs are also different as the vacuum and the matter terms are different for the three off-diagonal elements. In the subsequent discussions, we will see if these differences survive in a realistic stellar collapse and their possible effects into the overall flavor evolution.

The anti-neutrino matrices $\bar{\varrho}_{\mathbf{p}}$ have the same EOM (2.14) with a sign change of the vacuum oscillation term. Thus the off-diagonals in the anti-neutrino sector will have similar equations (3.1-3.3) with a sign change of the vacuum oscillation term.

Previous studies of the collective oscillations have been carried out for an effective two flavor neutrino system. In this chapter, we focus on the evolution of the three flavor system based on [212].

3.1.1 Three flavor neutrino system

According to the structure of the EOMs, the difference of the original neutrino distributions decides the flavor oscillations. The diagonal entries of the matrices drop out due to the commutation nature of the evolution equations and the off-diagonals of the occupation number matrices carry the flavor changing information.

We choose the following form of the neutrino matrices involving the spectral difference,

$$\varrho_{\mathbf{p}} = \frac{f_{\nu_e,\mathbf{p}} + f_{\nu_\mu,\mathbf{p}} + f_{\nu_\tau,\mathbf{p}}}{3}\,\mathbf{1} + \frac{f_{\nu_e,\mathbf{p}} - f_{\nu_\mu,\mathbf{p}}}{3}\begin{pmatrix} s_{\mathbf{p}} & S_{1\mathbf{p}} & 0 \\ S^*_{1\mathbf{p}} & -s_{\mathbf{p}} & 0 \\ 0 & 0 & 0 \end{pmatrix} + \frac{f_{\nu_e,\mathbf{p}} - f_{\nu_\tau,\mathbf{p}}}{3}\begin{pmatrix} s_{\mathbf{p}} & 0 & S_{2\mathbf{p}} \\ 0 & 0 & 0 \\ S^*_{2\mathbf{p}} & 0 & -s_{\mathbf{p}} \end{pmatrix} + \frac{f_{\nu_\mu,\mathbf{p}} - f_{\nu_\tau,\mathbf{p}}}{3}\begin{pmatrix} 0 & 0 & 0 \\ 0 & s_{\mathbf{p}} & S_{3\mathbf{p}} \\ 0 & S^*_{3\mathbf{p}} & -s_{\mathbf{p}} \end{pmatrix} \tag{3.4}$$

where $s_{\mathbf{p}}$ is a real number and $s_{\mathbf{p}} = 1$ in the linear order. $S_{j\mathbf{p}}$ are complex with $s^2_{\mathbf{p}} + |S_{j\mathbf{p}}|^2 = 1$, $j = 1, 2, 3$. Hence, the evolution of the off-diagonals ($j = 1, 2, 3$) in the linearized regime becomes

$$i\,v^\beta \partial_\beta S_{j\mathbf{p}} = \big(\omega_j + v^\beta \lambda_{j\beta}\big) S_{j\mathbf{p}} - \sqrt{2}\,G_F\,v^\beta \int d\mathbf{p}' v'_\beta \,(S_{j\mathbf{p}'} g_{j\mathbf{p}'} - \bar{S}_{j\mathbf{p}'} \bar{g}_{j\mathbf{p}'}\,). \tag{3.5}$$

The vacuum oscillation frequencies are given by $\omega_1 = \frac{(m_1^2 - m_2^2)}{2E}$, $\omega_2 = \frac{(m_1^2 - m_3^2)}{2E}$, $\omega_3 = \frac{(m_2^2 - m_3^2)}{2E}$. The spectrum for the neutrinos are taken as $g_{1\mathbf{p}} = (f_{\nu_e,\mathbf{p}} - f_{\nu_\mu,\mathbf{p}})$, $g_{2\mathbf{p}} = (f_{\nu_e,\mathbf{p}} - f_{\nu_\tau,\mathbf{p}})$, $g_{3\mathbf{p}} = (f_{\nu_\mu,\mathbf{p}} - f_{\nu_\tau,\mathbf{p}})$ and for anti-neutrinos, the spectrums are given as $\bar{g}_{1\mathbf{p}} = (f_{\bar{\nu}_e,\mathbf{p}} - f_{\bar{\nu}_\mu,\mathbf{p}})$, $\bar{g}_{2\mathbf{p}} = (f_{\bar{\nu}_e,\mathbf{p}} - f_{\bar{\nu}_\tau,\mathbf{p}})$, $\bar{g}_{3\mathbf{p}} = (f_{\bar{\nu}_\mu,\mathbf{p}} - f_{\bar{\nu}_\tau,\mathbf{p}})$.

The effective matter terms (λ^β_j) combining the effects of the charged and neutral leptons contributions are defined as,

$$\lambda^\beta_1 = (\lambda^\beta_e - \lambda^\beta_\mu) = \sqrt{2}\,G_F \int d\mathbf{p}\,\Big[2\,\Big(v^\beta_e\,(f_{e,\mathbf{p}} - \bar{f}_{e,\mathbf{p}}\,) - v^\beta_\mu\,(f_{\mu,\mathbf{p}} - \bar{f}_{\mu,\mathbf{p}}\,)\Big) + v^\beta\,\Big((f_{\nu_e,\mathbf{p}} - \bar{f}_{\nu_e,\mathbf{p}} - f_{\nu_\mu,\mathbf{p}} + \bar{f}_{\nu_\mu,\mathbf{p}}\,)\Big)\Big]$$

$$\lambda^\beta_2 = (\lambda^\beta_e - \lambda^\beta_\tau) = \sqrt{2}\,G_F \int d\mathbf{p}\,\Big[2\,\Big(v^\beta_e\,(f_{e,\mathbf{p}} - \bar{f}_{e,\mathbf{p}}\,) - v^\beta_\tau\,(f_{\tau,\mathbf{p}} - \bar{f}_{\tau,\mathbf{p}}\,)\Big) + v^\beta\,\Big((f_{\nu_e,\mathbf{p}} - \bar{f}_{\nu_e,\mathbf{p}} - f_{\nu_\tau,\mathbf{p}} + \bar{f}_{\nu_\tau,\mathbf{p}}\,)\Big)\Big]$$

$$\lambda_3^\beta = (\lambda_\mu^\beta - \lambda_\tau^\beta) = \sqrt{2}\, G_F \int d\mathbf{p} \Big[2 \Big(v_\mu^\beta \, (f_{\mu,\mathbf{p}} - \bar{f}_{\mu,\mathbf{p}}) - v_\tau^\beta \, (f_{\tau,\mathbf{p}} - \bar{f}_{\tau,\mathbf{p}}) \Big) + v^\beta \Big((f_{\nu_\mu,\mathbf{p}} - \bar{f}_{\nu_\mu,\mathbf{p}} - f_{\nu_\tau,\mathbf{p}} + \bar{f}_{\nu_\tau,\mathbf{p}}) \Big) \Big] \quad (3.6)$$

To keep the description compact we follow the flavor isospin convention, i.e, antiparticles as particles with negative energy and negative occupation numbers. In this convention, the neutrino modes are described by $-\infty < E < +\infty$ and the three flavor spectrums are given by,

$$g_{1E,\mathbf{v}} = \begin{cases} f_{\nu_e,\mathbf{p}} - f_{\nu_\mu,\mathbf{p}} & \text{for } E > 0, \\ f_{\bar{\nu}_\mu,\mathbf{p}} - f_{\bar{\nu}_e,\mathbf{p}} & \text{for } E < 0, \end{cases}$$

$$g_{2E,\mathbf{v}} = \begin{cases} f_{\nu_e,\mathbf{p}} - f_{\nu_\tau,\mathbf{p}} & \text{for } E > 0, \\ f_{\bar{\nu}_\tau,\mathbf{p}} - f_{\bar{\nu}_e,\mathbf{p}} & \text{for } E < 0, \end{cases}$$

$$g_{3E,\mathbf{v}} = \begin{cases} f_{\nu_\mu,\mathbf{p}} - f_{\nu_\tau,\mathbf{p}} & \text{for } E > 0, \\ f_{\bar{\nu}_\tau,\mathbf{p}} - f_{\bar{\nu}_\mu,\mathbf{p}} & \text{for } E < 0. \end{cases} \quad (3.7)$$

This choice of the spectrum makes the EOMs more compact and the integration term in equation 3.5 simplifies to give new form,

$$i\, v^\beta \partial_\beta S_{jE,\mathbf{v}} = (\omega_j + v^\beta \lambda_{j\beta}) S_{jE,\mathbf{v}} - \sqrt{2}\, G_F\, v^\beta \int d\Gamma'\, v'_\beta\, g_{jE',\mathbf{v}'} S_{jE',\mathbf{v}'} \quad (3.8)$$

where $j = 1, 2, 3$ and the phase-space integration is $\int d\Gamma = \int_{-\infty}^{+\infty} \frac{E^2 dE}{2\pi^2} \int \frac{d\mathbf{v}}{4\pi}$. Here, $\int d\mathbf{v}$ is an integral over the unit surface, i.e., over all polar angles of $\mathbf{p}$.

The vacuum oscillation frequency changes sign for antineutrinos, i.e, for negative E. For the mass ordering we consider the usual convention from [166] and describe the energy spectrum of the neutrinos by the ω spectrum. Here, ω_1 and ω_2 corresponds to the solar and the atmospheric sector, respectively and the $\omega_3 = \frac{(m_2^2 - m_3^2)}{2E} \simeq \omega_2$ as $\frac{\omega_2}{\omega_1} \approx 10^2$. Therefore, in the convention of [166], $\omega_2, \omega_3 > 0$ for inverted mass ordering (IO) and $\omega_2, \omega_3 < 0$ for the normal ordering (NO). For the solar sector, $\omega_1 = \frac{(m_1^2 - m_2^2)}{2E} < 0$, thus only the solutions in the normal ordering are physical. However, in our analysis to be consistent with the other two sectors, we consider both the mass orderings even for the solar sector. The equations 3.8 denote the evolution of the off-diagonal terms in the matrix of densities.

Now we focus on 3.8 and study the only radial evolution (slow conversions) and both space and time evolution (fast conversions) of the system.

3.2 Stability analysis

We carry out the usual stability analysis method which is employed in the literature [166, 171, 203, 205, 206] to understand the flavor instabilities in these dense neutrino systems. The linearized evolution equations of the off-diagonal elements obtained above are checked for any substantial growths. One may begin with a small seed for the off-diagonals and any exponential growth of these seeds denotes possibility of flavor instability. Another more compact way of looking into the stability is the dispersion picture. The stability picture becomes complicated if both the time-space evolution is considered. However, the equations 3.8 show that the complete picture requires simultaneous analysis in both space and time, hence the dispersion picture. The idea is to look for imaginary Fourier modes of the disturbances in time (K_0) and space ($\mathbf{K}$). The relation between these Fourier modes gives the dispersion relation ($D(K_0, \mathbf{K}) = 0$).

In the remaining chapter, we first begin with a simpler picture of only spatial evolution and look for flavor instabilities for the slow modes, i.e instabilities growing slowly with ω_i. Here we employ the method of stability analysis for three flavor neutrino system. Later we look into the three flavor dispersion picture as well.

3.2.1 Slow modes

In this stability picture the problem is interpreted as an instability in propagating flavor indicating the onset of the oscillations. Here, we consider the stationary solutions, i.e., the evolution is independent of time. Since we want to focus on the slow modes we ignore the angular distribution of the spectra ($g_{i,E,v} \equiv g_{i,E}$). The reason to focus on such a simple scenario is that we want to compare our three flavor results with the existing literature [169, 208]. The previous non-linear studies in three flavor were simple in the sense of the multi-angular treatment but had some very important realization. It showed that if the fluxes of the heavy lepton flavors neutrinos (usually denoted as ν_x) were degenerate then the three flavor analysis can be factorized in the two, two flavor sectors, i.e, the solar and atmospheric. The solar sector grows much slowly compare to the atmospheric one due to the smaller Δm^2_{ij} and the picture remains effectively a two flavored one. However, the absence of such

a degeneracy will couple these two sectors and make the solar modes grow faster, thus making the three flavor effects important. Here we try to see if the stability analysis gives the same feature at least qualitatively.

Our aim is to compare the three flavor results with the existing non-linear results presented in [169, 208]. In [169, 208], the dense neutrino systems considered are stationary and only radially evolving. Moreover, the systems are taken to be isotropic and the charged lepton matter terms are neglected. So, in order to accommodate these systems, we consider the linearized system in accordance with [149] but with three flavors.

Radial evolution

To have an analogy to [149] we have to understand the effective matter terms as in the present analysis the matter terms are more involved. The effective matter terms $\lambda_{j\beta} = \lambda^l_{j\beta} + \lambda^\nu_{j\beta}$, has contributions from both the charged leptons (l) and neutrinos (ν). The assumption of isotropy allows us to drop the current terms, i.e. $\lambda_{j1} = \lambda_{j2} = \lambda_{j3} = 0$. The remaining λ_{j0} terms denote the charged lepton and the neutrino densities. The charged lepton densities are denoted by $\lambda^l_{j0} = \lambda_j$ and the terms corresponding to the neutrino (λ^ν_{j0}) leads to the neutrino density parameter μ_0 and the lepton asymmetry parameter ϵ. Note that in comparison to the [149], there are three ϵ and λ in the present framework. Considering the stationary and radial evolution of the system, i.e., taking $\beta = 1$ only, the equations 3.8 take the form

$$i\partial_r S_{j,r,\omega_j,u,\phi} = \Big[\omega_j + u(\lambda_j + \epsilon_j\mu_0)\Big] S_{j,r,\omega_j,u,\phi} - \mu_0 \int d\Gamma'_j \left[u + u' - 2\sqrt{uu'}\cos(\phi - \phi')\right] g_{j,\omega'_j,u',\phi'} S_{j,r,\omega'_j,u',\phi'} \quad (3.9)$$

where $\int d\Gamma_j = \int_{-\infty}^{+\infty} d\omega_j \int_0^1 du \int_0^{2\pi} d\phi$ and $j = 1, 2, 3$. Here, $u = \sin^2\theta_R$ lies in the range $0 \leq u \leq 1$ where θ_R is the emission angle relative to the radial direction of the neutrino sphere at radius R. The radial velocity at a radius r can be expressed as $v^1 = v_{u,r} = (1 - \frac{R^2}{r^2}u)^{1/2}$. Also note that the evolution equations have been written under the assumption of large distance approximation, i.e., $\frac{R}{r} << 1$, (see [149] for more detail).

In this analysis the main difference is the three flavors of charged leptons and neutrinos, contrary to the usual two flavor analysis. Thus in principle there are

three matter densities and three lepton asymmetry parameters,

$$\lambda_1 = \frac{\sqrt{2}G_F R^2}{2r^2}\big[2((n_e-\bar{n}_e)-(n_\mu-\bar{n}_\mu))\big], \quad \lambda_2 = \frac{\sqrt{2}G_F R^2}{2r^2}\big[2((n_e-\bar{n}_e)-(n_\tau-\bar{n}_\tau))\big],$$

$$\lambda_3 = \frac{\sqrt{2}G_F R^2}{2r^2}\big[2((n_\mu-\bar{n}_\mu)-(n_\tau-\bar{n}_\tau))\big], \tag{3.10}$$

where n_e, n_μ, n_τ are the net electron, muon and tauon densities respectively. The effective neutrino density is defined as ,

$$\mu_0 = \sqrt{2}G_F \frac{\Big[\,2(N_{\nu_e}+N_{\bar{\nu}_e})-(N_{\nu_\tau}+N_{\bar{\nu}_\tau}+N_{\nu_\mu}+N_{\bar{\nu}_\mu})\,\Big]}{4\pi r^2}\frac{R^2}{2r^2}, \tag{3.11}$$

here $N_{\nu_e}, N_{\bar{\nu}_e}$ are the total number of electron neutrinos and antineutrinos and similarly for other flavors. Therefore lepton asymmetry parameters are

$$\epsilon_1 = \frac{\int d\Gamma_1\,(f_{\nu_e}-f_{\nu_\mu})}{N} = \frac{(N_{\nu_e}-N_{\bar{\nu}_e})-(N_{\nu_\mu}-N_{\bar{\nu}_\mu})}{N},$$
$$\epsilon_2 = \frac{\int d\Gamma_2\,(f_{\nu_e}-f_{\nu_\tau})}{N} = \frac{(N_{\nu_e}-N_{\bar{\nu}_e})-(N_{\nu_\tau}-N_{\bar{\nu}_\tau})}{N},$$

$$\epsilon_3 = \frac{\int d\Gamma_3\,(f_{\nu_\mu}-f_{\nu_\tau})}{N} = \frac{(N_{\nu_\mu}-N_{\bar{\nu}_\mu})-(N_{\nu_\tau}-N_{\bar{\nu}_\tau})}{N}, \tag{3.12}$$

where $N = \Big[\,2(N_{\nu_e}+N_{\bar{\nu}_e})-(N_{\nu_\tau}+N_{\bar{\nu}_\tau}+N_{\nu_\mu}+N_{\bar{\nu}_\mu})\,\Big]$.
In order to find the unstable modes, we assume the solutions of the linearized equations to be of the form $S_{j,r,\omega_j,u,\phi} = Q_{j,\omega_j,u,\phi}e^{-i\Omega_j r}$, leading to the eigenvalue equations in Q_js.

$$\Big[\omega_j + u(\lambda_j+\epsilon_j\mu) - \Omega_j\Big]Q_{j,\omega_j,u,\phi} = \mu_0 \int d\Gamma'_j\,[u+u'-2\sqrt{uu'}\cos(\phi-\phi')]\,g_{j,\omega_j}Q_{j,\omega_j,u,\phi} \tag{3.13}$$

The eigenvalues in principle are complex ($\Omega_j = \gamma_j + i\kappa_j, j = 1,2,3$). Any non-zero imaginary part ($\kappa_j \neq 0$) would signify unstable modes with the growth rates κ_j. Notice that as we are focussing on slow collective modes the spectrum ($g_{j,\omega}$) is only energy dependent. There is no angular dependence (u,ϕ) on spectrum as necessary for finding fast flavor oscillation modes.
Here, we consider monochromatic neutrinos, i.e., delta functions with some fixed

energy $\omega_j = \pm\omega_{j'}$,

$$g_{j,\omega_j} = \left(1 + \frac{\epsilon_j}{2}\right)\delta(\omega_j - \omega'_j) - \left(1 - \frac{\epsilon_j}{2}\right)\delta(\omega_j + \omega'_j)\,, \tag{3.14}$$

where ϵ_j is the spectral asymmetry.

Now the focus on a 'realistic' scenario of the usual SN environment. The usual practice is to assume that all three heavy lepton flavor neutrinos (i.e., $\nu_\mu, \bar{\nu}_\mu, \nu_\tau, \bar{\nu}_\tau$) have identical number density and spectra. However, our analysis shows that the minimal requirement is that the number of mu and tau type neutrinos to be identical to their corresponding antineutrinos, i.e., $N_{\nu_\mu} = N_{\bar{\nu}_\mu}$ and $N_{\nu_\tau} = N_{\bar{\nu}_\tau}$. Moreover, the usual supernova scenario, muons and tauons are considered to be absent or negligible. Recent SN simulations [87] show the possibility of presence of muons in the late accretion phase. Thus, from equations 3.10 and 3.12,

$$\lambda_1 = \lambda_2 = \lambda\ ;\ \lambda_3 = 0 \quad and \quad \epsilon_1 = \epsilon_2 = \epsilon\ ;\ \epsilon_3 = 0\,.$$

Now, the evolution equations 3.13 become,

$$\Big[\omega_1 + u\bar{\lambda} - \Omega_1\Big] Q_{1,\omega_1,u,\phi} = \mu_0 \int d\Gamma'_1\, [u + u' - 2\sqrt{uu'}\cos(\phi - \phi')]\, g_{1,\omega_1} Q_{1,\omega_1,u,\phi}\,, \tag{3.15}$$

$$\Big[\omega_2 + u\bar{\lambda} - \Omega_2\Big] Q_{2,\omega_2,u,\phi} = \mu_0 \int d\Gamma'_2\, [u + u' - 2\sqrt{uu'}\cos(\phi - \phi')]\, g_{2,\omega_2} Q_{2,\omega_2,u,\phi}\,, \tag{3.16}$$

$$\Big[\omega_2 - \Omega_3\Big] Q_{3,\omega_3,u,\phi} = \mu_0 \int d\Gamma'_2\, [u + u' - 2\sqrt{uu'}\cos(\phi - \phi')]\, g_{3,\omega_3} Q_{3,\omega_3,u,\phi}\,, \tag{3.17}$$

where, $\bar{\lambda} = \lambda + \epsilon\mu_0$. In order to solve the equations (3.15 - 3.17), we adopt a similar mechanism as done in [149, 155, 166] for the two flavor case. We can reasonably employ the 2 flavor method as the three flavor evolution is factorized into three independent two flavor evolution. In the linearized picture this independent evolution of the three off-diagonal elements makes the job simple and give qualitative understanding of the onset of the evolution. In the nonlinear evolution all the three modes will not be independent and onset in one sector will speed up the onset in other sectors due to their coupled nature of evolution.

Instability conditions

In particular, to make things simpler we consider the scenario where ($\bar{\lambda} = 0$). The main impact of this matter term is to 'suppress' the growth of the instability. However, our focus is to understand the dynamics of the three off-diagonal elements in this linear regime and to check if they qualitatively give the same picture obtained in the simple nonlinear analysis [169]. Thus the instability conditions in each of the 2 flavor systems are [149, 155],

$$(I_{j1} - 1)^2 = I_{j0} I_{j2} \quad \text{and} \quad I_{j1} = -1\,, \tag{3.18}$$

where

$$I_{1n} = \mu_0 \int d\omega_1\, du\, \frac{u^n g_{1,\omega_1}}{\omega_1 - \Omega_1}\,, \tag{3.19}$$

$$I_{2n} = \mu_0 \int d\omega_2\, du\, \frac{u^n g_{2,\omega_2}}{\omega_2 - \Omega_2}\,, \tag{3.20}$$

and

$$I_{3n} = \mu_0 \int d\omega_2\, du\, \frac{u^n g_{3,\omega_2}}{\omega_2 - \Omega_3}\,. \tag{3.21}$$

Note that the equations (3.19 - 3.21) has a dependency on the asymmetry parameter ϵ through the spectrum g_{j,ω_j}

Solving the equations 3.18 and using the spectrum of equation 3.14 leads to a quartic equation for the first block and a quadratic equation for the second one in the instability conditions whose general form are as follows,

$$\frac{-\mu_0^2}{3}\left(\frac{1+\frac{\epsilon_j}{2}}{\omega_j' - \Omega_j} + \frac{1-\frac{\epsilon_j}{2}}{\omega_j' + \Omega_j}\right)^2 + \left[-1 + \frac{\mu_0}{2}\left(\frac{1+\frac{\epsilon_j}{2}}{\omega_j' - \Omega_j} + \frac{1-\frac{\epsilon_j}{2}}{\omega_j' + \Omega_j}\right)\right]^2 = 0 \tag{3.22}$$

$$1 + \frac{\mu_0}{2}\left(\frac{1+\frac{\epsilon_j}{2}}{\omega_j' - \Omega_j} + \frac{1-\frac{\epsilon_j}{2}}{\omega_j' + \Omega_j}\right) = 0 \tag{3.23}$$

where $j = 1, 2, 3$.

Given the values of ω_j' and ϵ, one may look for the imaginary solutions of these equations. The presence of imaginary solutions for the equations 3.22 indicates the presence of two kinds of instabilities, namely Bimodal (BM) and Multi Zenith Angle (MZA) instability whereas, for equations 3.23, it shows the Multi Azimuthal Angle (MAA) instability [166].

Numerical solutions

To probe the solutions numerically, we estimate the values of ω'_j and ϵ similar to the supernova case. Here, ω'_1, ω'_2 and ω'_3 depends on the relevant mass square values. We take $\frac{\omega'_1}{\omega'_2} = \frac{7.3\times10^{-5}\,eV^2}{2.4\times10^{-3}\,eV^2} \simeq 3\times10^{-2}$ [213]. We use $\omega'_2 = 0.5$ and then ω'_1 becomes 0.015. For the asymmetry parameter we take $\epsilon = 0.5$. Thus the evolution of the first two off-diagonal elements (S1 and S2) are similar but driven by two different scales due to the difference in solar and atmospheric mass square difference.
However, for the third off-diagonal element the evolution is trivial for the spectrum $g_{3,\omega_3} = 0$ or $\epsilon_3 = 0$. In case the spectrum of the μ and τ neutrinos are same then $g_{3,\omega_3} = 0$ thus the evolution effectively factorizes in 2 two flavor evolutions. The solar and the atmospheric sector would decouple. This scenario is shown in the upper two panels of figure 3.1.

From the solutions of equations 3.22 and 3.23, it is possible to understand the variation of the maximum growth rate κ^{max} and the corresponding interaction strength μ_0^{onset} with the chosen vacuum frequency ω'_j and the asymmetry parameter ϵ. The relation between them comes out to be $\kappa^{max} = \sqrt{(2/\epsilon)^2 - 1}$ [149], where κ^{max} is expressed in the units of vacuum frequency ω'_j. For our chosen numerical values of ω'_j and ϵ we find $\mu_0^{onset}(j=2) > \mu_0^{onset}(j=1)$ and correspondingly $\kappa_2^{max} > \kappa_1^{max}$. In particular, $\kappa_1^{max} = 0.06$ and $\kappa_2^{max} = 1.9$ is in excellent agreement with the upper two panels of figure 3.1.

For all the cases BM, MAA and MZA instabilities are present. The BM happens for positive μ_0, i.e, IO and the MAA and MZA happens for the negative μ_0, i.e, NO. From the figures it is clear that for S1 (solar sector) the instability happens at much smaller μ_0 in comparison to the S2 (atmospheric sector). Smaller μ_0 would mean larger radius. Thus the instabilities for the atmospheric sector happen at a smaller radius, closer to the core. Due to the smaller mass squared difference the instabilities slow down in the solar sector. In fact, the neutrino density μ_0 with its $1/r^4$ dependence would be too small to sustain the solar instability to any substantial flavor conversion. However, the realistic SN case might be different than this idealistic situation, even a small $\nu_\mu - \nu_\tau$ asymmetry would trigger the third off-diagonal element S3. In that case, equations 3.22 and 3.23 would also hold for S_3 and result in a similar evolution in the $\nu_\mu - \nu_\tau$ sector as well. This has been shown in the lower most panel in figure 3.1. We have used $\omega'_3 = \omega'_2 = 0.5$ and $\epsilon_3 = 10^{-1}$. Clearly, even for this small asymmetry S3 grows much faster than the other two off-diagonals. Here, the maximum growth rate comes out to be $\kappa_3^{max} = 9.987$. Thus the linear evolution is decoupled in these three two flavor evolutions. Hence, the non

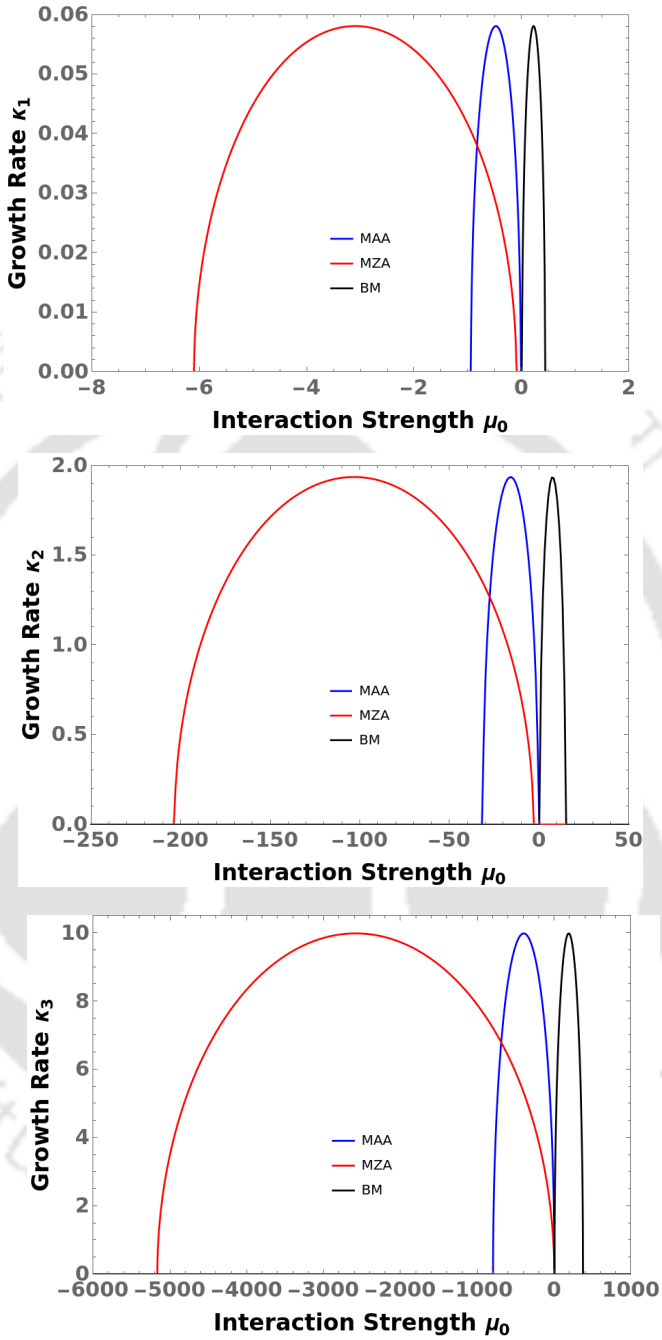

Figure 3.1: Growth rate κ versus interaction strength μ_0 for the unstable modes in the homogeneous (k=0) case for the evolution of S_1(First Panel), S_2(Second Panel), S_3(Third Panel). Here, we take $\epsilon_1 = \epsilon_2 = \epsilon = 0.5, \epsilon_3 = 10^{-1}$, $\omega_1' = 0.015, \omega_2' = 0.5, \omega_3' = 0.5$. The first block in equation 3.18 yields the bimodal and MZA instability (black and red curves) and the second block yields multi-azimuth-angle instability (blue curve).

linear evolution will not decouple the solar and atmospheric sector as the $\nu_\mu - \nu_\tau$ sector will act as the coupling factor and speed up the conversion [169].

Thus the simple stability analysis in the linear regime for the three flavor system helps in gaining analytic understanding of the system. We reproduce the existing understanding of the three flavor system of collective neutrino evolution in SN environment. The system we considered is a simple one, without temporal evolution, homogeneous and no angular distributions for the spectrum, i.e, no fast oscillations. In the following, we discuss the three flavor fast conversion in the dispersion picture for evolution in both time and space.

3.2.2 Fast modes

One common assumption in the discussions of dense neutrino systems was stationary solutions for the flavor evolution. However, the breaking of stationarity came out with surprising development of new instabilities, termed as 'temporal instabilities'. Around the same time it was also found that there is a complete different class of instability connected to the angular distributions of different flavors. In particular, the angular (u, ϕ) dependence of the spectrum $(g_{j,\omega_j,u,\phi})$ is the origin to these new instabilities. These new class of instabilities grow very fast, growth rates comparable to the neutrino density (μ_0), termed as fast instabilities resulting in fast conversions! These instabilities are markedly different from the usual 'slow conversions' growing at the rate of the vacuum frequencies (ω_j). In this regard, it is necessary that both the temporal and spatial instabilities are studied together to understand the true nature of the fast oscillations. Hence, the approach of dispersion relation, i.e, the relation between frequencies $(K_j^0,)$ and the wave numbers $(\mathbf{K}_j)$ of the temporal and spatial disturbances, respectively, indicates the presence of instability [120].

In particular, any imaginary K_j^0 for real $\mathbf{K}_j$ and vice versa will denote exponential growth of the temporal and spatial disturbances. Here, it is worth noting that the dispersion relation approach can also be used for slow conversion. Here, in order to understand the fast flavor conversions for a three flavor system we keep it simple and study the dispersion relation only for the fast instabilities without any coupling to slow conversion.

Consider the space-time dependent solutions for the three $(j = 1, 2, 3)$ off-diagonal elements

$$S_{j,\Gamma,r} = Q_{j,\Gamma,K}\, e^{-i(K_j^0 t - \mathbf{K}_j \cdot \mathbf{r})}\,, \tag{3.24}$$

where $\Gamma = (E, \mathbf{v})$, $r = (t, \mathbf{r})$ and $K_j = (K_j^0, \mathbf{K}_j)$. Inserting the above ansatz in

equations 3.8, we get

$$\Big[v_\beta(K_j^\beta - \lambda_j^\beta) - \omega_j\Big] Q_{j,\Gamma,K} = v_\beta A^\beta_{j,K}, \qquad \text{with} \qquad A^\beta_{j,K} = -\int d\Gamma'\, v'^\beta\, g_{j,\Gamma'}\, Q_{j,\Gamma',K}. \tag{3.25}$$

Provided the quantity $v_\beta(K_j^\beta - \lambda_j^\beta) - \omega_j \neq 0$ $(j = 1, 2, 3)$, possible solutions for equations 3.25 will take the form $Q_{j,\Gamma,K} = \frac{v_\beta A^\beta_{j,k}}{v_\beta(K_j^\beta - \lambda_j^\beta) - \omega_j}$. Thus the evolution equations take the form

$$v_\beta A^\beta_{j,k} = -v^\beta A^\alpha_{j,K} \int d\Gamma'\, g_{j,\Gamma'} \frac{v'_\beta v'_\alpha}{v'_\gamma(K_j^\gamma - \lambda_j^\gamma) - \omega_j}\,. \tag{3.26}$$

In the following the equations are written in a compact form with the help of the 'polarization' tensor $\Pi^{\alpha\beta}_{j,K}$. There are total three sets of equations one for each j,

$$v_\beta\, \Pi^{\alpha\beta}_{1,K} A_{1,K,\alpha} = 0 \qquad \text{with} \qquad \Pi^{\alpha\beta}_{1,K} = \eta^{\alpha\beta} + \int d\Gamma'\, g_{1,\Gamma'} \frac{v^\alpha v^\beta}{v'_\gamma(K_1^\gamma - \lambda_1^\gamma) - \omega_1}\,,$$

$$v_\beta\, \Pi^{\alpha\beta}_{2,K} A_{2,K,\alpha} = 0 \qquad \text{with} \qquad \Pi^{\alpha\beta}_{2,K} = \eta^{\alpha\beta} + \int d\Gamma'\, g_{2,\Gamma'} \frac{v^\alpha v^\beta}{v'_\gamma(K_2^\gamma - \lambda_2^\gamma) - \omega_2}\,, \tag{3.27}$$

$$v_\beta\, \Pi^{\alpha\beta}_{3,K} A_{3,K,\alpha} = 0 \qquad \text{with} \qquad \Pi^{\alpha\beta}_{3,K} = \eta^{\alpha\beta} + \int d\Gamma'\, g_{3,\Gamma'} \frac{v^\alpha v^\beta}{v'_\gamma(K_3^\gamma - \lambda_3^\gamma) - \omega_3}\,,$$

where $\eta^{\alpha\beta} = \text{diag}(+,-,-,-)$ is the metric tensor. The equations hold for any v_β leading to four independent equations $\Pi^{\alpha\beta}_{j,K} A_{j,K,\alpha} = 0$, where j=1,2,3 corresponding to each evolution equation. Non-trivial solutions of these equations give the resultant dispersion relation connecting the frequency (K_j^0) and the wave numbers $(\mathbf{K}_j)$,

$$\det \Pi^{\alpha\beta}_{j,K} = 0 \tag{3.28}$$

In our simplified system, these dispersion relations depend on the neutrino flavor spectrum $g_{j,\Gamma}$ and the vacuum oscillation frequency ω_j. In the following, we focus our analysis to the problem of fast flavor oscillations dominated by the neutrino densities rather than the vacuum frequency ω_j.

In the fast flavor limit, we consider $M^2 = 0$, i.e., $\omega_j \to 0$. In this case, the EOM no longer depends on E and we deal with the angular modes only. Therefore, the energy integrals in 3.27 can be performed on the distribution functions alone. So,

we define

$$G_{1,\mathbf{v}} = \int_{-\infty}^{+\infty} \frac{E^2 dE}{2\pi^2}\, g_{1,E,\mathbf{v}} = \sqrt{2}\, G_F \int_0^{\infty} \frac{E^2 dE}{2\pi^2} \left(f_{\nu_e,\mathbf{p}} - f_{\bar{\nu}_e,\mathbf{p}} - f_{\nu_\mu,\mathbf{p}} + f_{\bar{\nu}_\mu,\mathbf{p}}\right)$$
$$G_{2,\mathbf{v}} = \int_{-\infty}^{+\infty} \frac{E^2 dE}{2\pi^2}\, g_{2,E,\mathbf{v}} = \sqrt{2}\, G_F \int_0^{\infty} \frac{E^2 dE}{2\pi^2} \left(f_{\nu_e,\mathbf{p}} - f_{\bar{\nu}_e,\mathbf{p}} - f_{\nu_\tau,\mathbf{p}} + f_{\bar{\nu}_\tau,\mathbf{p}}\right)$$
$$G_{3,\mathbf{v}} = \int_{-\infty}^{+\infty} \frac{E^2 dE}{2\pi^2}\, g_{3,E,\mathbf{v}} = \sqrt{2}\, G_F \int_0^{\infty} \frac{E^2 dE}{2\pi^2} \left(f_{\nu_\mu,\mathbf{p}} - f_{\bar{\nu}_\mu,\mathbf{p}} - f_{\nu_\tau,\mathbf{p}} + f_{\bar{\nu}_\tau,\mathbf{p}}\right) \quad (3.29)$$

with $\mathbf{p} = E\mathbf{v}$. For each j, the polarization tensors $\Pi^{\alpha\beta}_{j,K}$ become,

$$\Pi^{\alpha\beta}_{j,K} = \eta^{\alpha\beta} + \int \frac{d\mathbf{v}}{4\pi}\, G_{j,\,\mathbf{v}}\, \frac{v^\alpha v^\beta}{v_\gamma (K^\gamma_j - \lambda^\gamma_j)} \quad (3.30)$$

The denominator $v_\gamma(K^\gamma_j - \lambda^\gamma_j)$ is takes the form $(K^0_j - \lambda^0_j) - \mathbf{v}\cdot(\mathbf{K}_j - \boldsymbol{\lambda_j})$ and solved to form the dispersion relation $D(K^0_j, \mathbf{K}_j) = 0$.

Two beam case

In the following, we use the widely used 'simplest yet non-trivial' example [120, 172] of the two beam case. With two angle modes representing two zenith ranges, it is termed as the 'two beam' neutrino model. In particular, we use the general formalism of the classification of instabilities [172],

$$G_{j,\mathbf{v}} = g'_j \frac{4\pi\,\delta(\mathbf{v} - \mathbf{v}_1)}{1 - \mathbf{v}_1\cdot\mathbf{v}_2} + g''_j \frac{4\pi\,\delta(\mathbf{v} - \mathbf{v}_2)}{1 - \mathbf{v}_1\cdot\mathbf{v}_2} \quad (3.31)$$

The equations 3.5 govern the evaluation of the off-diagonal elements and in the fast flavor limit they are written as,

$$i\, v^\beta \partial_\beta S_{1\mathbf{v}} = \left(v^\beta \lambda_{1\beta}\right) S_{1\mathbf{v}} - v^\beta \int \frac{d\mathbf{v}}{4\pi}\, v'_\beta\, G_{1,\mathbf{v}'} S_{1\mathbf{v}'}\,, \quad (3.32)$$

$$i\, v^\beta \partial_\beta S_{2\mathbf{v}} = \left(v^\beta \lambda_{2\beta}\right) S_{2\mathbf{v}} - v^\beta \int \frac{d\mathbf{v}}{4\pi}\, v'_\beta\, G_{2,\mathbf{v}'} S_{2\mathbf{v}'}\,, \quad (3.33)$$

$$i\, v^\beta \partial_\beta S_{3\mathbf{v}} = \left(v^\beta \lambda_{3\beta}\right) S_{3\mathbf{v}} - v^\beta \int \frac{d\mathbf{v}}{4\pi}\, v'_\beta\, G_{3,\mathbf{v}'} S_{3\mathbf{v}'}\,, \quad (3.34)$$

where the angular distributions $G_{j,\mathbf{v}}$ is given above. For our system we assume azimuthal symmetry with respect to the propagation direction (say z-direction) and translational symmetry in the transverse directions, hence the relevant dynamics

involves only one space coordinate z or its conjugate K_z (henceforth denoted as K). In the formalism of [172], find the general dispersion relation for K_j^0 and K_j $(j = 1, 2, 3)$,

$$(K_j^0 - \lambda_j^0 - v_1 K_j + \lambda_j)(K_j^0 - \lambda_j^0 - v_2 K_j + \lambda_j) = g_j' \, g_j''. \tag{3.35}$$

Here, v_1, v_2 and λ_j are the projections of the neutrino velocities and matter density along the z direction, respectively. The dispersion relation from the equation 3.35 can be solved either in terms of K_j^0 or K_j and the solutions are:

$$K_j^0 = \frac{1}{2}\left[2\lambda_j^0 + (v_1 + v_2)(K_j - \lambda_j) \pm \sqrt{4g_j' g_j'' + (K_j - \lambda_j)^2 (v_1 - v_2)^2}\right] \tag{3.36}$$

$$K_j = \frac{1}{2v_1 v_2}\left[2\lambda_j v_1 v_2 + (v_1 + v_2)(K_j^0 - \lambda_j^0) \pm \sqrt{4g_j' g_j'' v_1 v_2 + (K_j^0 - \lambda_j^0)^2 (v_1 - v_2)^2}\right] \tag{3.37}$$

Given the angular distribution $(v_1, v_2, g_j' \, g_j'')$ and the density (λ) one may find the dispersion relation $D(K_j^0, \mathbf{K}_j) = 0$.

Numerical examples

To exhibit the 3 flavor dispersion relations we consider the following numerical examples. Usually the SN like examples are simplified with the argument that the fluxes of ν_μ and ν_τ are almost equal to their corresponding antineutrino fluxes. In our case, from the definition of the distribution functions in equations 3.29, this would result in $G_{3,\mathbf{v}} = 0$ and $G_{1,\mathbf{v}} = G_{2,\mathbf{v}}$. Thus effectively there will be only one dispersion relation, similar to that of two flavor evolution. Hence, the limit $F_{\nu_\mu} = F_{\bar{\nu}_\mu}$ and $F_{\nu_\tau} = F_{\bar{\nu}_\tau}$ would effectively reproduce the two flavor results. However, for our purpose we consider the simplest two beam model where each beam consists of all the three flavors of neutrino. Therefore, to separate the three flavor effects we consider a slight difference in the fluxes, i.e, the g_j' and g_j'' fluxes are not same for different j's. Another interesting fact is that, the values of the matter terms in equations 3.10 are constant but can be different [87] for the three evolution equations as they involve the densities of the charged leptons and neutrinos (see equation 3.6). Thus the matter term can not be rotated away by redefining the K_j^0 and K_j, unlike the previous studies [172]. Here, that would mean different rotations for the three different evolution equations as a result of which the new 'homogeneous' modes [119]

will not be same for the three different off-diagonals. Hence we do not drop the matter terms.

For our example, we consider the effects of the heavy charged leptons (n_μ, n_τ) to be secondary compared to the order of the asymmetry in matter densities of electrons-positrons. This is in analogy to a SN like situation. Even if there are some muons present in the system, the presence of τ are considered to be extremely negligible. Thus the asymmetry between the different charged leptons and their antiparticles will have the hierarchy, $n_e - n_{\bar{e}} > n_\mu - \bar{n}_\mu \gg n_\tau - \bar{n}_\tau$ and similarly for neutrinos. In particular, we consider the following example, $\lambda_1^\gamma = 0.9\lambda_2^\gamma$ and $\lambda_3^\gamma = 0.1\lambda_2^\gamma$, where $\lambda_j^\gamma = (\lambda_j^0, \boldsymbol{\lambda}_j)$. We choose the numerical values analogous to the early accretion phase [77, 214] where the neutrino densities are similar to the lepton densities. Here, we also take into consideration the neutrino and lepton current terms (spatial parts of λ_j^γ) unlike the previous case of stability analysis where they have been neglected. In particular, we consider $\lambda_2^0 = \lambda_2 = 10$ thus $\lambda_1^0 = \lambda_1 = 9$ and $\lambda_3^0 = \lambda_3 = 1$.

Now that the densities are chosen, the angular densities $(v_1, v_2, g_j'\, g_j'')$ have to be fixed for our numerical example. In reference, [172] it is shown that the angular distribution can create 4 different kind of instabilities namely the completely stable, damped stable, convectively unstable and absolutely unstable. In the following, we take the same angular distributions to generate the different kind of instabilities for our three flavor example. To keep the example simple we consider the nature of the instability to be the same for all the three off-diagonal elements, i.e, same for the $\nu_e - \nu_\mu$, $\nu_e - \nu_\tau$ and $\nu_\mu - \nu_\tau$ sectors. The stability properties of the system can be analyzed by studying the conditions which lead to imaginary parts for K_j^0 or K_j in the dispersion relation in equations 3.35. The presence of instability indicates the possibility of flavor conversion. We plot the real and imaginary parts of K_j^0 vs real values of K_j and vice versa in the figures 3.2 and 3.3. The gap in $K_j^0(K_j)$ corresponds to the presence of it's complex values in that particular range of real $K_j(K_j^0)$ indicating instability.

The 4 different kind of instabilities mentioned above arises by choosing different numerical values of the parameters v_1, v_2 and g_j', g_j''. Based on these values, the solutions of the dispersion relation are real or complex which in turn decides the type of instability which will arise. This classification of instabilities is mainly dependent on the relative sign of g_j' and g_j'' which results in two different situations. The transition from stability to instability requires a change in sign (positive to negative) of the R.H.S of equation 3.35. If $g_j' g_j'' < 0$ i.e. the two terms in equation

3.31 have opposite sign, then the system becomes unstable and $g'_j g''_j > 0$ leads to the stable cases. The stable cases include the completely and damped stable ones while the unstable ones can be convective and absolutely unstable. In addition to this, the sign of the product of v_1 and v_2 is also an important factor for further classifying these cases. $v_1 v_2 > 0$ results in completely stable and convective unstable cases whereas $v_1 v_2 < 0$ are for damped stable and absolutely unstable scenarios. Taking into account the above conditions, we choose the values of the parameters and plot the solutions of the dispersion relation for the two unstable cases in figures 3.2 and 3.3.

The three sectors i.e., $j = 1, 2, 3$ show similar behaviour as in the 2 flavor case [172] for all the four kinds of instabilities. The only difference is that the region of instability is shifted due to the presence of non zero matter terms. However, we are more interested in the unstable cases giving an insight to the possibility of flavor conversions, so the two unstable cases, convectively unstable and absolutely unstable, are explained in detail with plots. For the stable cases we do verify both the completely stable ($v_1 v_2 > 0$ and $g'_3 g''_3 > 0$, $v_1 = 0.7$, $v_2 = 0.2$, $g'_3 = 0.04$ and $g''_3 = 0.06$) and the damped stable ($v_1 v_2 < 0$ but $g'_3 g''_3 > 0$, $v_1 = 0.6$, $v_2 = -0.3$, $g'_3 = 0.04$ and $g''_3 = 0.06$) cases for j=3. They mimic the two flavor results with the matter shifting. Assuming the same angular distribution for the other two ($j = 1, 2$) modes for the stable cases, we find the same behaviour.

The convective instability is shown in figure 3.2 for all the j values, i.e., $j = 1$, 2 (lower two panels) and $j = 3$ (upper two panels), corresponding to all the three sectors (e-μ, e-τ and $\mu - \tau$) respectively. It is called convective as in this case the perturbation decays locally, but blows up elsewhere as it moves away. We can see that there is a gap in both K_j^0 and K_j. Both K_j^0 and K_j develops imaginary part for a particular range of real values of each other. Here, $v_1 v_2 > 0$ and $g'_j g''_j < 0$. In particular, we take $v_1 = 0.7$, $v_2 = 0.2$, $g'_1 = -0.4$, $g''_1 = 0.6$, $g'_2 = -0.44$, $g''_2 = 0.66$, $g'_3 = -0.04$ and $g''_3 = 0.06$.

Similarly, the absolute instability case is shown in figure 3.3 for all the three sectors. In this case, the perturbation grows "on site" and around and thus the name absolutely unstable. Here, the imaginary part arises only in K_j^0 for real values of K_j. There is a relative change in sign in both v_1, v_2 as well as g'_j, g''_j. We take the values as $v_1 = 0.6$, $v_2 = -0.3$, $g'_1 = -0.4$, $g''_1 = 0.6$, $g'_2 = -0.44$, $g''_2 = 0.66$, $g'_3 = -0.04$ and $g''_3 = 0.06$.

One interesting feature which is evident from the lower two panels of figures 3.2 and 3.3 is that the range of values of K_j^0 for which K_j is imaginary and vice versa

for the two different sectors are shifted with respect to each other. This means that instability gets shifted. This signifies that the modes unstable for one sector (say $\nu_e - \nu_\mu$) may turn out to be stable for the other (say $\nu_\mu - \nu_\tau$). Moreover, some parts of the two ranges are also overlapping, indicating modes which are unstable in both the cases. Note that in our example, we choose λ's to be of similar order and in units of $\lambda_3 \sim 1$. Large values of λ's will make this effect of different homogeneous modes more pronounce. However, the fast growth of the instabilities may act against these effects. It would be interesting to see in a nonlinear analysis if the presence of matter will have any dominant effect or not. Also our assumption of all the three sectors having same kind of instability may not hold in a realistic situation. Thus, the effect of these different kind of instabilities on each other would be another interesting aspect.

In particular, for the two flavor picture the fast conversions are only governed by the 'electron lepton number' or ELN ($\nu_e - \bar{\nu}_e$ sector). Thus, $G_{1,v}$ is solely dependent on $\nu_e - \bar{\nu}_e$. The fast oscillations are connected to the 'crossings' in the ELN spectra. The size of the crossings are also important. The impact of the fast conversions on SN dynamics is one crucial factor [177]. Our analysis shows that in the three flavor picture it is not only ELN but in principle all the three flavors are important. It may lead to the curious scenario when the ELN crossing is small or absent, however the MuLN or TauLN contribute to the effective lepton crossing. In the non-linear evolution, the instability in one off-diagonal element will influence the growth of instability in the other sectors. Thus the growth of S_3 governed by crossings in MuLN / TauLN can impact the instability growth in S_1 which is otherwise only dependent on ELN in the two flavor scenario. Given the recent SN simulations [87] with muons being produced in the late accretion phase results in larger difference of fluxes of different flavors than the previous results. It would be interesting to see the sizes of the MuLN or TauLN in these SN simulations and their possible impact on the fast conversions in a SN environment.

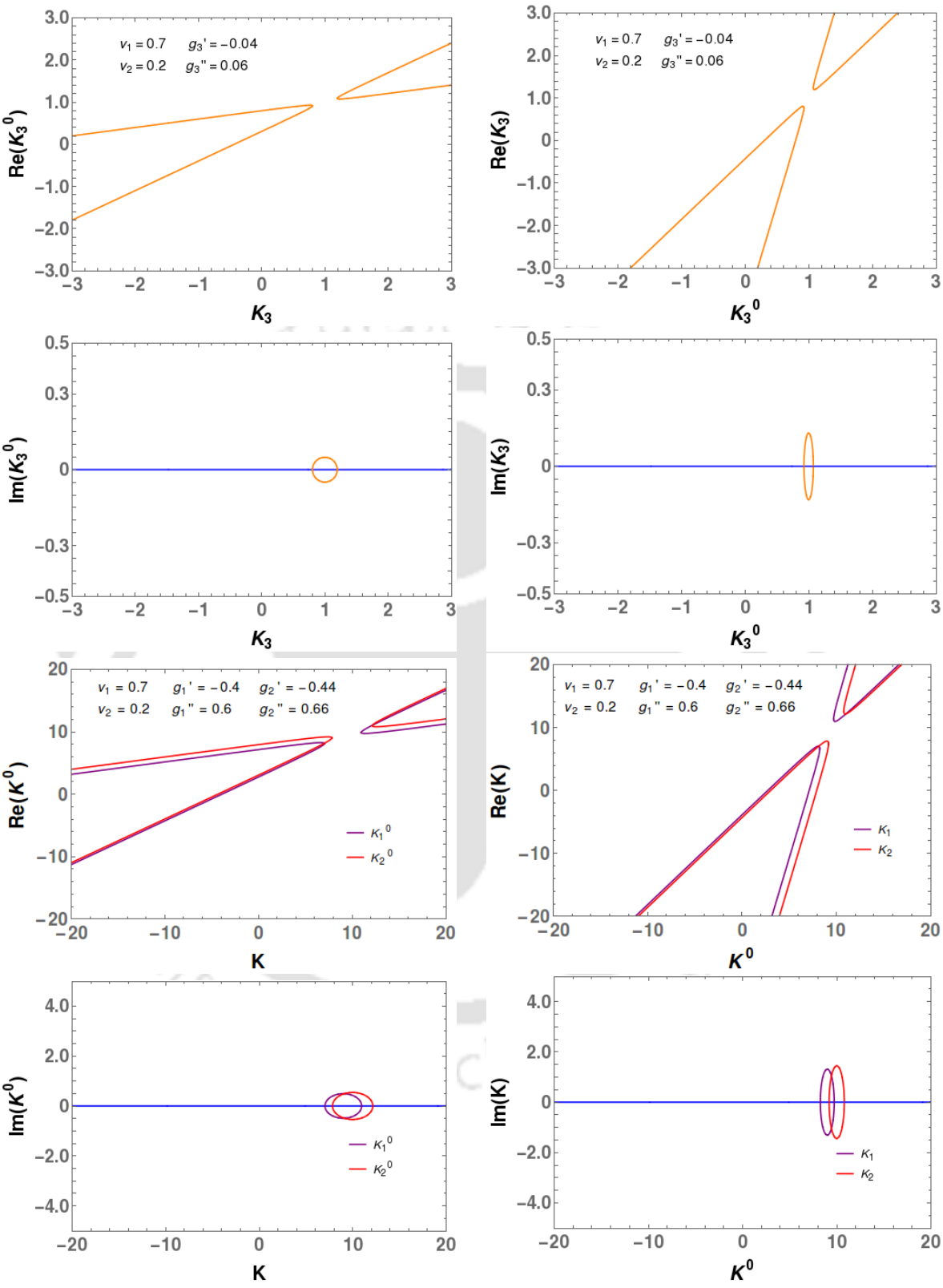

Figure 3.2: Example of solutions of the dispersion relation 3.35 for a convectively unstable case. The upper two panels are for j=3 and lower two panels for j=1,2. Here $v_1 = 0.7, v_2 = 0.2$. $g_3' = -0.04, g_3'' = 0.06$ and $g_1' = -0.4, g_1'' = 0.6$, $g_2' = -0.44, g_2'' = 0.66$.

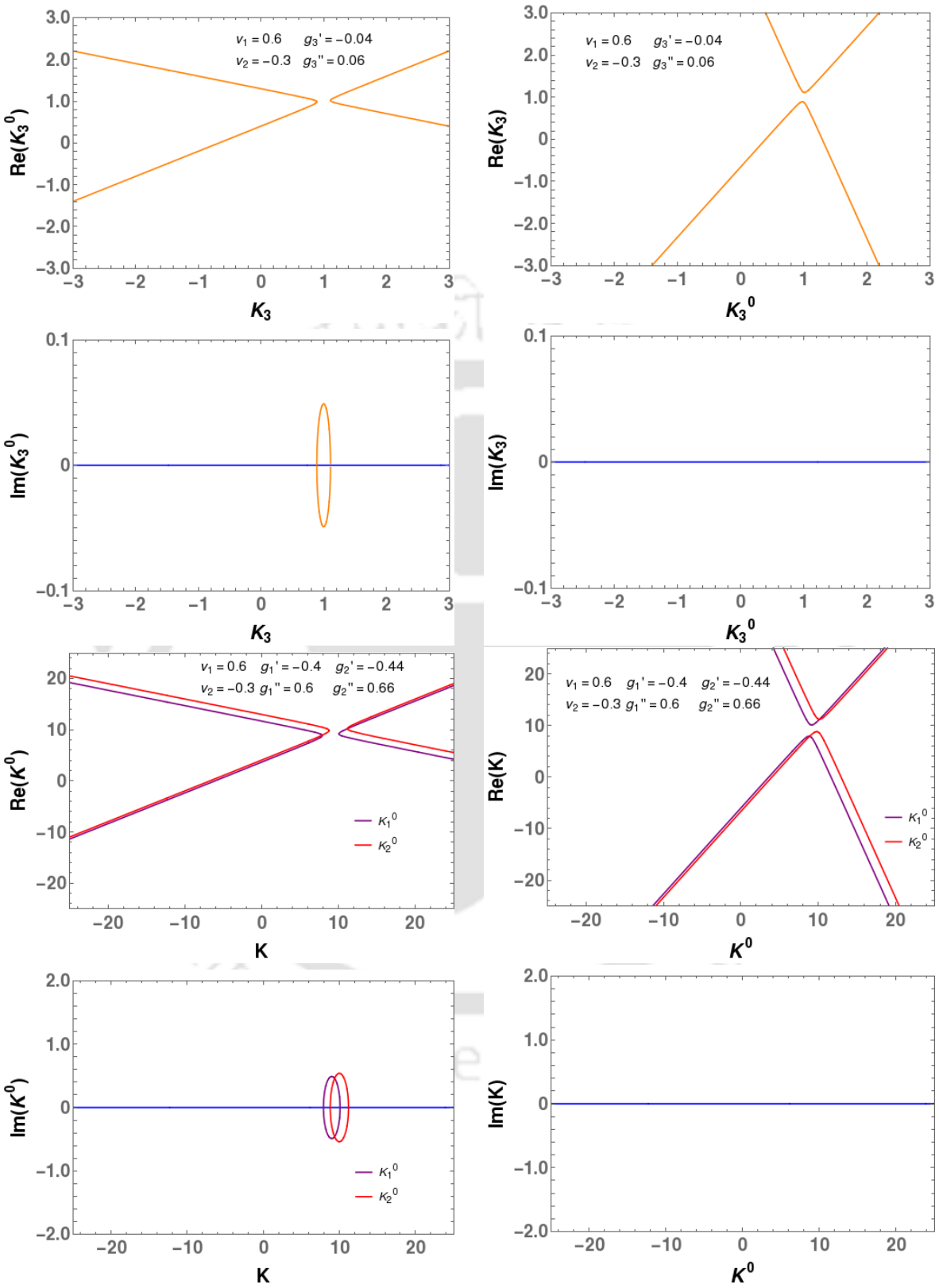

Figure 3.3: Example of solutions of the dispersion relation 3.35 for an absolutely unstable case. The upper two panels are for j=3 and lower two panels for j=1,2. Here $v_1 = 0.6, v_2 = -0.3$. $g_3' = -0.04, g_3'' = 0.06$ and $g_1' = -0.4, g_1'' = 0.6$, $g_2' = -0.44, g_2'' = 0.66$.

3.3 Discussion

The phenomena of self induced flavor conversions in the regions of dense neutrinos (stellar core) have been previously studied using the method of linear stability analysis in the 2 flavor scenario. In this chapter, we have discussed the evolution of the system considering all the three flavors of the neutrinos based on [212]. Here, we obtained three linearized equations of motion for ϱ, i.e two more compared to the usual two flavor scenario and studied these equations for both the slow and the fast instabilities. For the slow oscillations, assuming the system to be isotropic and taking into account only the homogeneous modes, we studied the stationary solutions, i.e., only the spatial evolution. This simple system is similar to the previous three flavor studies done for the dense neutrino problems. We found our linear analysis results are in excellent qualitative agreement with these previous non linear three flavor studies. Further, for the fast conversions we did a generalized analysis. We adopted the dispersion relation approach to study both the temporal as well as spatial evolution. The consideration of the three flavor effects on the fast oscillations has been done for the first time in [212]. The addition of the third flavor shows possibilities impacting the rate of growth of the instabilities when compared to the two flavor case. Given the suitable conditions, addition of the third flavor may slow or speed up the instabilities and in turn may affect the flavor conversions.

In the three flavor analysis, the assumption of different distributions for all the three flavors of neutrinos lead to the non trivial effect of the third flavor. The three linearized equations of motion found corresponds to the three off-diagonal elements S_1, S_2 and S_3 describing ν_e - ν_μ, ν_e - ν_τ and ν_μ - ν_τ sectors respectively. We found that the minimum requirements to reduce the three flavor evolution to an effective two flavor one are $f_{\nu_\mu} = f_{\bar{\nu}_\mu}$ and $f_{\nu_\tau} = f_{\bar{\nu}_\tau}$. This is clearly different than the present assumptions on fluxes, i.e, $f_{\nu_\mu} = f_{\nu_\tau}$ and $f_{\bar{\nu}_\mu} = f_{\bar{\nu}_\tau}$ to generate the effective two flavor description. Moreover, for the three flavor case, we found instabilities for both the mass orderings. This is similar to the two flavor studies except that here, the instabilities may remain present corresponding to the ν_μ - ν_τ sector as well. We obtained all the three different kinds of instabilities namely Bimodal (BM), Multi Zenith Angle (MZA) and Multi Azimuthal Angle (MZA). The BM happens for positive μ_0, i.e., inverted mass ordering and the MZA and MAA for negative μ_0, i.e., normal mass ordering.

The overall matter effect defined in our framework includes the contributions of both the charged leptons and the corresponding neutrinos. It consists of both the

current as well as the normal matter term. So in general, the effects from both would be important for the study of the three flavor evolution. We have assumed isotropy for the linearized stability analysis of the slow conversions and the currents have been neglected. However, both the contributions have been taken into account for the dispersion picture of the fast conversions.

According to the previous effective two flavor studies, the onset of the growth of the instability in the solar sector is found to be at a later radius compared to that of the atmospheric sector, however the onset of the solar sector may get faster in the three flavor analysis. Our 3 flavor linearized stability analysis showed that the onset of the growth of the third off-diagonal term (ν_μ - ν_τ) occurred at a larger value of μ_0 i.e., at a lower radius. In the non linear scenario the three evolution equations are coupled to each other, thus the early growth of the third off-diagonal can affect (speed up) the other off-diagonals and may speed up the solar sector conversions. This is in perfect agreement with the previous three flavor nonlinear studies. We performed the slow conversion stability analysis without considering the ordinary matter effects. However, the consideration of non-zero matter could have substantial effect on the evolution. The slow onset of the solar sector compared to the atmospheric one has been discussed in [215] in the context of two simple models of colliding and intersecting neutrino beams. Here, we identified all the different instabilities involved and demonstrated that this slow onset is happening for all the cases BM, MAA and MZA instabilities. Indeed, the speed up due to the $\nu_\mu - \nu_\tau$ sector would be true to all the three instabilities.

In the dispersion picture for the fast oscillations, we obtained three dispersion relations for the three flavor scenario. Here also $f_{\nu_\mu} = f_{\bar{\nu}_\mu}$ and $f_{\nu_\tau} = f_{\bar{\nu}_\tau}$ are the conditions to get back the effective two flavor picture. For the three flavor case we considered the simplest two beam model where each beam consists of all the three flavors of neutrinos. Depending on the values of the angular densities chosen, we obtained four kinds of instabilities, namely the completely stable, damped stable, convectively unstable and absolutely unstable corresponding to each of the off-diagonal element. For simplicity, we assumed same angular distributions for all the three sectors resulting in the presence of similar kind of instabilities for all of them. However, the different angular distributions may result in different stability picture in different flavors. In the non-linear evolution this might result in an interesting impact, as in the non linear picture the instability in one flavor sector may have strong influence on the evolution of another flavor sectors. This becomes interesting when fluxes for the three flavors of neutrinos and their respective

antineutrinos are different [87]. It would be crucial to understand the influence of these flux differences in the context of these 'three flavor speed up (or slow down!)' in the non-linear evolution.

In the earlier studies involving the dispersion relations, the matter term, being a constant is often rotated away. Similarly, in case of three flavor analysis also, we have constant matter terms but they are different for the three sectors. As a result, they cannot be rotated away simultaneously. The presence of this term shows a very interesting result. It indicates that the modes unstable for some λ may not be the same for the others i.e, the effective 'homogeneous' mode for one sector may be 'inhomogeneous' for the other sectors. However, in the context of fast oscillations these instabilities are growing at an enormous rate. Hence negligible 'cascading' between the modes [162] may reduce this effect. In particular, for our numerical example the separation of these modes were reasonably small.

This discussion on linear analysis of three flavor case motivates us to see the influence of these effects in non-linear simulations. Thus, we explore this idea of presence of other flavor lepton numbers (MuLN and TauLN) in addition to the ELN in the context of fast flavor oscillations in the next chapter. We discuss the role played by the presence of third flavor in modifying the crossings in the angular spectra in the usual two flavor scenario. Overall, we show the importance of the study of the fast flavor conversions in complete three flavor scenario using some toy examples in the next chapter.

Chapter 4

Non-linear analysis of fast oscillations

In the previous chapter, we talked about the method of linear stability analysis for studying slow as well as fast conversions. This method can predict whether flavor conversions take place or not. However, it cannot provide any information about the outcome. To understand the behaviour of the system, we need to solve the complete non-linear equation of motion numerically. In addition, we expand our non-linear analysis to system beyond 'effective two flavor'. As the linear stability discussion in the previous chapter signals substantial difference between effective two flavor and complete three flavor analysis, in this chapter, we carry out the non-linear analysis of the fast oscillations taking into account different toy examples. Note that our main focus here will be the three flavor scenario.

4.1 Fast oscillations : Three flavor

The presence of the fast flavor conversions (FFCs) well inside a SN can lead to paradigm changes in our understanding of the explosion dynamics, requiring a more detailed analysis of the different approximations going into the studies. One of such assumptions is the consideration of the effective two flavor scenario (e and x flavor, where $x = \mu, \tau$ or a linear combination of both) where ELN is considered to be the only driving quantity inspite of the presence of neutrinos of other flavors in the SN environment. The studies [116–118, 120, 170–183, 185] have suggested that a necessary and sufficient condition for the existence of these fast instabilities is the presence of a *zero-crossing* in the angular distribution of the neutrino electron lepton number (ELN), i.e., the difference between the electron neutrino and the antineutrino angular emission spectra should go through a zero for some emission angle. These crossings are naively expected to occur near the neutrino free-streaming zone

and require a comprehensive study of the interplay of collisions and fast conversions, thereby necessitating the use of quantum kinetic equations [199, 216–218]. This assumption of effective two flavor is based on the fact that in the absence of muons and taus in traditional SN simulations, the heavy lepton neutrinos have identical microphysics and similar number density ($n_{\nu_\mu} = n_{\nu_\tau} = n_{\bar{\nu}_\mu} = n_{\bar{\nu}_\tau} = n_{\nu_x}$) for all emission angles. This set up has severe limitations as the ν_x and $\bar{\nu}_x$ flux would differ naturally if nucleon recoil effects, implying different neutral-current scattering cross sections, are taken into account. Moreover, it would be also natural to expect that the high temperatures during the accretion phase would create muons in the nascent neutron stars. In fact, [87] has shown that the addition of muons can enhance neutrino energy deposition to the stalled shockwave, leading to a successful explosion. Muon production in a SN [87] can create differences in the heavy lepton flavor neutrino fluxes. In [87], it has been shown that due to the creation of muons in the accretion phase, the difference in the ν_μ and $\bar{\nu}_\mu$ increases ($\sim 5\%$) as compared to the already present difference ($\sim 0.5\%$) between them due to different neutral current scattering cross sections with nucleons. However, for ν_τ and $\bar{\nu}_\tau$, the difference is only due to the different cross sections as the temperatures are not enough to create tauons in that environment. Thus the inclusion of three-flavor effects is necessary. The oscillation treatment of such a scenario was pointed out in [119] and in [212] we have done a detailed analysis of fast conversions taking into account all the three neutrino flavors. Using the linear stability analysis, we demonstrated the possibility of altering the instability growth rates obtained in the standard two-flavor setup which is explained in chapter 3.

Going a step forward with respect to current literature, we, for the first time, perform a fully non-linear computation of FFCs in the presence of three neutrino flavors in [219]. Motivated by the difference in the heavy lepton flavor neutrino fluxes observed in [87], we propose some toy models and demonstrate that it is not only the ELN, but also MuLN and TauLN that drives the onset of these rapid conversions. In fact, it is the difference of any of the two-flavor lepton numbers that goes into the evolution equations [212]. This emphasizes the incompleteness of a two-flavor analysis, especially while analyzing the presence of FFC in the pre-shock region, where tiny crossings in the ELN can get erased by the MuLN and/or TauLN. Our results suggest the importance of such a fully non-linear three-flavor study of FFC with detailed hydrodynamic SN simulations, including muon production, to gauge its impact on SN dynamics. Furthermore, in [220] it has been pointed out that even considering the same flavor content in the three and six neutrino species cases, the

flavor conversion probabilities obtained as output of numerical simulations can have appreciable differences. However, these conclusions have been obtained assuming only the evolution in time, i.e. spatial homogeneity has been imposed. So, we extend the studies performed in [212, 219, 220] by considering the dependence of flavor evolution on the spatial dimension as well in [221]. In the subsequent sections, we discuss our three flavor setup and present the results showing the effects of the addition of the third flavor in contrast to the effective two flavor scenario.

4.2 Evolution equation

The spatial and temporal evolution of the neutrinos is governed by the equation 2.5 mentioned in chapter 2. In absence of collisions, the form of the equation becomes :

$$i\left(\partial_t + \mathbf{v_p}\cdot\nabla_{\mathbf{x}}\right)\varrho_{\mathbf{p},\mathbf{x},t} = \left[H_{\mathbf{p},\mathbf{x},t}, \varrho_{\mathbf{p},\mathbf{x},t}\right] \tag{4.1}$$

where, $\varrho_{\mathbf{p},\mathbf{x},t}$ are the neutrino occupation number matrices, $H_{\mathbf{p},\mathbf{x},t}$ is the Hamiltonian of the system which consists of three parts, i.e., vacuum term, MSW potential and the neutrino-neutrino interaction terms given by:

$$H_{\mathbf{p}}^{vacuum} = \Delta m^2/2\,E \tag{4.2}$$

$$H_{\mathbf{p}}^{matter} = \sqrt{2}G_F n_\alpha \tag{4.3}$$

$$H_{\mathbf{p}}^{\nu\nu} = \mu_0 \int d^3\mathbf{q}/(2\pi)^3(1-\mathbf{v_p}\cdot\mathbf{v_q})(\varrho_{\mathbf{q},\mathbf{x},t} - \bar{\varrho}_{\mathbf{q},\mathbf{x},t}) \tag{4.4}$$

Here, n_α denotes the charged lepton density (α denotes the flavor), $\mu_0 = \sqrt{2}G_F n_\nu$, n_ν being the background neutrino density and G_F is the Fermi constant.

In the fast flavor limit, the evolution of the system is mainly dependent on the matter and the neutrino-neutrino interaction terms ($\mathrm{H}_{\mathbf{p}}^{matter}$ and $\mathrm{H}_{\mathbf{p}}^{\nu\nu}$) as the only role played by the vacuum term is to seed the fast oscillations. Further, while studying space and time evolution, the matter term ($\mathrm{H}_{\mathbf{p}}^{matter}$) can be neglected [175, 222]. Thus the whole system is driven only by the neutrino-neutrino interaction term. We also ignore the small radiative corrections in the nonlinear term ($\mathrm{H}_{\mathbf{p}}^{\nu\nu}$) [210].

Now, we will discuss the significance of the angular distributions of different flavors of neutrinos and antineutrinos in the mechanism of fast flavor conversions.

4.2.1 Angular distributions

To study fast flavor conversions, the angular distribution of the neutrinos is an important factor. The requirement is that different flavors of neutrinos should have significantly different angular distributions. This is the cause of the creation of zero crossing in the difference between the fluxes of neutrinos and their anti-neutrino counterparts which is the necessary and sufficient condition for the occurrence of fast oscillations. Since the interaction rates of different flavors of neutrinos are different, they are decoupled from the matter at different radii. The non-electron flavors, $\nu_\mu, \nu_\tau, \bar{\nu}_\mu, \bar{\nu}_\tau$ are decoupled much earlier (deeper) as compared to $\bar{\nu}_e$ which is further followed by ν_e. As a result, it is expected that near the SN core, the zenith-angle distribution of the non-electron flavors of neutrinos and anti-neutrinos would be more forward peaked than the electron anti-neutrino which is further more forward peaked than the electron neutrino.

In the effective two flavor scenario where the fluxes of non-electron flavors of neutrinos and anti-neutrinos are considered to be identical, a quantity known as the electron lepton number (ELN) is defined which determines the possibility of the existence of instabilities. The ELN is defined as the difference between the occupation numbers of the electron neutrino and its anti-neutrino integrated over energy which is given as :

$$G^e_{\mathbf{v}} = \sqrt{2} G_F \int_0^\infty \frac{dE\, E^2}{2\pi^2} \left[\varrho_{ee}(E, \mathbf{v}) - \bar{\varrho}_{ee}(E, \mathbf{v})\right] \ . \tag{4.5}$$

Now as described in the previous chapter if we relax this assumption of equal fluxes of the non-electron flavors, then in addition to the ELN there will be two more flavor lepton numbers which we term MuLN and TauLN.

$$G^\mu_{\mathbf{v}} = \sqrt{2} G_F \int_0^\infty \frac{dE\, E^2}{2\pi^2} \left[\varrho_{\mu\mu}(E, \mathbf{v}) - \bar{\varrho}_{\mu\mu}(E, \mathbf{v})\right] \ , \tag{4.6}$$

$$G^\tau_{\mathbf{v}} = \sqrt{2} G_F \int_0^\infty \frac{dE\, E^2}{2\pi^2} \left[\varrho_{\tau\tau}(E, \mathbf{v}) - \bar{\varrho}_{\tau\tau}(E, \mathbf{v})\right] \ . \tag{4.7}$$

Unlike the effective two flavor case where we search for crossings in the ELN, now the quantities of interest in case of three flavor scenario are the differences of these flavor lepton numbers which are given as :

$$\begin{aligned} G^{e\mu}_{\mathbf{v}} &= G^{e}_{\mathbf{v}} - G^{\mu}_{\mathbf{v}} \,, \\ G^{e\tau}_{\mathbf{v}} &= G^{e}_{\mathbf{v}} - G^{\tau}_{\mathbf{v}} \,, \\ G^{\mu\tau}_{\mathbf{v}} &= G^{\mu}_{\mathbf{v}} - G^{\tau}_{\mathbf{v}} \,. \end{aligned} \tag{4.8}$$

where, $G^{e\mu}_{\mathbf{v}}, G^{e\tau}_{\mathbf{v}}$ and $G^{\mu\tau}_{\mathbf{v}}$ are the differences of the lepton numbers in the e$-\mu$, e$-\tau$ and $\mu - \tau$ sectors respectively. So, equation 4.8 becomes :

$$\begin{aligned} G^{e\mu}_{\mathbf{v}} &= \sqrt{2}\, G_F \int_0^\infty \frac{dEE^2}{2\pi^2} \left[\varrho_{ee}(E,\mathbf{v}) - \bar{\varrho}_{ee}(E,\mathbf{v}) - \varrho_{\mu\mu}(E,\mathbf{v}) + \bar{\varrho}_{\mu\mu}(E,\mathbf{v})\right] \,, \\ G^{e\tau}_{\mathbf{v}} &= \sqrt{2}\, G_F \int_0^\infty \frac{dEE^2}{2\pi^2} \left[\varrho_{ee}(E,\mathbf{v}) - \bar{\varrho}_{ee}(E,\mathbf{v}) - \varrho_{\tau\tau}(E,\mathbf{v}) + \bar{\varrho}_{\tau\tau}(E,\mathbf{v})\right] \,, \\ G^{\mu\tau}_{\mathbf{v}} &= \sqrt{2}\, G_F \int_0^\infty \frac{dEE^2}{2\pi^2} \left[\varrho_{\mu\mu}(E,\mathbf{v}) - \bar{\varrho}_{\mu\mu}(E,\mathbf{v}) - \varrho_{\tau\tau}(E,\mathbf{v}) + \bar{\varrho}_{\tau\tau}(E,\mathbf{v})\right] \,, \end{aligned} \tag{4.9}$$

This is the same as equation 3.29 which is described in the previous chapter. The presence of instability in any one of these sectors is indicated by the presence of the zero crossing in the corresponding lepton number difference shown above. Note that under the assumption of $\varrho_{\mu\mu} = \bar{\varrho}_{\mu\mu} = \varrho_{\tau\tau} = \bar{\varrho}_{\tau\tau}$, equation 4.9 reduces to the usual ELN.

Focussing on equation 4.9, it is clear that now the difference between the fluxes of the non-electron flavors will influence the ELN. It can either enhance or erase the crossing originally present in ELN. Also in case, there is no crossing in ELN originally, the MuLN and TauLN can create one. As a result, the consideration of three flavors can affect the crossings in the two flavor scenario and thus can affect the fast flavor conversions. To investigate this point, we consider four toy examples of angular distributions as mentioned in the following.

Numerical examples

To study the fast flavor oscillations in the three flavor scenario, we consider four toy examples. The angular distributions as a function of $v = \cos\theta$ are given by the following expression:

$$\varrho_{\alpha\alpha} = \frac{1}{2\pi}\left[\frac{1+\Delta_\alpha}{1-v^\alpha_{min}}\mathcal{H}(\cos\theta - v_{min}) + h\mathcal{H}(-\cos\theta + v_{min})\right] \tag{4.10}$$

where, $\alpha = e, \bar{e}, \mu, \bar{\mu}, \tau, \bar{\tau}$ and the parameters $\Delta_\alpha, v^\alpha_{min}$ and h for four different cases are mentioned in tables 4.1 and 4.2.

α	v^α_{min}	Δ_α	h
e	-1.00	0.80	0
$\bar{e}$	-0.60	0.70	0
μ	-0.80	0.10	0
$\bar{\mu}$	-0.70	0.45	0
τ	-0.80	0.10	0
$\bar{\tau}$	-0.70	0.45	0

α	v^α_{min}	Δ_α	h
e	-1.00	0.80	0
$\bar{e}$	-0.60	0.70	0
μ	-0.80	0.30	0
$\bar{\mu}$	-0.70	0.15	0
τ	-0.80	0.30	0
$\bar{\tau}$	-0.70	0.15	0

Table 4.1: Parameter values for case 1 (left) and case 2 (right).

α	v^α_{min}	Δ_α	h
e	-1.00	0.90	0
$\bar{e}$	-0.60	0.30	0
μ	-0.80	0.10	0
$\bar{\mu}$	-0.70	0.50	0
τ	-0.80	-0.20	0
$\bar{\tau}$	-0.70	-0.10	0

α	v^α_{min}	Δ_α	h
e	-0.30	0.60	0.00
$\bar{e}$	0.00	0.29	0.00
μ	-0.20	0.00	0.08
$\bar{\mu}$	-0.10	0.20	0.02
τ	-0.20	0.10	0.08
$\bar{\tau}$	-0.10	0.17	0.00

Table 4.2: Parameter values for case 3 (left) and case 4 (right).

Figures 4.1 and 4.2 show the angular distributions of different flavors and the differences between them given by equation 4.8 respectively for the four different cases mentioned above. Note that in figure 4.2, the ELN for the two flavor case is shown by blue dotted line.

The upper left panel of figures 4.1 and 4.2 represent the case 1. The parameter values for them are given in the left panel of table 4.1. Here, all the three flavor lepton number distributions (ELN, MuLN and TauLN) have crossings, whereas the differences i.e., $G^{e\mu}_{\mathbf{v}}$, $G^{e\tau}_{\mathbf{v}}$ and $G^{\mu\tau}_{\mathbf{v}}$ (shown by the blue, green and red solid lines in figure 4.2 respectively) do not have crossings.

The upper right panel of figures 4.1 and 4.2 show the case 2, whose angular

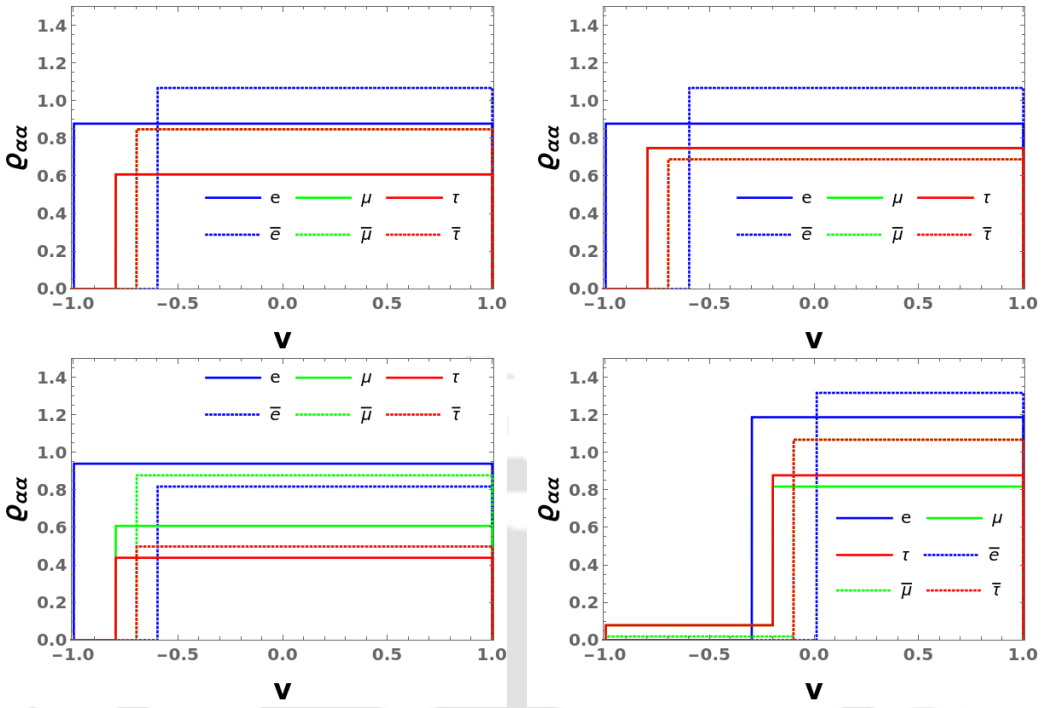

Figure 4.1: The above panels show the angular distributions for different flavors of the four toy examples mentioned in the text. The upper left panel corresponds to case 1 and upper right panel is for case 2. The lower left and right panels represent the case 3 and case 4 respectively.

distributions are given by the parameter values in the right panel of table 4.1. In this case, ELN has a crossing but MuLN and TauLN do not have. However, in figure 4.2, there is a crossing in $G_{\mathbf{v}}^{e\mu}$ (blue solid line) and $G_{\mathbf{v}}^{e\tau}$ (green solid line) but there is none in $G_{\mathbf{v}}^{\mu\tau}$ (red solid line).

The case 3 is represented by the lower left panel of figures 4.1 and 4.2 and the parameter values of its angular distributions are given by the left panel of TABLE 4.2 . In this scenario, there is no crossing in ELN but it is present in MuLN and TauLN. Focussing on the differences in figure 4.2, $G_{\mathbf{v}}^{e\mu}$ (blue solid line) and $G_{\mathbf{v}}^{e\tau}$ (green solid line) do not have a crossing whereas it is there in $G_{\mathbf{v}}^{\mu\tau}$ (red solid line).

The last example, i.e., case 4 (lower right panel of figures 4.1 and 4.2) is given by the angular distributions with parameter values in the right panel of table 4.2. Here, there is a shallow crossing in the ELN in the forward direction and also there are crossings in the MuLN and TauLN. Unlike the other three cases, here the differences $G_{\mathbf{v}}^{e\mu}$ (blue solid line) and $G_{\mathbf{v}}^{e\tau}$ (green solid line) have shallow backward crossings as shown in the lower right panel of figure 4.2. However, $G_{\mathbf{v}}^{\mu\tau}$ (red solid line) does not have any crossing.

Taking these angular distributions into account, in the rest of the chapter we

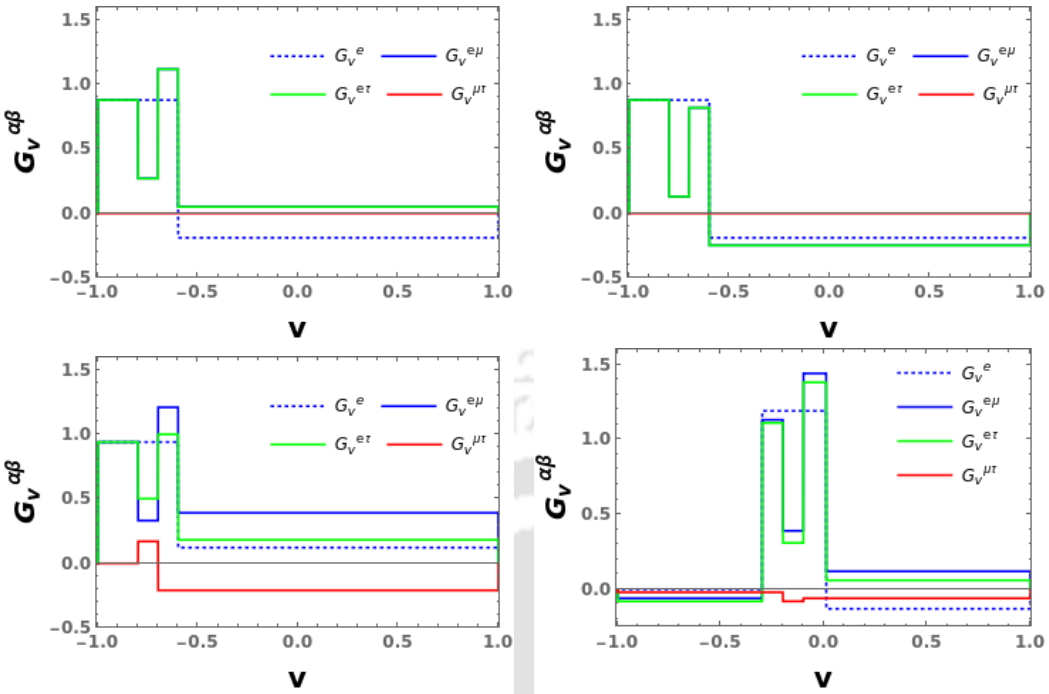

Figure 4.2: The above panels show the effective lepton numbers for different flavors for the angular distributions of the four toy examples mentioned in the text. The upper left panel corresponds to case 1 and upper right panel is for case 2. The lower left and right panels represent the case 3 and case 4 respectively.

study the fast flavor conversions by solving the non-linear equations of motion first considering only time evolution and then both time and space (1+1 D). This study is based on [219, 221]. Note that current state of the art SN simulations [87] can only provide angular moments of the neutrino distribution, from which one can construct realistic angle-dependence of the neutrino flavor intensity but only near the neutrinosphere. However, these distributions are not very reliable at larger radii [223].

4.3 Non-linear analysis : Time evolution

First, we aim to solve the evolution equation 4.1 by considering only the time derivative part for which we assume a spatially homogeneous flavor composition. We assume that the initial neutrino angular distributions are axially symmetric around the $z-$axis, i.e., they only depend on the zenith angle. Nevertheless, we do consider the azimuthal angles in our calculations, so that also axially breaking instabilities are allowed to develop [155]. We consider 100 zenith angles and 10 azimuthal angles in our calculations. We take $\mu_0 = \sqrt{2}G_F n_\nu = 4 \times 10^5$ km^{-1}, which is a typical value in

the neutrino decoupling region. Concerning the vacuum term, we use as oscillation frequencies $\Delta m^2_{31}/(2E) = 0.5$ km^{-1} and $\Delta m^2_{21}/(2E) = 0.01$ km^{-1}, whereas we set the mixing angles to be $\theta_{12} = \theta_{13} = \theta_{23} = 10^{-3}$. In this way, we mimic the suppression of θ_{ij} induced by the large potentials. Moreover, as we focus only on the time evolution we neglect the matter terms, $\lambda_e = \lambda_\mu = \lambda_\tau = 0$. We solve the evolution equation and plot the angle averaged off-diagonal elements of ϱ in figures 4.3 and 4.4 for the two flavor and three flavor scenarios respectively which will be discussed in detail below. The angle average of the elements of the occupation number matrix is defined as:

$$|\langle \varrho_{\alpha\beta} \rangle| = \left| \int d\mathbf{v} \varrho_{\alpha\beta}(\mathbf{v}) \right| . \tag{4.11}$$

where, α, β are the indices corresponding to the e, μ and τ flavors.

4.3.1 Two flavor

As mentioned earlier, the quantity of interest to study fast flavor oscillations in the two flavor scenario ($n_{\nu_\mu} = n_{\bar{\nu}_\mu}$) is the electron lepton number (ELN). The presence of zero crossing in ELN indicates the occurrence of flavor conversion. The blue dotted lines in figure 4.2 represent the ELN for the four toy examples considered. Figure 4.3 shows the time evolution of the angle averaged off-diagonal elements in the case of two flavor.

The upper left and right panels correspond to the cases 1 and 2 respectively. It is evident from figure 4.2 (blue dotted lines in upper left and right panels) that there is a crossing in the ELN ($G^e_{\mathbf{v}}$). So we expect growth in the off-diagonals and the same is seen in figure 4.3. Note that the ELN is similar for both cases 1 and 2.

Case 3 does not have any crossings in the ELN (as shown in lower left panel of figure 4.2) and thus there is no growth in $|\langle \rho_{e\mu} \rangle|$. The time evolution is shown in the lower left panel of figure 4.3.

In case 4, there is a shallow crossing in forward direction in the two flavor scenario in lower right panel of figure 4.2. However, it does not lead to a significant growth (lower right panel of figure 4.3) in the off diagonal element.

4.3.2 Three flavor

In figure 4.4, the time evolution of the angle averaged off-diagonal elements of $\varrho_{\alpha\beta}$ is shown for the four toy examples. Firstly, we consider the scenario, where each of $G^e_{\mathbf{v}}$, $G^\tau_{\mathbf{v}}$ and $G^\mu_{\mathbf{v}}$ have crossings as can be interpreted from the angular distribution of the

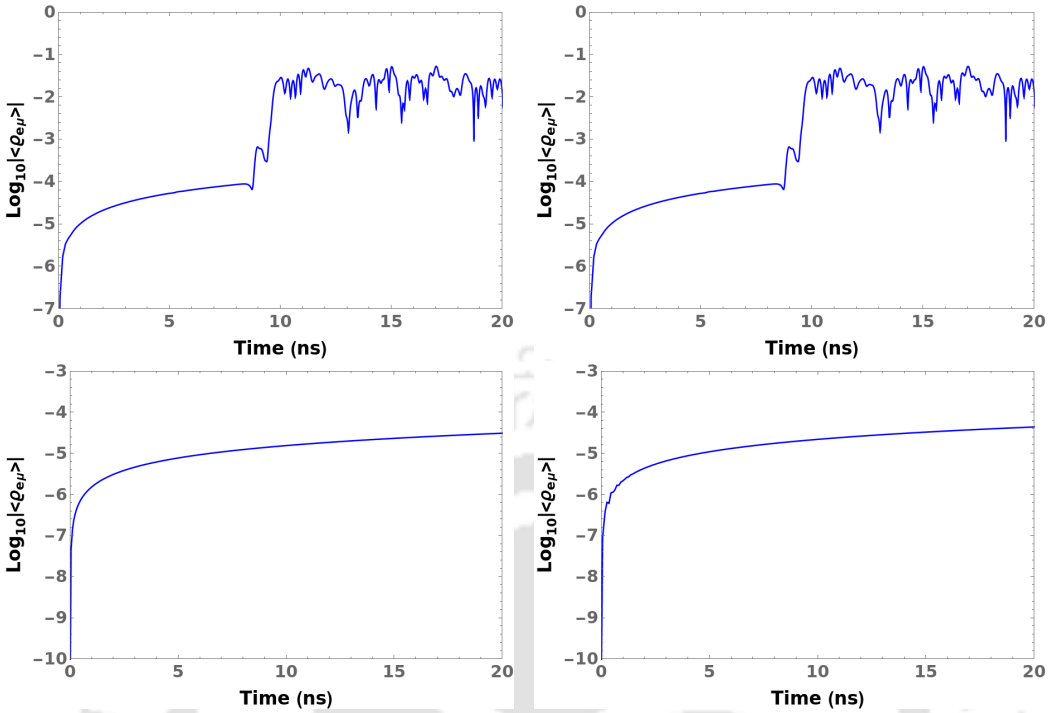

Figure 4.3: The panels show the evolution of the angle-averaged off-diagonal elements $|\langle\varrho_{\alpha\beta}\rangle|$ of the occupation number matrix with time (in ns) for the case of two flavor. Upper left panel : It shows case 1 where the effective two-flavor evolution, assuming $\nu_x = \bar{\nu}_x$, shows large exponential growth due to crossing in $G^e_{\mathbf{v}}$. Upper right panel : This is for case 2 where again due to crossing in $G^e_{\mathbf{v}}$ substantial flavor conversions are seen. Lower left panel : It represents case 3. Here, the two-flavor evolution shows no instability as there is no ELN crossing. Lower right panel : This is for case 4 where due to very shallow crossing, the two-flavor evolution shows no instability.

fluxes (upper left panel in figure 4.1). Thus, in the two-flavor scenario ($n_{\nu_\mu} = n_{\bar{\nu}_\mu}$), there is an exponential growth in angle averaged $\varrho_{e\mu}$ (upper left panel in figure 4.3), due to this crossing in $G^e_{\mathbf{v}}$. However, there is no crossing in $G^{e\mu}_{\mathbf{v}}$, $G^{e\tau}_{\mathbf{v}}$ or $G^{\mu\tau}_{\mathbf{v}}$, and thus the time evolution of the off-diagonal elements $|\langle\varrho_{\alpha\beta}\rangle|$ does not show any exponential growth (upper left panel in figure 4.4). This simple but crucial example clearly demonstrates that some of the crossings found in [179, 195, 224] might disappear once the corresponding hydrodynamical simulation include the full three-flavor neutrino transport, including the production of muons.

As a second example, consider the case (figure 4.2 (upper right panel), where the ELN ($G^e_{\mathbf{v}}$) has a regular crossing (dashed line) and thus there is a growth in the off-diagonal $\varrho_{e\mu}$ (upper right panel of figure 4.3), but there are none in the MuLN or the TauLN. The spectra are designed such that the flavor lepton number difference $G^{e\mu}_{\mathbf{v}}$, $G^{e\tau}_{\mathbf{v}}$ exhibit deep crossings (solid lines in figure 4.2). On the other hand, there is no crossing in $G^{\mu\tau}_{\mathbf{v}}$. The naive two-flavor intuition is that there should be exponential growths in the $e-\mu$ and $e-\tau$ sector. However, the non-linear, coupled nature of the

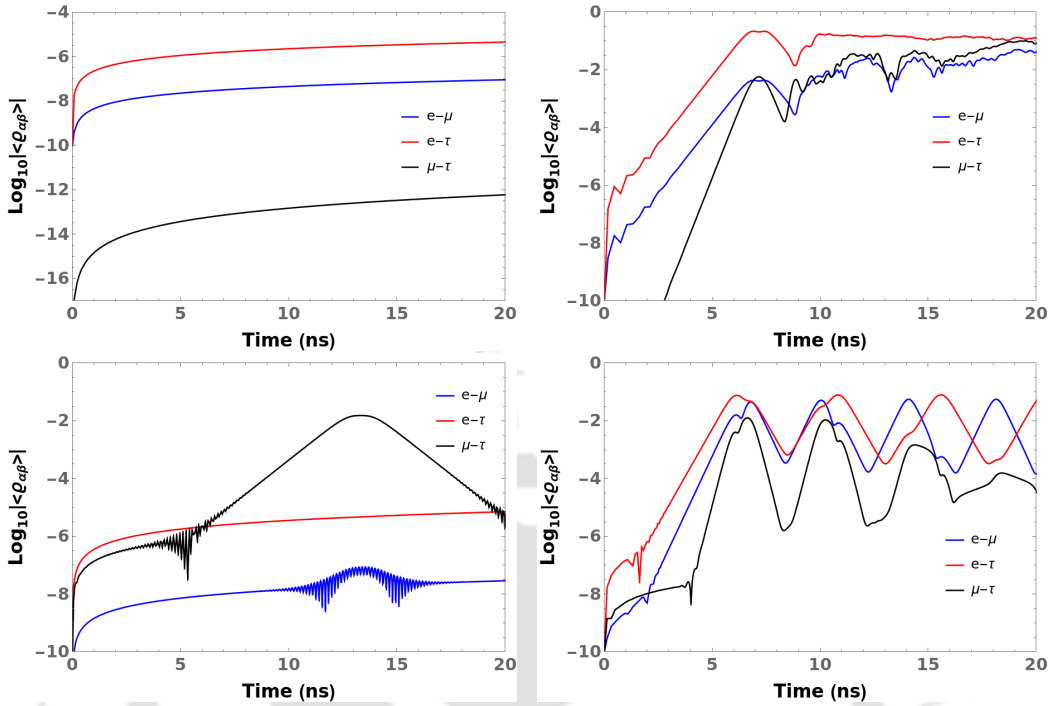

Figure 4.4: The panels show the evolution of the angle-averaged off-diagonal elements $|\langle \varrho_{\alpha\beta} \rangle|$ of the occupation number matrix with time (in ns) in the three flavor scenario. Upper left panel : It shows case 1 where the three-flavor evolution has no instability in any of the sectors. Upper right panel : This is for case 2 where due to large crossings in $G_{\mathbf{v}}^{e\mu}$, $G_{\mathbf{v}}^{e\tau}$, substantial flavor conversions are seen in all the sectors. Lower left panel : It represents case 3. Here, crossing only in $G_{\mathbf{v}}^{\mu\tau}$ causes an exponential growth in $\mu - \tau$ sector. Lower right panel : This is for case 4 where shallow crossings are present in $G_{\mathbf{v}}^{e\mu}$, $G_{\mathbf{v}}^{e\tau}$ in the backward direction, leading to exponential growths in $|\langle \varrho_{\alpha\beta} \rangle|$ for the three-flavor setup.

problem intertwines the growths in all the sectors. This is borne by the upper right panel of figure 4.4, where substantial flavor conversion is seen in all the sectors, though with different growth rates. Note that the growth in $\varrho_{\mu\tau}$ is inherently a non-linear effect, and will not be captured by a linear stability analysis. It can be seen clearly from upper right panel of figure 4.3 that the two-flavor evolution is very different, with a larger onset time and growth rate.

The third case, shown in lower left panel of figure 4.2, presents a crossing only in $G_{\mathbf{v}}^{\mu\tau}$. There exists a reasonable asymmetry between ν_μ and ν_τ (and between their antiparticles as well) to generate an exponential growth in the $\mu - \tau$ sector. This is what is seen in the lower left panel of figure 4.4, where the $\mu - \tau$ sector experiences a flavor instability, while the other two do not. Indeed, the two-flavor analysis (lower left panel of figure 4.3) also does not exhibit any instability due to the lack of a crossing in the ELN ($G_{\mathbf{v}}^{e}$). This example advances the hypothesis

that those regions where no ELN crossing was found in [179, 195, 224] might, in reality, have fast instabilities once the differences between ν_μ and $\bar{\nu}_\mu$ are taken into account. Another comment is in order: the amplitude of the exponential growth in our toy model is not enough to cause substantial flavor conversions. However, the background conditions for these solutions may dynamically change in a realistic SN environment, or if spatial evolution is taken into account, and may result in flavor conversions.

As a final example, we consider a scenario in the lower right panel of figure 4.2 where shallow crossings are present in $G^{e\mu}_{\mathbf{v}}$, $G^{e\tau}_{\mathbf{v}}$ in the backward direction, whereas $G^{\mu\tau}_{\mathbf{v}}$ does not show any crossing. To contrast with the two-flavor examples, the setup is constructed such that the ELN ($G^{e}_{\mathbf{v}}$) also has a shallow crossing in the forward direction only but does not lead to the growth of the off-diagonal element (lower right panel of figure 4.3). We find that such shallow crossings readily lead to an instability in the three-flavor case (lower right panel of figure 4.4). This example is motivated from [195], where it was pointed out that shallow crossings in the backward directions can lead to a fast instability. In [195], such backward crossings were associated with residual coherent scattering on heavy nuclei, which is slightly enhanced for $\bar{\nu}_e$ with respect to ν_e, because of their larger average energy. Our toy model advances the hypothesis that the existing differences between ν_μ and $\bar{\nu}_\mu$ could (at least in principle) be the real cause of these crossings. Similarly, the non negligible muon lepton number can also erase a potential shallow (backward) crossing in the ELN.

4.4 Non-linear analysis : Space and time evolution

In the previous section, we focussed on the non-linear analysis of fast oscillations for a spatially homogeneous case, i.e., considering the evolution only in time. Now we present a more general scenario in this section. Moving a step forward, now we solve the evolution equation 4.1 considering one space and time dimension. Here, we take into account the same four toy examples and study the evolution of the off-diagonals. For the numerical analysis, we employ the d03pff routine from the NAG library, which is built for solving a system of nonlinear convection-diffusion partial differential equations in one space dimension. The method of lines is employed to reduce the system of partial differential equations to a system of ordinary differential equations, and the resulting system is solved using a backward differentiation formula method. We use this routine with 10^3 points in space and we discretize the

angular variable $\mathbf{v}$ with 30 points. We fix $\mu_0 = 4 \times 10^5$ km^{-1} and we consider a spatial range $z \in [0, 0.01]$ km. We set

We discuss our non-linear analysis for the complete three flavor scenario in one space and time dimension (1+1 D). Since we, for the first time are doing the 1+1 non-linear analysis for the complete three flavor scenario and the results are not well understood, we first perform the linear analysis by solving the dispersion relation. This provides us an idea about the results to be expected from the non-linear analysis.

Linearized analysis : Dispersion

The onset of the fast flavor conversions is studied through the method of linear stability analysis [119, 120, 172, 187, 188, 212]. We linearize equation 4.1 at first order in the off-diagonal elements of the density matrices $S^{\alpha\beta}_{\mathbf{v}}$, $(\alpha \neq \beta)$, assuming the diagonal elements to be $O(1)$ which leads to the following equations.

$$i\, v^\gamma \partial_\gamma S^{\alpha\beta}_{\mathbf{v}} = \big(v^\gamma(\Lambda^{\alpha\beta}_\gamma + \Phi^{\alpha\beta}_\gamma)\big) S^{\alpha\beta}_{\mathbf{v}} - v^\gamma \int \frac{d\mathbf{v}'}{4\pi}\, v'_\gamma\, G^{\alpha\beta}_{\mathbf{v}'} S^{\alpha\beta}_{\mathbf{v}'}\,, \tag{4.12}$$

where, $\alpha\beta$ corresponds to the three sectors i.e., $e-\mu$, $e-\tau$ and $\mu-\tau$ respectively. These are same as the equations (3.32 - 3.34) in chapter 3. Here, $\gamma = 0, 1, 2, 3$ and $\Lambda^{\alpha\beta}_\gamma$ is the charged lepton matter term and the corresponding current. Similarly, $\Phi^{\alpha\beta}_\gamma$ is the neutral lepton matter term and the corresponding current. Since we are neglecting the ordinary matter term, we take $\Lambda^{\alpha\beta}_\gamma = 0$ and $\Phi^{\alpha\beta}_\gamma = \int \frac{d\mathbf{v}}{4\pi}\, v_\gamma\, G^{\alpha\beta}_{\mathbf{v}}$.

We then take the ansatz $S^{\alpha\beta}_{\mathbf{v}} = Q^{\alpha\beta}_{\mathbf{v}}\, e^{-i(\Omega t - K\cdot\mathbf{x})}$. Note that Ω and K are the frequency and wave vector and are same as K^0 and $\mathbf{K}$ in equation 3.24 in chapter 3. Substituting this back in equation 4.12, we obtain the following dispersion relation for each choice of $\alpha\beta$.

$$\det\left[\Pi^{\gamma\delta}_{\alpha\beta}(\Omega, K)\right] = 0\,, \tag{4.13}$$

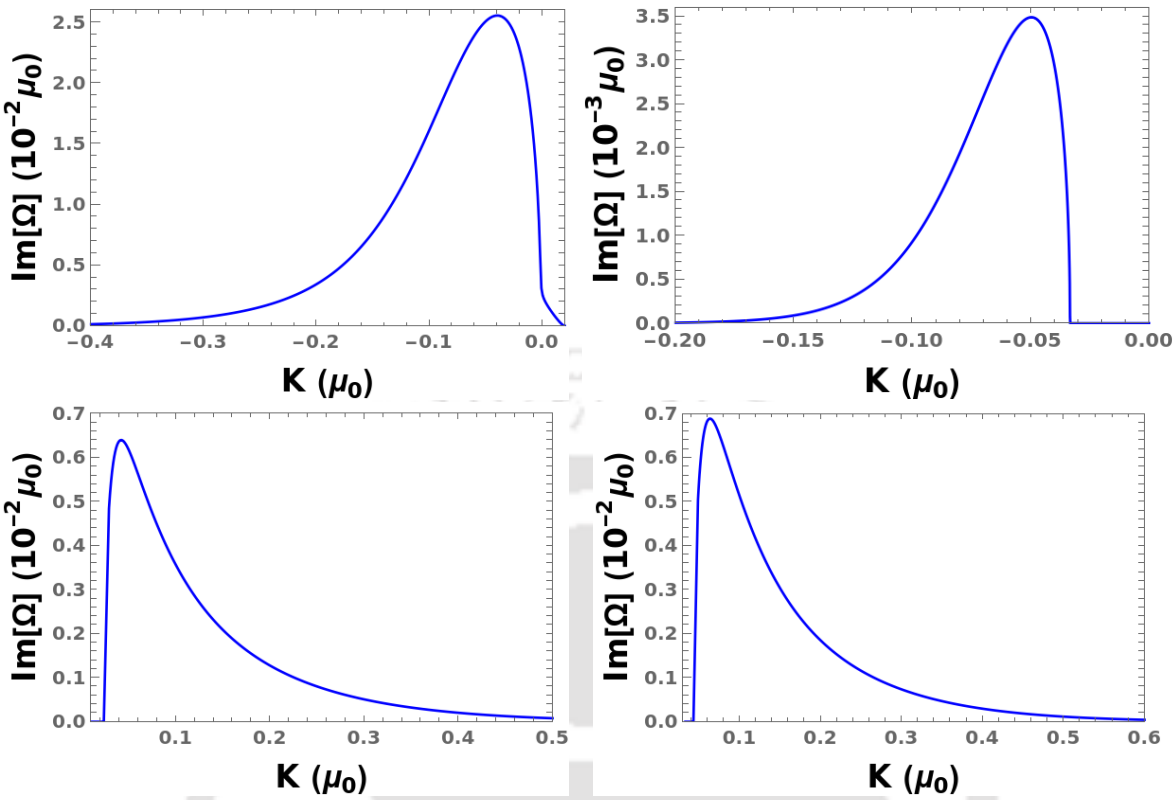

Figure 4.5: The above panels show the plots of the Im[Ω] vs K for the above mentioned examples. Case 1 has no instability and thus there is no Im[Ω]. The upper left panel shows Case 2 (eμ and eτ) and the upper right panel shows Case 3 ($\mu\tau$). Case 4 (eμ and eτ) are represented by the lower left and lower right panels respectively .

where the rank 2 polarization tensor $\Pi^{\gamma\delta}_{\alpha\beta}$ is given by:

$$\Pi^{\gamma\delta}_{\alpha\beta} = \eta^{\gamma\delta} + \int \frac{d\mathbf{v}}{4\pi} G^{\alpha\beta}_{\mathbf{v}} \frac{v^{\gamma} v^{\delta}}{\Omega - (K - \Phi^{\alpha\beta}).\mathbf{v}} \tag{4.14}$$

where $\eta^{\gamma\delta}$ is the metric tensor and it is equal to diag(+1, -1, -1, -1). Note that the subscripts α, β of Π denote the flavor of neutrinos and γ, δ are the spacetime indices. Here, there are three dispersion relations corresponding to the three sectors, i.e., $e-\mu$, $e-\tau$ and $\mu-\tau$. To investigate the presence of instabilities in the system, for each sector we solve equation 4.13 numerically as a function of real values of K. If, we find $\mathrm{Im}[\Omega(K)] \neq 0$, then we have an instability.

In case1, since there are no crossings in the difference spectrum ($G^{e\mu}_{\mathbf{v}}$, $G^{e\tau}_{\mathbf{v}}$, $G^{\mu\tau}_{\mathbf{v}}$), there are no instabilities and thus no Im(Ω) for real values of K. Fig. 4.5 shows the plots of Im(Ω) vs K for the cases 2, 3 and 4. The upper left panel represents the e-μ and e-τ sector of case 2. Since the angular distributions of both sectors are similar, the solutions to the dispersion relation are same. It can be seen that the instabilities

are present for both positive and negative values of K for case 2. The upper right panel is for the $\mu\tau$ sector of case 3. Here, we note that the instabilities are present only for negative values of K. The e-μ and e-τ sectors of case 4 are represented by the lower left and right panels respectively. Note that in case 4, the instabilities are present only for the positive K.

We can define the wavevector 'k' in a co-rotating frame as k = $K-\Phi$ where Φ is the current term. In [175], the presence of instabilities have been identified by the method of moments. It is interesting to note from the plots of case 3 and case 4 that there are no instabilities for the K=Φ mode which is equivalent to saying k=0. In case 3, the value of $\Phi^{\mu\tau}= -0.00528$ and for case 4, $\Phi^{e\mu}= 0.00371$ and $\Phi^{e\tau}= 0.0298$ in units of μ_0. This also agrees with the fact that when we calculate the Im(Ω) following the formalism of [175] by finding the moments, we do not obtain any instability. This is because of the fact that the moments formalism is based on the calculation of Im(Ω) for the case of k=0.

Non-linear analysis

The results for the four cases, shown in figure 4.6, demonstrates the growth rates of flavor instabilities in terms of the evolution of $\log_{10}|\langle\varrho^{\alpha\beta}\rangle|$ in the $z-t$ plane. The leftmost panels depict the evolution in the $e-\mu$ sector, while the middle panels show the same for the $e-\tau$ sector and the $\mu-\tau$ sector respectively. Note that the dispersion plots shown in figure 4.5 are also shown in the insets of the corresponding plot in figure 4.6.

We find that, as expected, there is no flavor instabilities for Case 1 (top panel). This is consistent with the fact that the angular distributions in Case 1 show no crossing in three-flavors. In tandem with these results, we find null results for the growth rates using a stability analysis shown in figure 4.5. For Case 2 (second panel from top), there exists a crossing in the $e-\mu$ and the $e-\tau$ sector. Consequently, the values of $\log_{10}|\langle\varrho_{e\mu}\rangle|$ and $\log_{10}|\langle\varrho_{e\tau}\rangle|$ start growing in space and time, indicating a flavor instability. The corresponding plots in figure 4.5 (upper left panel) show the instabilities in the Im$\Omega - K$ plane in the linear regime. We also get a quantitative agreement among the amplitudes of the growth rates in the linear as well as non-linear regime. The growth-rate in the $\mu-\tau$ sector is driven by a combination of the couplings in the different sectors, and is purely driven by the non-linearity of the problem. Hence, this growth rate is not captured by a stability analysis.

The toy spectra in Case 3 (third panel from top) shows a crossing only in the $\mu-\tau$ sector. As a result, we find a flavor instability in the $\mu-\tau$ sector only. The

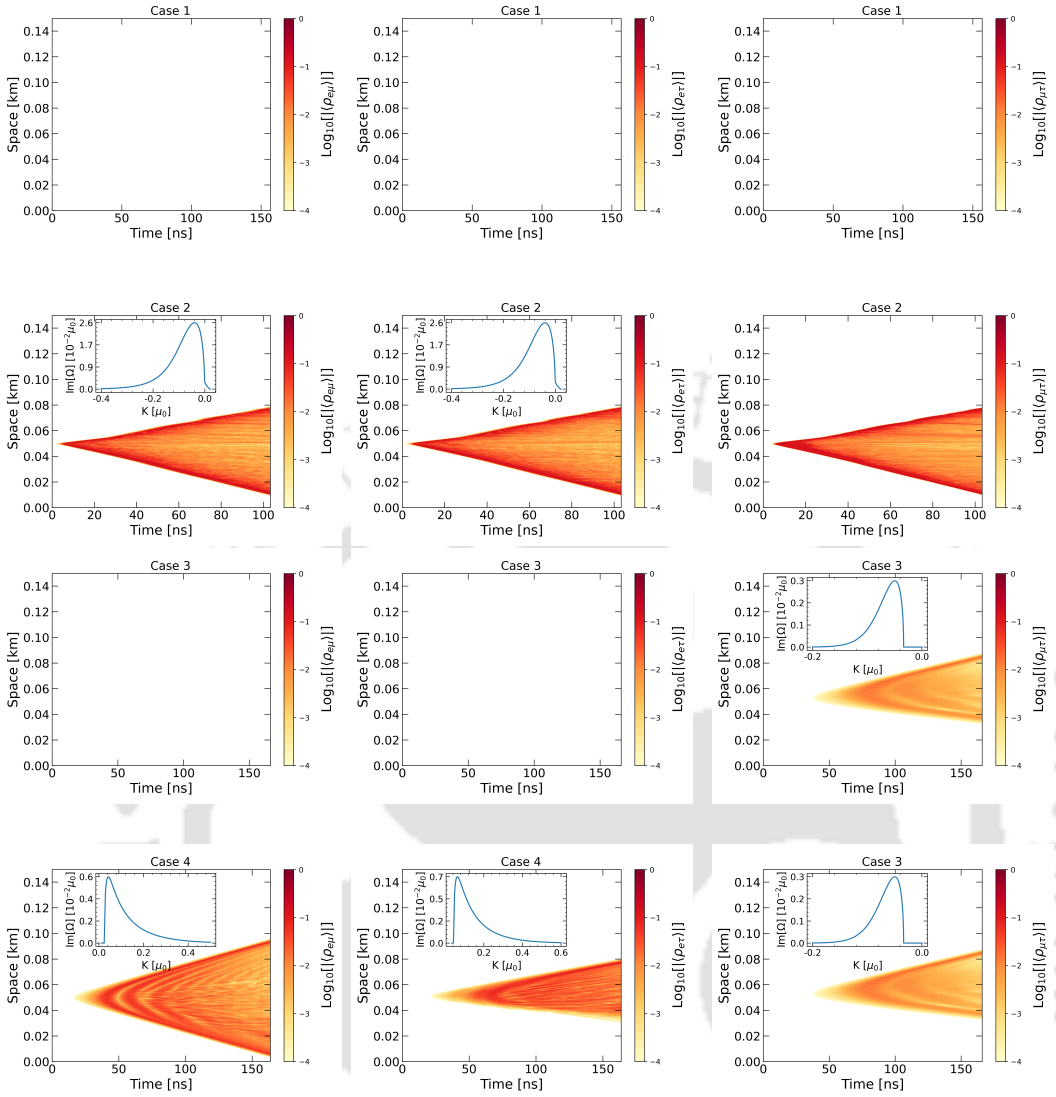

Figure 4.6: Growth rate of flavor instability ($\log_{10}|\langle\varrho_{\alpha\beta}\rangle|$) in the three-flavor study for the 4 different cases. The rows (from top to bottom) correspond to case 1,2,3, and 4 respectively. The left panel depicts the $e-\mu$ sector, while the middle and right panel depicts the $e-\tau$ and the $\mu-\tau$ sector respectively.

linear stability analysis also obtains imaginary values of Ω only in the $\mu-\tau$ sector and not in the other two (upper right panel of figure 4.5).

For Case 4 (bottom panel), we find that all three flavor sectors show a non-zero growth of the off-diagonal components of the density matrix. The $e-\mu$ and the $e-\tau$ sector show a spectral crossing, and hence have a faster growth rate. The growth in the $\mu-\tau$ sector is completely a three flavor artefact, and does not depend on any spectral crossing in that sector. The same is captured in a linear stability analysis, where there is an instability only in the $e-\mu$ and the $e-\tau$ sector, as shown in the

lower panels of figure 4.5.

4.5 Discussion

The evolution of neutrino fast flavor conversions in a core-collapse supernova depends on the occurrence of crossings in the angular distributions of flavor lepton number. In this context it is usually assumed that the flavor content of ν_μ, ν_τ, $\bar{\nu}_\mu$ and $\bar{\nu}_\tau$ is equal. Consequently only three neutrino species are used (ν_e, $\bar{\nu}_e$ and ν_x) in numerical simulations, as well as linear stability analyses. Within this two-flavor formalism, these ultra-rapid flavor conversions are believed to occur mainly when the ELN, i.e., the difference between the ν_e and $\bar{\nu}_e$ angular spectra, exhibit a zero-crossing. However, the first hydrodynamical simulations with six neutrino species performed in [87] have motivated us to extend the study of fast conversions in complete three flavor picture.

Based on [219, 221], it has been demonstrated in this chapter through toy examples that the differences expected between ν_μ and $\bar{\nu}_\mu$, which are induced by a non-negligible population of negatively charged muons in the core, can introduce some observable modifications of the angular distributions of lepton number. As a result, those angular crossings that are expected to occur with three neutrino species can be either erased or actually created. We find that the inclusion of three-flavors can significantly alter our understanding of the conditions for fast conversions. Using toy spectra, we demonstrate that it is not the ELN, or correspondingly, the MuLN, and TauLN, but rather their differences that govern these fast modes. The examples studied clearly show that three-flavor evolution can result in instabilities that are not captured by a two-flavor study; conversely, it can also wash out the instabilities predicted by a two-flavor study. These results also show that the linear stability analysis cannot capture all the instability signatures of the full non-linear analysis, i.e the triggering of instabilities in otherwise stable sector $\rho_{\alpha\beta}$, because of the absence of a crossing at $t = 0$, can only be observed at the non linear level. These conclusions have been obtained considering a spatially homogeneous neutrino system as well as considering evolution in both space and time (1+1 D). Overall, we find that the qualitative nature of the results obtained in only time evolution case remain robust even when considering flavor evolution in both space and time.

Our findings further indicate caution against claiming the presence of fast conversions for shallow crossings in the ELN, because such crossings can easily be nullified by an opposite crossing in the MuLN. This is particularly relevant in the shock re-

gion, where a significant population of ν_μ, ν_τ can be expected in the accretion phase. This fast flavor mixing can have a drastic impact on the shockwave revival, as well as nucleosynthesis. Hence, it is crucial to appreciate these flavor conversions, using a complete three-flavor analysis. This motivates the necessity of including muons in a dedicated analysis of fast-flavor conversions to gauge their impact on supernova dynamics. Moreover, our examples clearly establish the importance of detailed three-flavor treatments to assess whether such possibilities are indeed realized in nature. Future muon SN simulations will hold the key to the answer.

Chapter 5

Diffuse supernova neutrino background

In the previous chapters, we discussed the phenomenon of collective oscillations in the dense environment of a supernova core. We particularly focussed on the study of slow and fast oscillations in a three flavor framework. In this chapter, we will talk about the phenomenological implications of the SN neutrino oscillations on the Diffuse Supernova Neutrino Background.

5.1 Introduction

The detection of SN neutrinos directly from a core-collapse supernova is a challenging task. Though the CCSN is accompanied by a huge number of neutrinos, the weakly interacting nature of these neutrinos limits their detection. Even the present super large neutrino detectors would not be able to probe much beyond our galaxy. Moreover, the core collapse supernova rate in our galaxy being $1 \sim 3$ per century [225] makes such detection rare. The only observations of supernova neutrinos available to us till date are that from SN1987A [226–228] in the Large Magellanic Cloud. Although this observation provided good amount of information about SN dynamics on a broader scale, the small number of events captured in the detector restricted our detailed understanding.

Another opportunity to detect these neutrinos can be provided by the far away supernovae in the form of the Diffuse Supernova Neutrino Background (DSNB) [229–235]. It is the cummulative background formed by the neutrinos and antineutrinos emitted during the past supernova explosions in the universe. These neutrinos are also known as the supernova relic neutrinos. It is interesting to study DSNB

as it explores the entire population of collapsing stars, taking into account both the diverse nature and cosmological evolution of the stars. This background is expected to be uniform and time independent to a great extent. Thus the possibility of observing DSNB is extensively dependent on the advancements in the detector technology.

The main factors governing the calculation of the DSNB flux are the rate of core collapse supernova and the flavor dependent spectrum of the neutrinos and antineutrinos from supernovae. The cosmic star formation rate can be measured by studying how the stars are distributed according to their luminosities and masses on which an analytical fit to the star formation rate can be obtained [235–238]. There are many uncertainties associated with these methods [239]. The other ingredient, i.e. the flux of neutrinos from a supernova is also not well known as the only experimental information about CCSNe are the small number of events detected from SN1987A. Thus, to determine the SN neutrino spectra, one has to rely on the hydrodynamical simulations [240]. Although the fluxes predicted by different simulation groups vary due to the different values of the input parameters, the idea of representing the SN neutrino spectra by the pinched thermal spectra is well accepted [91]. In addition to this, the neutrinos undergo flavor oscillations while passing through the SN which further modify the spectra. Deep inside the SN, collective oscillations [108, 111–142] take place which is then followed by the MSW effect [24, 26] at larger distances from the core. The uncertainties in the prediction of spectra by SN simulations together with different flavor conversion possibilities are fundamental sources of the uncertainties in the diffuse neutrino flux.

The usual predictions of the diffuse supernova neutrino background were commonly done considering the collapse into a neutron star [241–255]. But then the detailed studies have been done over the last decade taking into consideration the rarer case of failed supernova i.e., the direct collapse into a black hole without explosion [256–268]. In this case, the luminosities and the energy of the neutrino emitted are found to be more than the neutron star forming collapse. This suggests that the diffuse flux due to black hole forming collapses might dominate at the higher energy part of the spectrum.

In this chapter, we will study two different oscillation scenarios, the motivation being the fast oscillations and the impact of that on DSNB. The extreme effect of fast oscillations would be to equilibrate the fluxes of the different flavors of neutrinos. Further we focus on the uncertainties in the DSNB flux due to different black hole fractions considering the uncertainty in the normalization of the supernova rate.

We study the phenomenological prospect in the water Cherenkov and liquid Argon detectors.

5.2 Calculation of the DSNB flux

The total differential flux of diffuse supernova neutrino background (DSNB) is defined as the number of neutrinos of a particular flavor arriving at the detector on Earth per unit area per unit time per unit energy due to all the supernovae in the Universe. This background is calculated upto the maximum redshift. The expression for the differential DSNB flux for ν_α ($\alpha = e, \mu, \tau$) flavor is given by

$$\varphi_{\nu_\alpha}(E) = \frac{c}{H_0} \int_{10M_\odot}^{125M_\odot} \int_0^{z_{max}} R_{SN}(z, M)\, F_{\nu_\alpha}(E', M)\, \frac{dz}{\sqrt{\Omega_M (1+z)^3 + \Omega_\Lambda}}\, dM \quad (5.1)$$

where α denotes the neutrino flavor, c is the speed of light, z_{max} is the maximum redshift, $\Omega_M = 0.3$, $\Omega_\Lambda = 0.7$ are the matter and dark energy cosmic energy densities respectively, and the Hubble parameter $H_0 = 67.36$ km s^{-1} Mpc^{-1} [45]. As it is evident from the above equation, the differential flux depends on the supernova rate R_{SN} and the oscillated time integrated spectrum of the neutrinos F_ν for a progenitor mass M. E' represents the neutrino energy at the site of production at redshift z and is related to the energy at the Earth (E) by $E' = E(1+z)$. The integration on M in equation 5.1 includes both the contribution of the neutron star forming collapses as well as the ones forming black holes.

The comoving supernova rate (R_{SN}) is defined as the rate at which the core collapse supernova occurs in the universe. This R_{SN} is considered to be proportional to the star formation rate (R_{SF}) and is given by

$$R_{SN}(z, M) = R_{SF}(z)\, \frac{\phi(M)}{\int_{0.5M_\odot}^{125M_\odot} M\, \phi(M)\, dM} \quad (5.2)$$

where $M_\odot$ is the mass of Sun and $\phi(M)$ is the Initial Mass Function. The initial mass function represents the mass distribution of stars at birth. Here, we use the Salpeter IMF [269] i.e. $\phi(M) \propto M^{-2.35}$. The star formation rate R_{SF} is fitted by the following functional form [270] which is also adopted in [262].

$$R_{SF}(z) = R_{SF}(0) \begin{cases} (1+z)^{\gamma} & 0 < z < 1, \\ 2^{\gamma-\beta}\,(1+z)^{\beta} & 1 < z < 4.5, \\ 2^{\gamma-\beta}\,5.5^{\beta-\delta}\,(1+z)^{\delta} & 4.5 < z < 5, \end{cases} \tag{5.3}$$

where, $\beta = -0.26, \gamma = 3.28, \delta = -7.8$. The total normalization of the supernova rate is taken to be $R_{cc}(0) = \int_{8M_\odot}^{125M_\odot} R_{SN}(0, M)\, dM = (1.25 \pm 0.5) \times 10^{-4}\,\mathrm{yr}^{-1}\,\mathrm{Mpc}^{-3}$ [258]. Note that in our calculations, we have used the fiducial value of $\mathrm{R}_{cc}(0)$ i.e. $1.25 \times 10^{-4}\,\mathrm{yr}^{-1}\,\mathrm{Mpc}^{-3}$.

Now, for the spectra (F_{ν_α}) of SN neutrinos as mentioned earlier (chapter 2), the average energies and luminosities may change within the duration of emission. However, this is of minimal interest for DSNB as we take into consideration the time integrated spectra from each supernova. The spectrum of the neutrinos emitted from a supernova is parametrized in the form of a pinched thermal spectrum [91] as

$$F^0_{\nu_\alpha}(E) = \frac{L_{\nu_\alpha}}{\langle E \rangle^2_{\nu_\alpha}} \frac{(1+s_{\nu_\alpha})^{(1+s_{\nu_\alpha})}}{\Gamma(1+s_{\nu_\alpha})} \left(\frac{E_{\nu_\alpha}}{\langle E \rangle_{\nu_\alpha}}\right)^{s_{\nu\alpha}} e^{-(1+s_{\nu_\alpha})E/\langle E \rangle_{\nu_\alpha}} \tag{5.4}$$

where, the spectral parameter s is given in terms of average energies and the average of the energy squared as

$$s_{\nu_\alpha} = \frac{\langle E^2 \rangle_{\nu_\alpha} - 2\langle E \rangle^2_{\nu_\alpha}}{\langle E \rangle^2_{\nu_\alpha} - \langle E^2 \rangle_{\nu_\alpha}} \tag{5.5}$$

and $\alpha = e, x$, i.e., different flavors of the neutrinos.

Now we wish to calculate the DSNB flux in the above framework by taking into consideration the different model uncertainties contributing in the DSNB flux. The uncertainties in DSNB can arise from two factors, i.e. R_{SN} and F_{ν_α} as these are the two main ingredients in the calculation of DSNB flux. The supernova R_{SN} depends on the fraction of the core-collapse supernovae occurring in the universe which in turn depends on the distribution of the masses of the stars at the time of their birth (IMF). The second factor, F_{ν_α} is dependent on the simulations as well as the oscillation scenario considered. In the next section, we discuss the impact of these uncertainties in the calculation of the DSNB flux.

5.3 Model uncertainties

The diffuse supernova neutrino background has not been detected yet. However, there are upper bounds from the Super Kamiokande experiment [271–273]. One of

the goals of the ongoing and future neutrino experiments is to measure this background. The main challenge is the presence of various other backgrounds which hinders the detection of this smaller DSNB flux. We will discuss about these backgrounds in detail later (section 5.4). In this chapter, we focus on the detection of the $\bar{\nu}_e$ and ν_e flux in the gadolinium doped Super Kamiokande and the upcoming Hyper Kamiokande and DUNE detectors respectively.

When a core collapse supernova occurs, there are two possibilties about the final outcome, i.e. either it will be successful or failed, latter being a rarer event. The successful explosion is accompanied by the formation of a neutron star whereas in case of failed supernova, direct collapse occurs without explosion which results in the black hole formation [274–279]. Thus, the diffuse supernova neutrino background can have contribution from both neutron star forming collapses (NSFC) as well as black hole forming collapses (BHFC). Many studies [256–268] have been carried out taking into account the contribution of failed supernova in the calculation of the diffused flux. The black hole forming collapses are expected to have a harder neutrino spectra than NSFCs, i.e. the neutrino flux will be greater at the higher energies [274–279]. This is because of the rapid contraction of the protoneutron star which is formed before the black hole formation. As a result, their contribution to the total diffused flux in the higher energy range can be significant. However, the exact fraction of the stars resulting in the formation of black holes is not known.

In this study, we consider the contribution from both the NSFCs and BHFCs to compute the total DSNB flux. Motivated from [268], we take into consideration three scenarios (shown in figure 5.1) which differ in the fraction of the black hole forming progenitors. Moreover, focussing on equation 5.2, we can see that the supernova rate is dependent on the initial mass function $\phi(M)$. The power law dependence of ϕ on M indicates that the lower mass stars contribute more than the higher ones. If we take larger number of progenitors in the lower mass range, a good estimate of the diffused flux can be made. This would make the calculation relatively easier than the detailed study done in [268], where around 200 different progenitor models have been taken into account. Here, our aim is to compute the DSNB flux for ν_e and $\bar{\nu}_e$ and study the effect of different black hole fractions and the different oscillation scenarios. In order to do so, we use the parameter values of the progenitor models (listed in table 5.1) from the Garching simulations [35, 280, 281]. We consider two neutron star forming progenitors (11.2 $M_\odot$ and 27 $M_\odot$) and three black hole forming progenitors (15 $M_\odot$, 25 $M_\odot$ and 40 $M_\odot$). Table 5.1 gives the values of the time integrated luminosities, average energies and the second moment of energy for all the

Mass	L_{ν_e}	$L_{\bar{\nu}_e}$	L_{ν_x}	$\langle E_{\nu_e} \rangle$	$\langle E_{\bar{\nu}_e} \rangle$	$\langle E_{\nu_x} \rangle$	$\langle E^2_{\nu_e} \rangle$	$\langle E^2_{\bar{\nu}_e} \rangle$	$\langle E^2_{\nu_x} \rangle$
($M_\odot$)	(10^{52} ergs)			(MeV)			(MeV^2)		
11.2	3.56	3.09	3.02	10.43	12.89	12.93	137.52	213.18	220.86
15	2.83	2.31	1.25	13.19	16.91	15.84	230.95	370.47	341.84
25	7.08	6.51	3.7	15.32	18.2	17.62	318.92	437.57	427.22
27	5.87	5.43	5.1	11.3	13.89	13.85	164.68	249.97	255.38
40	9.38	8.6	4.8	15.72	18.72	17.63	343.65	470.76	440.71

Table 5.1: Time integrated parameter values of the progenitor masses taken from Garching simulation [35, 280, 281].

flavors of neutrinos. Here, the parameters for the non-electron type of neutrinos are taken to be identical ($\nu_x = \bar{\nu}_x$). The progenitors used are of solar metallicity from Woosley et al. [282] and the equation of state is LS220, i.e. Lattimer and Swesty Equation of State [283]. It can be seen from table 5.1 that the average energies for the black hole forming progenitors are larger than the neutron star forming ones. Moreover, ν_e and $\bar{\nu}_e$ have higher values of luminosities than ν_x in the case of BHFC as the rate of electron and positron capture on the nuclei in the hot accreted matter is very high. Also note that the luminosities of the neutrino flavors increase with the mass. However, the values of the parameters are dependent on the simulation details.

5.3.1 Black hole fractions

We calculate the diffuse flux for the three fractions of the black hole forming collapses as shown in Figure 5.1. The fraction of black hole forming collapses is defined as the number of stars resulting in the formation of black holes divided by the total number of stars undergoing core collapse. It is given by

$$f = \frac{\int \phi(M)\, dM}{\int_{10\,M_\odot}^{125\,M_\odot} \phi(M)\, dM} \tag{5.6}$$

where the integration in the numerator is on the mass range for which black holes are formed.

Figure 5.1 represents the three cases with different fractions of black hole forming stars. The markings on the horizontal axis represent the masses of the progenitors in

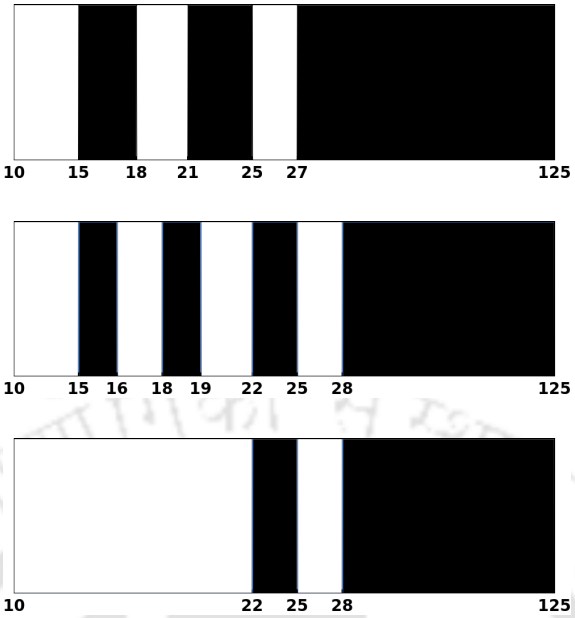

Figure 5.1: Range of progenitor masses forming black hole for three different cases. The topmost panel represents case 1 ($f = 44\%$), middle panel shows case 2 ($f = 36.3\%$) and lowermost panel refers to case 3 ($f = 28\%$). The black regions indicates the range which undergo black hole forming collapse.

units of solar masses. The topmost panel of figure 5.1 corresponds to case 1 where 44% of the stars form black hole. The middle panel represents the case 2 where the fraction of the black hole forming collapses is 36.3% and case 3 is shown in the lowermost panel having the fraction as 28%. The region enclosed by the black bars in figure 5.1 shows the mass range in which the black hole forming collapses occur and the white regions correspond to the neutron star forming mass ranges. Note that the possibility of a star collapsing to a failed supernovae does not depend directly on M. Rather, a lot of other factors also come into play [73, 284, 285]. Table 5.2 provide the mass intervals and their corresponding representative masses considered for the calculation of flux for the three cases.

5.3.2 Oscillation scenarios

To estimate the diffuse flux at the detector, we need to take into account the flavor conversions that is undergone by the neutrinos while travelling through the supernova envelope. The neutrinos can undergo collective oscillations at distances of $\mathcal{O}(10^2)$ km and MSW effects at larger distances of around $10^4 - 10^5$ km. The slow collective oscillations are usually suppressed by the multi-angle effects of the

	Representative ($M_\odot$)	Case 1 intervals	Case 2 intervals	Case 3 intervals
NSFC	11.2	10-15, 18-21	10-15, 16-18, 19-22	10-22
	27	25-27	25-28	
BHFC	15	15-18	15-16, 18-19	
	25	21-25	22-25	22-25
	40	27-125	28-125	28-125

Table 5.2: Masses of progenitors taken as representative for the intervals of NSFCs and BHFCs in Figure 5.1.

ordinary matter during the accretion phase [286]. Although they can be present in the cooling phase, very negligible (less than 10 %) effect has been found on the time-integrated neutrino spectra [287]. Here we neglect the oscillation effects due to the passage of neutrinos through Earth before reaching the detector as they have a very small impact on the pattern of oscillation [288]. The fluxes of ν_e and $\bar{\nu}_e$ at the detector after considering oscillations can be written as :

$$F_{\bar{\nu}_e} = \bar{P}_{ee} F^0_{\bar{\nu}_e} + (1 - \bar{P}_{ee}) F^0_{\nu_x} \tag{5.7}$$

$$F_{\nu_e} = P_{ee} F^0_{\nu_e} + (1 - P_{ee}) F^0_{\nu_x} \tag{5.8}$$

where, P_{ee} and $\bar{P}_{ee}$ are the survival probabilities for the electron neutrinos and electron antineutrinos respectively. $F^0_{\nu_\alpha}$ and $F^0_{\bar{\nu}_\alpha}$ are the initial fluxes of neutrino and antineutrino at the source for the flavor 'α'. We focus on the following two scenarios here.

(1) Only MSW oscillations : This is the case where we assume that the neutrino flux has an oscillation effect only due to the Mikheyev-Smirnov-Wolfenstein resonance occuring at lower density [24, 25]. The higher density oscillation effects, i.e. slow collective oscillations are neglected. We consider the scenario where the slow collective oscillations are suppressed due to matter multiangle effect [288]. The MSW effect being adiabatic, the values of the survival probabilities are taken to be $\bar{P}_{ee} = \cos^2\theta_{12}$, $P_{ee} = 0$ for normal ordering and $\bar{P}_{ee} = 0$, $P_{ee} = \sin^2\theta_{12}$ for inverted ordering [88].

(2) Flavor equilibration : This is the case which arises when the fast oscillations

come into picture deep inside SN. In the extreme scenario, these fast flavor conversions may equalize the fluxes of all the different flavors, thus the term 'flavor equilibration'. Although in principle flavor equalization cannot happen in both the sectors (neutrino and antineutrino) simultaneously keeping in mind the lepton number conservation [111], here to keep it simple, we consider the survival probability of the electron antineutrino to be also 1/3 [138]. In this extreme flavor equilibration scenario, SN flux are not affected by matter effect [138].

5.3.3 Dependence on SN simulations

The calculation of the DSNB flux depends on the various input parameters like the average energy, luminosity and the spectral parameter of the different flavors of neutrinos. These parameters are dependent on the simulation. Here, we study the difference in the diffuse flux that arises due to the variation in the input parameters. We compare the fluxes for progenitor models from two simulation groups which we denote here as Garching [35, 280] and Nakazato [289, 290].

The time integrated input parameters of the progenitors by the Garching group are shown in table 5.1. These are obtained from spherical symmetric simulations and the equation of state used is the Lattimer equation of state [283]. The processes which are considered for the neutrino transport are neutrino pair conversions between different flavors, transfer of energy in the interactions of neutrinos with nucleons and the nucleon correlations in the dense medium [280]. Also the convection effects are considered through the mixing length treatment [35, 280]. The simulation continues till around 10s for the neutron star forming collapses and around 1s for the black hole forming collapses.

For the Nakazato group, the time integrated data for eight simulations in the mass range of 13-50 $M_\odot$ are considered. The metallicity of the progenitors are Z = 0.02 and Z = 0.004. There is only one black hole model of mass 30 $M_\odot$ with metallicity 0.004. The equation of state considered is from Shen et. al. [291, 292] whereas for the black hole forming progenitor, we consider the data for the LS220 equation of state [283]. The time of the simulations extend to about 20 s. Two different methods of simulations are used. For the early phase general relativistic neutrino-radiation hydrodynamic (νRHD) simulations are used. The other one is the general relativistic quasi-static evolutionary calculations of neutrino diffusion in a nascent neutron star which is used for the late phase. In addition to this, a new

parameter known as the shock revival time is considered so as to connect the early and later phases as the νRHD simulations do not result in a successful supernova explosion.

5.4 Detector configurations

The detection of the diffuse supernova neutrino background is a challenging task as the value of its flux is very small. In addition to this, another difficulty is the presence of other backgrounds [232, 293] in that particular energy range which will hinder the detection of DSNB. So, in order to detect it, either of the two requirements needs to be fulfilled : (1) we need very large detectors, (2) we need normal size detectors with large exposure time. The next generation of detectors are expected to be large enough to be able to differentiate the signal from background and detect DSNB in the next five to ten years [294, 295]. The current neutrino detector which is capable of detecting the DSNB is the 50 kton water Cherenkov detector Super-Kamiokande [293] in Japan. SK has provided upper bounds on the DSNB flux but only above neutrino energy greater than 17.3 MeV as below that energy range several backgrounds are prevalent. Recently, the SK has been doped with Gadolinium which is expected to increase its sensitivity by efficient neutrino tagging. Besides this, the other future neutrino detectors Hyper-Kamiokande [296], Jiangmen Underground Neutrino Observatory [297], Deep Underground Neutrino Experiment [298], Theia [299] are also expected to measure some of the properties of DSNB. The DSNB flux extends around the neutrino energies of order tens of MeV. In this energy range, there are many other background sources. The main neutrino sources which can mimic the DSNB signal and thus cause obstruction in its detection are the $\bar{\nu}_e$ from nuclear reactors, ν_e from Sun, atmospheric ν_e and $\bar{\nu}_e$, spallation products induced by cosmic ray muons and neutrinos coming from the invisible muons produced by atmospheric ν_μ and $\bar{\nu}_\mu$.

In the following discussion, we consider three types of detector out of which two are for observing $\bar{\nu}_e$ and one for ν_e :

(1) Water Cherenkov detectors

(2) Gadolinium loaded water Cherenkov detectors

(3) Liquid argon detectors

5.4.1 Water Cherenkov detectors

Water Cherenkov detectors are mainly composed of large volumes of water which is surrounded by photomultipliers tubes (PMTs). These PMTs are sensitive to the charged particles which are produced by the interactions of the incoming neutrinos whose energy range is from few MeV to few tens of MeV. Thus, they can be used to study neutrinos from Sun, atmosphere and core collapse supernovae and thus can be useful to observe the diffuse supernova neutrino background. For the typical energies of the DSNB neutrinos, the main detection channel is the inverse beta decay reaction of electron antineutrinos with the free protons in water because of its greater cross-section compared to other species. It is of the form :

$$\bar{\nu}_e + p \rightarrow n + e^+ \tag{5.9}$$

The detection of the positron emitted in IBD reaction is based on the principle of production of Cherenkov radiation when charged particles pass through a medium faster than the speed of light. The famous water Cherenkov detectors which observed the electron antineutrinos (around 20 events in total) from SN1987A are the IMB [226] and Kamiokande-II [227] detectors. The ongoing large water Cherenkov detector is the Super-Kamiokande (SK) [293] in Japan with a fiducial mass of 22.5 kton. It has provided the most stringent upper bound on the DSNB flux, i.e. the diffused flux is constrained to be $\lesssim$ (2.8-3.1) cm^{-2} s^{-1} for neutrino energy $>$ 17.3 MeV [272]. The upcoming water Cherenkov detector is the Hyper-Kamiokande (HK) [296] in Japan which will be around 10 times larger than SK with a fiducial volume of 187 kton. It is expected to record around hundreds of DSNB events in a decade.

The major backgrounds experienced in the water Cherenkov detectors are the reactor $\bar{\nu}_e$ in the lower enrgy range below 10 MeV and the "invisible muons" produced in the higher energy range above 30 MeV by atmospheric ν_μ, $\bar{\nu}_\mu$. These muons are produced with a kinetic energy below the threshold for emitting Cherenkov photons and thus they pass without getting detected. Later, the electrons or positrons produced by the decay of these photons are finally recorded at the detector. Below 30 MeV, the events due to the atmospheric ν_e and $\bar{\nu}_e$ are expected to be below the DSNB flux and thus does not cause much difficulty in the analysis of DSNB. So, taking into account all the backgrounds, the detectable neutrino energy window of DSNB in a water Cherenkov detector is limited to 19.3 MeV - 30 MeV.

5.4.2 Gadolinium doped water Cherenkov detectors

The production of positron in reaction 5.9 is accompanied with the emission of neutron. In water, these neutrons are absorbed by hydrogen which emits a 2.2 MeV photon. This is the usual way in which neutron tagging is done in SK and thus along with other backgrounds, the detectable range is restricted to $E_\nu = (19.3 - 30)$ MeV. However, in comparison to this, the cross-section for neutron capture is larger in gadolinium. This results in the emission of 8 MeV photons. Therefore, the neutron tagging with gadolinium increases the detectable energy range to (10-30) MeV by further reducing the backgrounds (particularly the muon spallation background) [295]. So, to increase the sensitivity to DSNB, SK has been doped with gadolinium in summer of 2020. Also in future, HK is expected to be doped with gadolinium.

5.4.3 Liquid argon detectors

Another type of detectors which are capable of detecting the DSNB signal are the liquid argon detectors. Due to low cost, high availability and outstanding scintillation properties, liquid argon is one of the most extensively used scintillators for detecting particles. A lot of research is going on currently in developing these kind of detectors. The ICARUS T600 detector [300] in Italy with 600 tons of purified liquid argon is the largest LAr TPC built so far. These detectors can be used in a wide range of energy from MeV to multi GeV and also have a high event reconstruction efficiency. Moreover, due to high granularity, low thresholds for particle identification are also possible. One of the speciality of liquid argon Time Projection Chambers (TPCs) is that they can detect the electron neutrinos and thus can be useful in detecting DSNB ν_e flux. The main detection channel is the absorption of ν_e in liquid argon given as follows :

$$\nu_e + {}^{40}Ar \rightarrow {}^{40}K^* + e^- \tag{5.10}$$

This is followed by the de-excitation of potassium nucleus which releases a cascade of photons. In this case, the major backgrounds are the atmospheric ν_e flux above 40 MeV and the solar ν_e below 16 MeV. Thus, (20-40) MeV can be the detectable energy window. DUNE [301] and MicroBooNE [302] are the upcoming liquid argon detectors. The DUNE far detector with fiducial volume of 40 kton is expected to be ready within 10 years.

5.5 Results

5.5.1 Black hole fractions

The diffuse fluxes vs neutrino energy for the above three mentioned black hole fractions using the parameters given in table 5.1 are plotted in Figure 5.2. Here, the oscillation scenario is considered to be only MSW resonance. The mass ordering is denoted by NO (normal) and IO (inverted) in the figure. The left and right panels correspond to $\bar{\nu}_e$ and ν_e respectively. The solid lines (blue : case 1, red : case 2, black : case 3) in the upper four panels of Figure 5.2 represent the fluxes of the fraction of neutron star forming collapses (NSFCs) and the corresponding dotted lines refer to the black hole forming collapses (BHFCs). Clearly, the fluxes due to the BHFCs are dominant in the higher energy range and that due to NSFCs are dominant in the lower energies. Focussing on the individual cases of the BHFCs, one can identify that the case having larger black hole fraction has larger diffuse flux at higher energies. On the other hand, the opposite is true for the neutron star fraction, i.e. the larger black hole fraction case has lower flux at lower energies. In particular, it is clear from figure 5.2 that the blue solid line which represents the case 1 (maximum f) is lower than the solid black line indicating case 3 (minimum f). Contrary to it, for BHFCs the blue dotted line is higher than black dotted line. As a result, when we calculate the total flux, there is not much difference between the two cases. The energy at which the diffuse flux curve due to BHFC crosses that of NSFC is determined by the several input parameters like average energy, luminosity of different species etc. and are dependent on simulations.

The lower four panels of Figure 5.2 show the total diffuse flux considering the contribution of both NSFC and BHFC. In this figure, the solid blue, red and black lines correspond to the total DSNB flux for cases 1, 2 and 3 respectively. Here, it can be seen that in normal ordering, the total flux for the higher energy range is largest for case 1 and case 3 is largest in lower energy range. This is expected as the contribution of the BHFC is the largest in this case 1 and thus it is more in higher energy range. More precisely, if we focus on the detectability window of our interest say neutrino energy range of 10 - 30 MeV, it is difficult to identify clearly which flux is largest. Thus, from the detection point of view, it may not be possible to distinguish between the different scenarios with different fractions of black hole formation. This result is true for our choice of the simulation models and it would be interesting to see if this changes for other simulations.

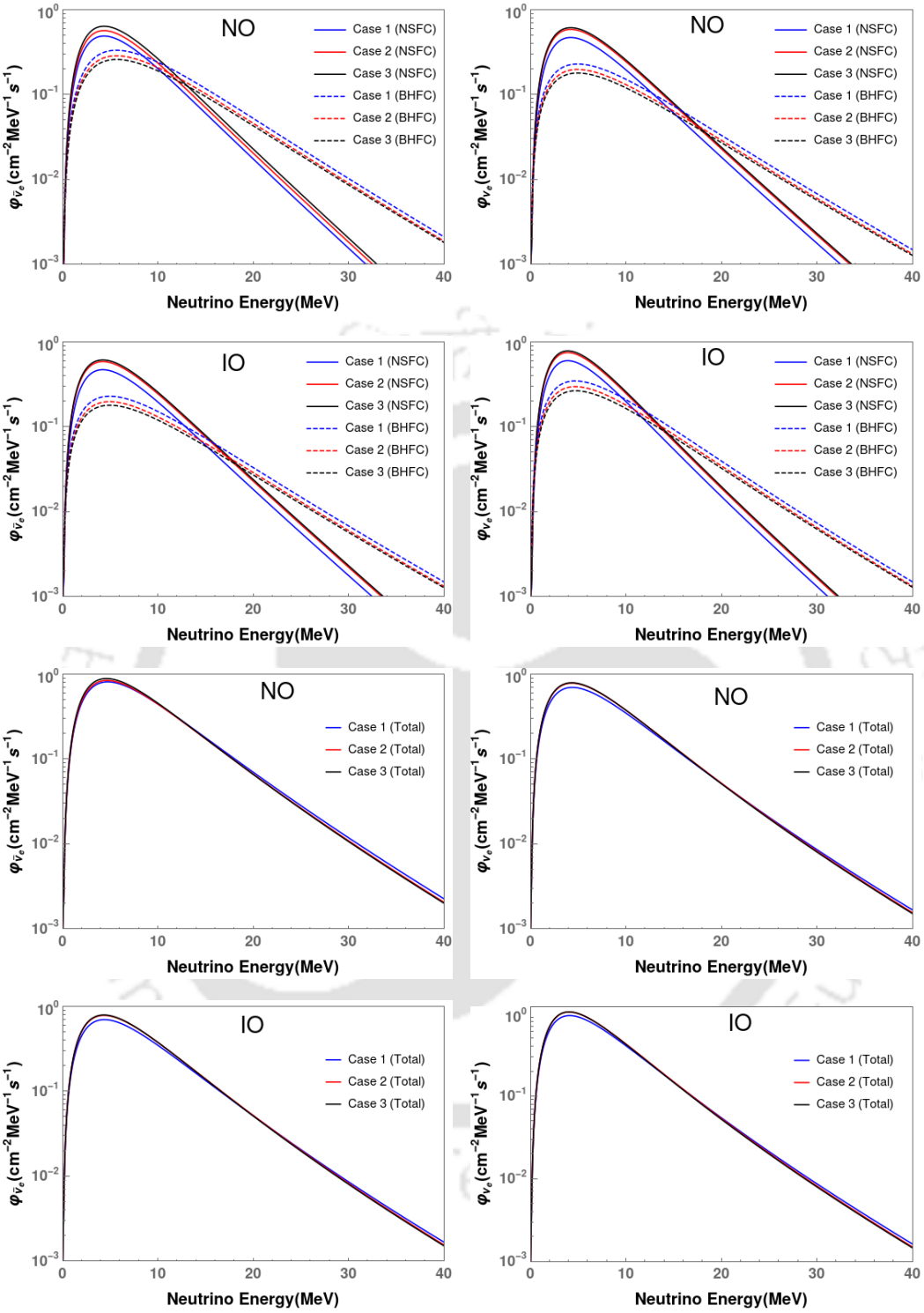

Figure 5.2: DSNB fluxes for the three different cases of black hole fractions. The left panels are for $\bar{\nu}_e$ flux and right panels are for ν_e. The top four panels represents the DSNB flux for both NSFCs and BHFCs. The lower four panels refer to the DSNB flux by summing up the contributions from the NSFCs and BHFCs for the three cases. Here, NO and IO denotes normal and inverted ordering respectively.

5.5.2 Oscillation scenarios

Now, we wish to see the effect of the two oscillation scenarios on the flux. So, we fix the fraction of black hole forming collapses $f = 44\%$. With this consideration we compute the total diffuse fluxes of $\bar{\nu}_e$ and ν_e. This is shown in Figure 5.3 where the left panel corresponds to flux of $\bar{\nu}_e$ and right panel is for ν_e. The solid blue and red lines represents the only MSW oscillation with normal and inverted ordering respectively. The solid black lines refer to the scenario of flavor equilibration. Note that as expected the DSNB flux in the scenario of flavor equilibrium is between that of the two extreme cases of normal and inverted ordering.

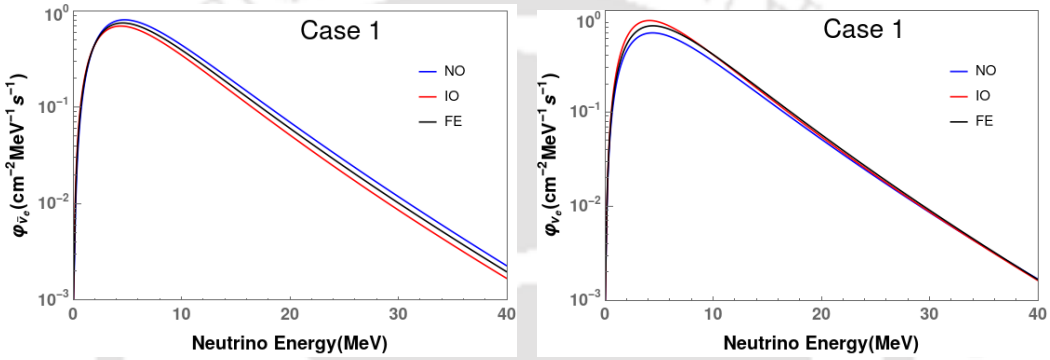

Figure 5.3: DSNB flux for the case 1 (f=44%) taking into consideration two oscillation scenarios. NO refers to normal ordering, IO is inverted ordering and FE represents the flavor equilibration scenario. The left panel shows the $\bar{\nu}_e$ flux and right one is for ν_e.

5.5.3 Dependence on SN simulations

Further, we present a comparison between the diffused fluxes calculated with parameter values from two different simulations in Figure 5.4. Fixing $f = 44\%$ and the oscillation scenario to be only MSW (normal ordering), we calculate DSNB flux taking into consideration progenitors from the Garching and Nakazato simulations. We consider the Nakazato models [289, 290], where we take into account three neutron star forming progenitors of masses $13M_\odot$, $20M_\odot$ and $50M_\odot$ and one progenitor mass of $30M_\odot$ for the black hole forming collapse. In Figure 5.4, the blue solid line corresponds to the diffuse flux by considering Garching models and red one is for Nakazato models. The difference in the fluxes in both scenarios is due to the differences in the average energies and the luminosities of different neutrino flavors.

To summarize the results, we consider the DSNB flux corresponding to the highest and lowest value of f. The DSNB flux vs neutrino energy for both the mass

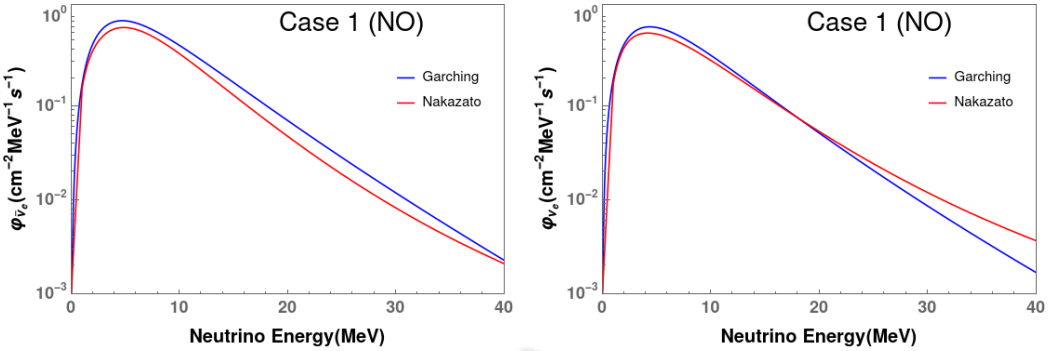

Figure 5.4: DSNB flux for the parameter values taken from two different simulations (Garching [35, 280, 281] and Nakazato [289, 290]) for case 1 ($f = 44\%$). The mass ordering is considered to be normal. The left panel shows the $\bar{\nu}_e$ flux and right one is for ν_e.

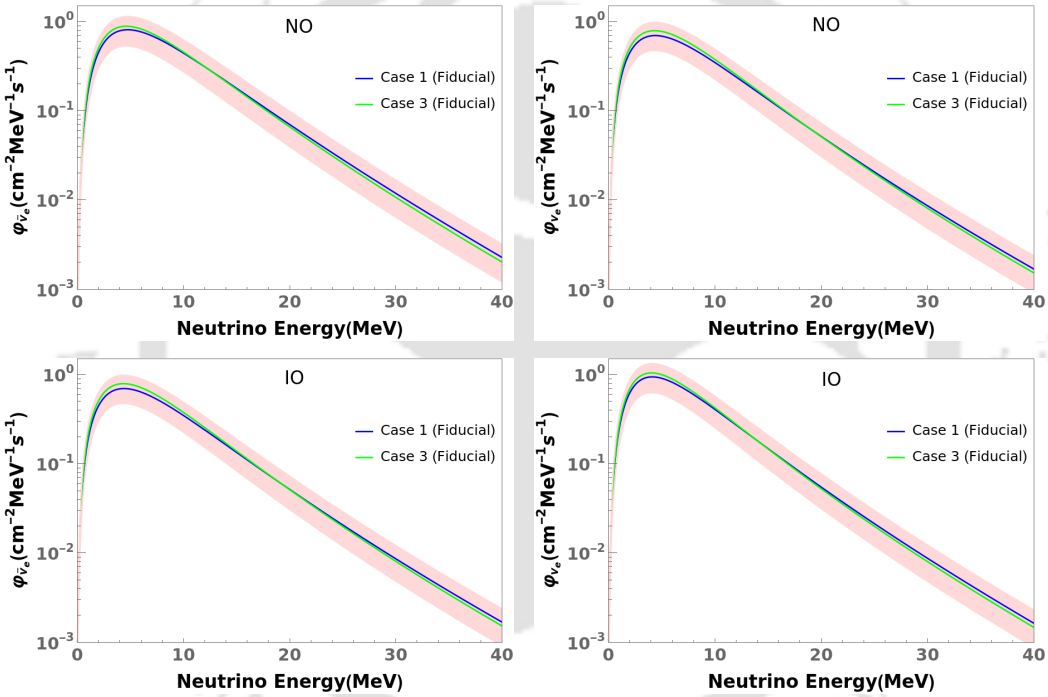

Figure 5.5: DSNB flux for the two extreme cases of black hole forming fraction, i.e. case 1 ($f = 44\%$) and case 3 ($f = 28\%$). The red band represents the uncertainty in the the DSNB flux due to the uncertainty in the black hole fractions (f) for our three cases considered. The upper curve of the red band is for case 1 taking into account $R_{cc}(0) = (1.25+0.5) \times 10^{-4}\,\mathrm{yr}^{-1}\,\mathrm{Mpc}^{-3}$ and the lower curve is for case 3 with $R_{cc}(0) = (1.25\text{-}0.5) \times 10^{-4}\,\mathrm{yr}^{-1}\,\mathrm{Mpc}^{-3}$. The left panels are for $\bar{\nu}_e$ and right panels are for ν_e. NO and IO refers to normal and inverted ordering respectively.

orderings is shown in figure 5.5. The upper panels depict the normal ordering and the lower ones are for inverted ordering. The left and right panels represent the fluxes for $\bar{\nu}_e$ and ν_e respectively. For each of the mass ordering, we choose the case having maximum and minimum flux. This flux is calculated taking into account

the fiducial value of the local supernova rate. The blue line corresponds to the flux for case 1, i.e. one having highest black hole fraction ($f = 44\%$) and the case 3 with lowest black hole fraction ($f = 28\%$) is represented by the green line. The red band depicts the range within which the DSNB flux can vary due to the uncertainty in the fraction of black hole forming collapses for our three considered scenarios taking into account the uncertainty in the local supernova rate. The upper line of the red band corresponds to the DSNB flux calculated for case 1 with $R_{cc}(0) = (1.25+0.5) \times 10^{-4}\,yr^{-1}\,Mpc^{-3}$ and the lower line is for case 3 with $R_{cc}(0) = (1.25-0.5) \times 10^{-4}\,yr^{-1}\,Mpc^{-3}$. This shows that the largest uncertainty in the DSNB flux arises due to the uncertainty in the normalization of the supernova rate. It is not possible to distinguish or detect any effects on DSNB which falls within this band.

5.6 Number of events

Taking into consideration all the above scenarios, we calculate the number of events which are expected to be recorded in a time period of 10 years. We use the public package SNOwGLoBES which makes use of the GLoBES front-end software to calculate the number of events [303]. The events are calculated for 22.5 kton Gd doped Super-Kamiokande, 187 kton Hyper-Kamiokande and 40 kton DUNE. We consider both the oscillation scenarios for our analysis. The event number is plotted with the detected energy (e^+ for GdSK, HK and e^- for DUNE) in figure 5.6. Here, we show only the scenario where only MSW resonance is taken into account. The left panels correspond to the case of normal ordering (NO) and right ones are for inverted ordering (IO). The topmost panel shows the events for the gadolinium doped SK, middle panel represents the HK events and the lowest panel is for DUNE. The blue and orange lines refer to the case 1 ($f = 44\%$) and case 3 ($f = 28\%$) respectively. The events are plotted in energy bins of 5 MeV.

The number of events corresponding to the detectable neutrino energy window for the three detectors are listed in Tables 5.3 and 5.4. Here, both the oscillation scenarios have been shown. Table 5.3 corresponds to the case 1 ($f = 44\%$) and case 3 ($f = 28\%$) is shown in table 5.4. Focussing on the number of events, it is clear that neither of the three detectors taken into consideration will be able to distinguish between the two oscillation scenarios. However, for higher black hole forming fraction case, i.e. case 1, we see that HK might be able to distinguish between the mass ordering at 1 σ.

Oscillation Scenario	Gd SK (10-30) MeV	HK (19.3-30) MeV	DUNE (20-40) MeV
Only MSW (NO)	18.97	63.27	6.53
Only MSW (IO)	14.20	46.33	6.72
FE	16.52	54.55	7.03

Table 5.3: Number of expected events in 10 years in 22.5 kton of GdSK, 187 kton of HK and 40 kton of DUNE for case 1 ($f = 44\%$). The neutrino energy ranges for which events are calculated are shown in paranthesis. Here events for both the oscillation scenarios have been shown.

Oscillation Scenario	Gd SK (10-30) MeV	HK (19.3-30) MeV	DUNE (20-40) MeV
Only MSW (NO)	18.28	58.84	6.26
Only MSW (IO)	14.45	45.27	6.28
FE	16.31	51.85	6.68

Table 5.4: Number of expected events in 10 years in 22.5 kton of GdSK, 187 kton of HK and 40 kton of DUNE for case 3 ($f = 28\%$). The neutrino energy ranges for which events are calculated are shown in paranthesis. Here events for both the oscillation scenarios have been shown.

5.7 Discussion

Various studies have been carried out in the literature to probe the detection prospects of DSNB flux in the current and upcoming neutrino detectors. Earlier studies were based on the contribution of only the neutron star forming collapses in the diffuse flux. However, the significance of the contribution of the black hole forming collapses has also been investigated in the later studies. In this chapter, we calculate the DSNB flux taking into account three different fractions of the black hole forming collapses motivated from [268]. Our main aim is to explore the various uncertainties in the DSNB flux and the detection prospect of that in Gadolinium doped Super

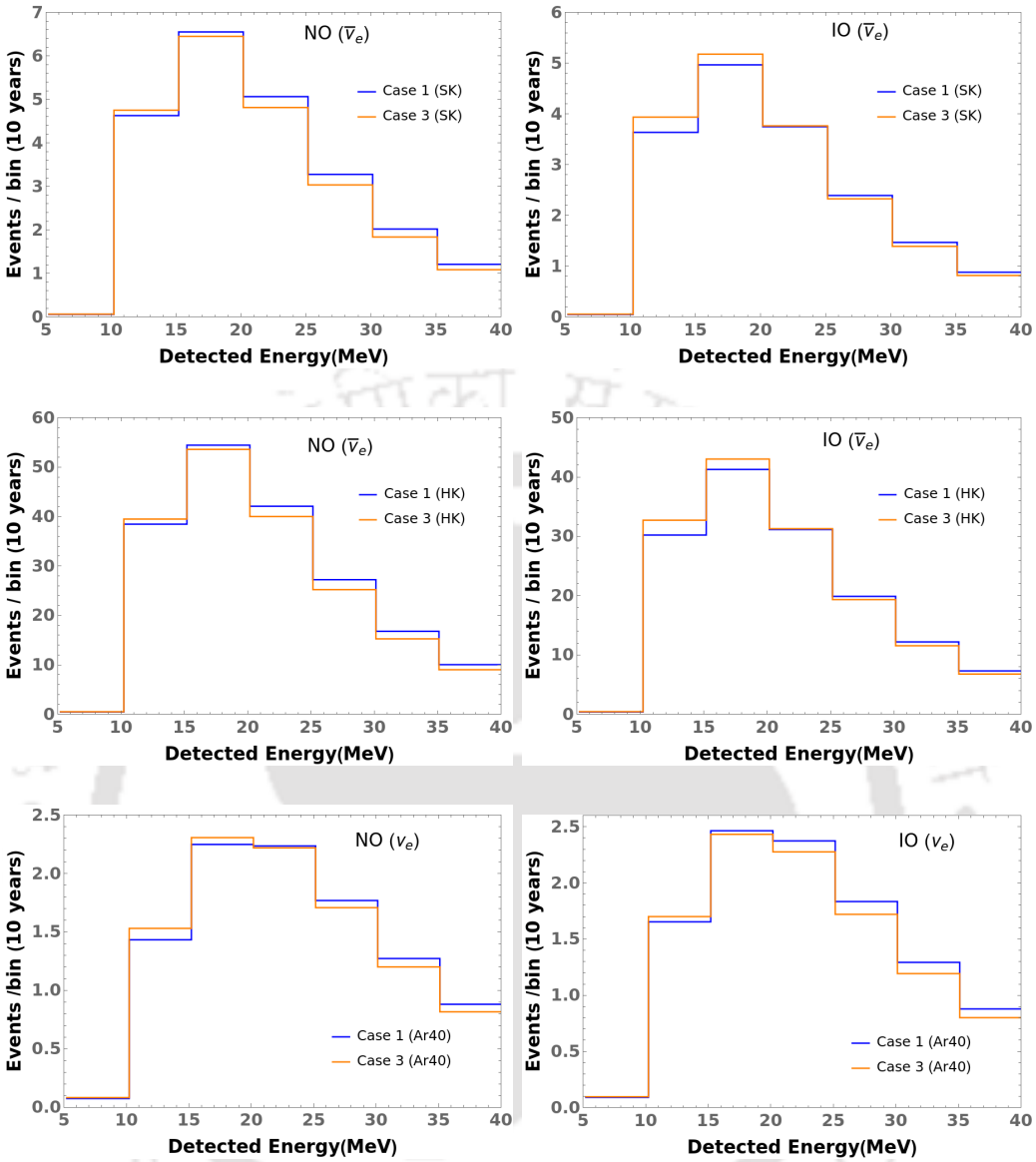

Figure 5.6: Expected number of events per bin vs the detected energy in 10 years. The bin size is taken to be 5 MeV. The topmost panels shows the $\bar{\nu}_e$ events in 22.5 kton GdSK, middle panels represent the $\bar{\nu}_e$ events in 187 kton HK and lowermost panels show the ν_e events in 40 kton of DUNE. Here, NO and IO denote normal and inverted ordering respectively.

Kamiokande, Hyper Kamiokande and DUNE detectors.

We first analyze the diffuse flux for the three cases of black hole fractions considered. As expected, we find that the DSNB flux at higher energies is dominated by BHFCs whereas NSFCs dominate at lower energies. Moreover, for the BHFCs, the flux for the case with highest fraction is more whereas it is opposite for that of NSFCs. So if we focus on the total diffuse flux which is the sum of the contribution

due to NSFCs and BHFCs, we see an interesting feature. At lower energy values where the diffuse flux due to the NSFCs is more compared to that of BHFCs, the total diffuse flux has the highest value for case 3 ($f = 28\%$). On the other hand, the total diffuse flux is largest for case 1 ($f = 44\%$) for higher energies as the BHFCs contribution to the flux dominates over that of NSFCs in that energy range. However, when we probe the total flux these effects compensate each other and the fluxes are very similar. Infact, distinguishing them at the detection level is difficult.

Taking into consideration the case having largest black hole fraction ($f = 28\%$), we investigate the two different oscillation scenarios. Firstly, we assume that there are only MSW conversions at large distances from the core and the collective oscillations are matter suppressed. Under this scenario, we study the effect in both the mass orderings. Secondly, we take into account the fast flavor conversions deep inside the SN which are believed to result in eqilibrium among all the neutrino flavors. We calculate the diffuse flux and find that the flux for the case of flavor equilibration lies in between the two extreme cases of normal and inverted ordering.

The value of the diffuse flux depends strongly on the input parameters in its calculation, i.e. average energy, luminosities etc. These input parameters are obtained from the simulations and thus vary with the different simulations. So we also calculate the diffuse flux for input parameters from two different simulation groups (Garching and Nakazato) and observe that there are differences between them.

We find that above all the uncertainties, the largest is due to the uncertainty in the local supernova rate. Taking this into account, we determine the range of DSNB flux for our considered cases of highest and lowest black hole fractions. Finally we calculate the number of events for 10 years in the detectable energy window for $\bar{\nu}_e$ flux in two water Cherenkov detectors (Gd doped SK and HK) and ν_e flux in the liquid Argon detector (DUNE). We find that the distinction between the two oscillation scenarios is not possible in any of the detectors.

In the Garching simulation, the average energies of the different flavors for the time integrated spectra are very similar. This might be due to the largest cooling phase of the emission where the fluences for different flavors are expected to be same. This in turn makes the phenomenology of oscillation scenarios difficult as the fluxes of different flavors are very similar.

However, the analysis with the Nakazato simulation shows departure from this behaviour. This is also due to the difference of neutrino spectra between the simulations. Hence it would be interesting to see if future simulations show closer or separable average energies for different flavors.

5.8 Observable effects

In addition to DSNB, there can be some potential observable signatures of neutrino flavor conversions for a galactic supernova. One of the implications of the self-induced flavor conversions is the spectral swap between the $\nu_e, \bar{\nu}_e$ and $\nu_x, \bar{\nu}_x$ for specific energy ranges which further lead to the spectral splits. The modification in the neutrino signal due to these spectral splits can be observed in the large underground detectors [304]. The detection of the neutronization burst signal can be one of the interesting probes of the flavor conversions in supernova as it has been found to be almost independent of the mass of the progenitor and the nuclear equation of state [305]. The oscillation effects on the neutronization burst signal is only due to MSW resonance as the self induced flavor conversions will be suppressed during this phase. Moreover, this signal is sensitive to the mass ordering. While the Water Cherenkov detectors can detect the neutronization burst through the elastic scattering of ν_e on e^-, liquid argon detectors are more sensitive to the signal through charged current interactions of ν_e. Various nonstandard effects like neutrino decay [306], active to light sterile neutrino oscillations [307], Lorentz invariance violation [308] and neutrino-antineutrino oscillations mediated by a neutrino magnetic moment [309] can also be constrained through the neutronization burst signal detection. Another way of identifying the neutrino mass ordering is through the analysis of the rise time of the $\bar{\nu}_e$ light curve of a galactic SN observable in large underground detectors like IceCube [310]. This is based on the fact that the ν_e flux at Earth is dependent on the original $\bar{\nu}_x$ for inverted ordering and original $\bar{\nu}_e$ for the normal one [88, 311–313]. From simulations, it has been seen that there is a significant difference in the temporal profiles of the original $\bar{\nu}_e$ and $\bar{\nu}_x$ in the accretion phase. This allows us to differentiate between the two mass orderings. In [314], a method has been shown for determining the mass ordering using the time information of the early supernova neutrino events at the future detectors like DUNE, JUNO and Hyper-Kamiokande. The Earth matter effects on the neutrino oscillations can cause modulations in the SN neutrino signal which has been studied in [88, 315, 316]. These effects are also sensitive to the mass ordering.

In addition to this, studies have been carried out regarding the effect of oscillations on the shock-wave propagation [97, 317–319] and turbulence [320–322] in the density of the stellar envelope. In [138], method have been shown to distinguish the flavor equalization due to fast flavor conversions from the scenario of MSW resonance during the accretion phase in a model independent way.

Chapter 6

Conclusion

The study of neutrino oscillations is one of the important aspects of the physics beyond Standard Model. While the Standard Model predicts the neutrino to be a massless particle, the discovery of the phenomenon of neutrino oscillations provides a proof contrary to it. The different neutrino experiments investigating the neutrinos from the Sun, atmosphere, reactors and accelerators provide an evidence for the existence of neutrino oscillations indicating that neutrinos are not massless. The flavor and mass eigenstates of the neutrinos are different and thus they can change their flavor from one to another through the quantum mechanical phenomenon known as the neutrino oscillation. In addition to the vacuum oscillations, neutrinos undergo flavor conversions while passing through a medium. The constituents of the medium create an effective potential for the neutrinos. This leads to the enhancement of the flavor oscillations which is known as the Mikheyev-Smirnov-Wolfenstein (MSW) resonance. The knowledge of the oscillation parameters governing the framework of the three flavor oscillations is crucial to have a complete understanding of the neutrino oscillation phenomenon. The main motive of the various neutrino oscillation experiments is to determine these parameters precisely. Currently, five out of the six oscillation parameters are known with great precision. The mass ordering and the CP violating phase still need to be determined. In chapter 1, we have presented an introduction to the phenomenon of neutrino oscillations. We have discussed the vacuum oscillations and the MSW resonance. Finally we have presented an overview of the current status of the understanding of the three flavor oscillations.

Another source of neutrino other than the Sun, reactors, atmosphere etc. is a core-collapse supernova. A Type II supernova explosion also known as the core-collapse supernova is accompanied by the emission of a large number of MeV energy neutrinos. These neutrinos carry away almost 99 % of the total gravitational energy

released in the explosion. The exact explosion mechanism of a star into a supernova is still not known. However the hydrodynamical simulations over the years suggest that the neutrinos might be the driving factor. Thus, the neutrinos released as a result of a supernova explosion can act as an indirect probe of the nuclear processes at the core. In the initial half of chapter 2, we have provided a detailed explaination of the explosion mechanism of the core-collapse supernova and the emisssion of neutrinos. The later part of chapter 2 focusses on the oscillations of the neutrinos in a dense environment like supernova.

The evolution of neutrinos through the medium of a core-collapse supernova is a complex problem. This is due to the non-linear nature of the equations of motion governing the system. The non-linearity arises due to the neutrino-neutrino interactions which become significant inside a dense medium like supernova. Therefore, in addition to the MSW resonance phenomenon which occurs due to the interaction of neutrinos with the ordinary background matter, flavor conversions known as collective oscillations also take place. In this phenomenon, the neutrinos having different energies undergo flavor conversions in a coherent manner. Both the presence and outcome of these collective oscillations have been extensively studied in more than last two decades. Due to the numerical complexities involved in solving the full evolution equation of the neutrinos in a dense medium, a semi-analytical method has been adopted. This method is known as the 'Linear Stability Analysis'. The onset of the collective flavor conversions can be predicted by this method. It has been found from the studies that these self-induced flavor conversions grow in two different time scales. The one depending on the vacuum oscillation frequency ω_{vac} is termed as the slow oscillation while the other one depending on the neutrino-neutrino strength μ_0 is called fast oscillations. The slow modes usually develop with a rate proportional to $\omega_{vac} \sim \mathcal{O}(1)$ km^{-1} at a distance of around few hundred kms from the neutrinosphere. On the other hand, the growth rate of the fast modes is proportional to $\mu_0 \sim 10^5$ km $^{-1}$ and takes place deeper inside close to neutrinosphere. There are three possible regions inside the supernova where the fast conversions can occur. Studies have shown that due to strong convective activity in the proto-neutron star, the fast flavor conversions can occur inside the neutrinosphere (10 km $\lesssim$ r $\lesssim$ 20 km) [132]. One possible location of the occurrence of fast conversions is the neutrino decoupling region [196, 224]. The angular crossings develop in the neutrino decoupling region (r $\sim$ 30-100 km) due to the difference in the interaction cross section of ν_e and $\bar{\nu}_e$ with the nucleons. Recent studies [195] have also shown the occurrence of fast oscillations in the pre-shock region at r $\sim \mathcal{O}(200)$ km as a result of backward

scattering of neutrinos from the heavy nuclei. Moreover these fast oscillations are found to occur even in the absence of neutrino mixing. Since these fast oscillations occur deep inside, near the neutrinospheres, they can have a drastic impact on the shockwave revival and nucleosynthesis.

All the previous studies in the context of slow and fast oscillations have been carried out in the effective two flavor case. In this scenario, the non electron flavors of neutrino and antineutrino are assumed to have similar fluxes. This assumption is based on the fact that in the absence of muons and taus in the supernova environment, the non electron flavors of neutrinos are produced only through the thermal pair processes and thus are expected to have similar fluxes. However, the 2D simulations with the presence of muons in the accretion phase leads to the softening of neutron star equation of state and its faster contraction. As a result, the luminosities and the average energies of the emitted neutrinos are found to be higher which further helps in successful neutrino driven explosions. So, now the presence of muons would lead to an asymmetry in the fluxes of the muon and tau neutrinos and antineutrinos. Motivated by this, we carry out the investigation of the slow and fast oscillations in the complete three flavor scenario.

In chapter 3, we present our analysis of the slow and fast instabilities in the linearized regime for the complete three flavor scenario based on [212]. We have considered the system to be isotropic and have studied only the spatial evolution for the slow oscillations. In case of fast oscillations, we performed a generalized analysis. In contrast to the effective two flavor studies, we obtained three independent linearized equations of motion. Each of the equations can be considered as a two flavor system corresponding to the e-μ, e-τ and $\mu - \tau$ sectors. The instabilities are found to be present for both the mass orderings, similar to the two flavor case. We find Bimodal instability for the inverted ordering and Multi Azimuthal Angle and Multi Zenith Angle for the normal ordering. Here, we also obtain the instabilities for the $\mu - \tau$ sector additionally. The onset of the growth of the instability in the solar sector is found to be at a lower radius as compared to the atmospheric sector. However, with the inclusion of the third flavor, the growth in the solar sector may get faster. In this way, our linearized slow oscillation results are in excellent qualitative agreement with the previous non-linear three flavor studies. We also a obtain a similar effect of the third flavor in the case of fast oscillations. Here we obtain three dispersion relations corresponding to the three sectors. In contrast to only one flavor lepton number, i.e. ELN, now there are two more corresponding to the other two flavors which we term as MuLN and TauLN. The crossings in MuLN

and TauLN would also be important now to study the fast oscillations. Depending on the values of the angular densities chosen, we obtain four kinds of instabilities, namely completely stable, damped stable, convective and absolute corresponding to each of the off-diagonal element. The presence of similar kinds of instabilities in all the sectors is a result of our assumption of same angular distributions. However, the different angular distributions may lead to different stability picture in different flavors. In contrast to the previous studies, here the matter terms cannot be rotated away simultaneously as they are different for the different sectors. This indicates that the modes unstable for some λ may be stable for the other. However, due to the larger growth rate in the scenario of fast conversions, this effect may be reduced due to negligible cascading between the modes. All our results are based on the linear analysis. The non-linear analysis will provide a better picture of the influence of the three flavor analysis on the collective oscillations.

In chapter 4, we discuss the non-linear analysis of particularly the fast oscillations in the complete three flavor scenario. This provides us a better understanding of the effects obtained in the linear analysis. Here, we consider four toy examples of the angular distributions of the neutrinos of different flavors. We solve the complete non-linear equation of motion considering only time evolution in [219] and then both space and time evolution (1+1 D) in [221]. The differences which are expected between ν_μ and $\bar{\nu}_\mu$ due to the presence of the muons in the core can create observable changes in the angular distributions of the lepton number. In addition to the usually considered ELN, there is also MuLN and TauLN. Since the quantity of interest in studying fast oscillations is the difference between the flavor lepton numbers, the combined effect of the ELN, MuLN and TauLN are found to be crucial. The consideration of the six neutrino species instead of three can modify the angular crossings originally present. To be precise, they can be either erased or created in the six species scenario which is shown in our examples. Moreover, one should be cautious especially in the case of shallow crossings in the ELN. This is because there is a possibility of such crossings being nullified by an opposite crossing in the MuLN. This would make an otherwise stable system in two flavor case unstable in the three flavor scenario. This particular case is relevant in the shock region where there can be an appreciable number of ν_μ and ν_τ. From the point of view of linear stability analysis, we find that the linear picture cannot capture all the instability signatures of the full non-linear analysis. The role of the third sector $(\mu - \tau)$ in triggering the instabilities in the otherwise stable sector can only be realized at the non-linear level. The qualitative nature of the results obtained in the case of

spatially homogeneous system (only time evolution) remain robust even for the both space and time evolution. Our non-linear results clearly explain the significance of detailed three-flavor treatments to find out whether these scenarios are actually realized in nature. The future muon SN simulations can provide a better insight in this direction.

In chapter 5, we discuss the phenomenological implication of the fast oscillations on the diffuse supernova neutrino background. We investigate the possibility of detecting the extreme effect of fast oscillations, i.e. flavor equilibration of the fluxes of different neutrino flavors in the upcoming water Cherenkov and liquid Argon detectors. Our analysis of the DSNB flux for three different fractions of black hole forming stars shows that as expected the contribution of the BHFCs is more at higher energy as compared to the lower energies. Moreover, when we compare the highest and lowest BH fraction (f) case, we find that for highest f, the flux is larger at the higher energies and smaller at lower energies. As a result, the total flux in both the cases are very similar. We also studied the dependence of the DSNB flux on the SN simulations. This is because the calculation of DSNB is based on the input parameters like average energy, luminosity etc. which vary with the different simulations. In the Garching simulations, from which we have used the input parameters, the average energies of the different flavors for the time integrated spectra are very similar. As a result, the DSNB fluxes we obtain are very similar. Thus, it is difficult to distinguish or detect the impact of the oscillation scenario in the detectors for the cases considered in our study. We find that the largest uncertainty in our DSNB fluxes correspond to the uncertainty in the local supernova rate and all other scenarios fall within it. It would be interesting to see if the future simulations show separable average energies for different flavors. This might make the study of impact of the oscillation scenarios on the DSNB flux possible from the detection point of view.

Thus, summarizing the thesis, it is focussed on the complete three flavor study of the collective oscillations in a core-collapse supernova. It broadly consists of two analyses. The first one focusses on the linear analysis of the three flavor treatment in the context of slow and fast collective oscillations. The second one investigates the non-linear aspect of that to have a better understanding of the linear results, particularly for the fast oscillation scenario. Finally the phenomenological implication of fast oscillations on DSNB is being discussed. We hope that the topics discussed in this thesis can be useful to have a better understanding of the neutrino flavor evolution in a core-collapse supernova.

6.1 Future outlook

The discussions presented in this thesis provide an explaination to some of the unsolved issues in the context of collective oscillations in supernova. However, this leads to many more ideas which can be explored further to enhance our understanding of the system. We present three of such ideas below.

In the method of linear stability analysis, the usual idea is to expand the evolution equation upto linear order of the off-diagonal elements of the matrix of densities ϱ [203]. Then the ϱ matrices are expressed in terms of the Hermitian matrix 'S' whose off-diagonals are taken upto linear order. Now instead of this, if we consider these off-diagonals of 'S' beyond linear order, the equations of motion will change. In that case, the usual way of considering an exponential ansatz may not be enough to solve the equations of motion. It would be interesting to look into this scenario and find out a way to solve the equations. It might be possible that this method would provide us some more information than just predicting the onset of the growth of the flavor instabilities.

One interesting aspect in the study of fast oscillations can be to look into the effect of the presence of sterile neutrinos in the supernova environment. The various studies in the literature [323–327] have shown that depending on the mass squared difference of the active and sterile species, two types of MSW resonances are possible. The inner resonance takes place at around few tens of km whereas the outer resonance occurs at around hundreds of km. We have performed some preliminary analysis to investigate the effect of the creation of the sterile neutrinos through MSW resonance on the fast oscillations. We have considered a 2+1 scenario, i.e. two active and one sterile species. We have found that these sterile neutrinos can modify the crossings present in ELN. One interesting thing we note is that although it is not possible to generate new crossings in the presence of sterile species, it can nullify the originally present crossing. As a result, in either of the cases, fast oscillations can be suppressed. It would be interesting to study the effect in a 3+1 flavor scenario.

The study of the diffuse supernova neutrino background can be useful in probing various new physics scenarios. One such scenario is the resonant absorption of these neutrinos while they pass through the intergalactic matter before reaching the detector on Earth. This topic has been investigated in the previous studies [328] and it has been found that such interactions can lead to a dip in the spectrum of the supernova relic neutrinos. The idea is that there is a scalar or fermion dark matter (DM) with the mass in the range of MeV or lower and has Yukawa couplings to

neutrinos and a new fermion or scalar, the mass being in the range of MeV or lower. In such a case, the resonant interaction of the DSNB with DM can result in a dip in the spectrum. This study has been done in the literature by taking into account only the contribution of the neutron stars in the calculation of DSNB spectrum. It would be interesting to see if in the framework of our analysis where we take both the BHFCs and NSFCs in calculating DSNB flux, similar or some new signature of this new physics interaction show up. Another point can be to probe this new physics signature in DSNB under the consideration of the flavor equilibration scenario.

Bibliography

[1] W. Pauli, *Dear radioactive ladies and gentlemen*, *Phys. Today* **31N9** (1978) 27.

[2] W. Pauli, *On the Earlier and more recent history of the neutrino*, *Camb. Monogr. Part. Phys. Nucl. Phys. Cosmol.* **14** (2000) 1.

[3] F. Reines, *The neutrino: from poltergeist to particle*, *Rev. Mod. Phys.* **68** (1996) 317.

[4] Particle Data Group collaboration, *Review of Particle Physics*, .

[5] B. T. Cleveland, T. Daily, J. Raymond Davis, J. R. Distel, K. Lande, C. K. Lee et al., *Measurement of the solar electron neutrino flux with the homestake chlorine detector*, *The Astrophysical Journal* **496** (1998) 505.

[6] GALLEX collaboration, *Results of the whole GALLEX experiment*, *Nucl. Phys. B Proc. Suppl.* **70** (1999) 284.

[7] SAGE collaboration, *Solar neutrino flux measurements by the Soviet-American Gallium Experiment (SAGE) for half the 22 year solar cycle*, *J. Exp. Theor. Phys.* **95** (2002) 181 [astro-ph/0204245].

[8] KamLAND collaboration, *Measurement of neutrino oscillation with KamLAND: Evidence of spectral distortion*, *Phys. Rev. Lett.* **94** (2005) 081801 [hep-ex/0406035].

[9] SNO collaboration, *Electron energy spectra, fluxes, and day-night asymmetries of B-8 solar neutrinos from measurements with NaCl dissolved in the heavy-water detector at the Sudbury Neutrino Observatory*, *Phys. Rev. C* **72** (2005) 055502 [nucl-ex/0502021].

[10] Super-Kamiokande collaboration, *Solar neutrino measurements in super-Kamiokande-I*, *Phys. Rev. D* **73** (2006) 112001 [hep-ex/0508053].

[11] Super-Kamiokande collaboration, *Evidence for oscillation of atmospheric neutrinos*, *Phys. Rev. Lett.* **81** (1998) 1562 [hep-ex/9807003].

[12] Super-Kamiokande collaboration, *Neutrino induced upward stopping muons in Super-Kamiokande*, *Phys. Lett. B* **467** (1999) 185 [hep-ex/9908049].

[13] MACRO collaboration, *Atmospheric neutrino oscillations from upward through going muon multiple scattering in MACRO*, *Phys. Lett. B* **566** (2003) 35 [hep-ex/0304037].

[14] Super-Kamiokande collaboration, *Evidence for an oscillatory signature in*

atmospheric neutrino oscillation, *Phys. Rev. Lett.* **93** (2004) 101801 [hep-ex/0404034].

[15] Daya Bay collaboration, *Observation of electron-antineutrino disappearance at Daya Bay*, *Phys. Rev. Lett.* **108** (2012) 171803 [1203.1669].

[16] RENO collaboration, *Observation of Reactor Electron Antineutrino Disappearance in the RENO Experiment*, *Phys. Rev. Lett.* **108** (2012) 191802 [1204.0626].

[17] Double Chooz collaboration, *Reactor electron antineutrino disappearance in the Double Chooz experiment*, *Phys. Rev. D* **86** (2012) 052008 [1207.6632].

[18] K2K collaboration, *Evidence for muon neutrino oscillation in an accelerator-based experiment*, *Phys. Rev. Lett.* **94** (2005) 081802 [hep-ex/0411038].

[19] MINOS collaboration, *Measurement of the Neutrino Mass Splitting and Flavor Mixing by MINOS*, *Phys. Rev. Lett.* **106** (2011) 181801 [1103.0340].

[20] T2K collaboration, *Measurement of Neutrino Oscillation Parameters from Muon Neutrino Disappearance with an Off-axis Beam*, *Phys. Rev. Lett.* **111** (2013) 211803 [1308.0465].

[21] B. Pontecorvo, *Inverse beta processes and nonconservation of lepton charge*, *Zh. Eksp. Teor. Fiz.* **34** (1957) 247.

[22] Z. Maki, M. Nakagawa and S. Sakata, *Remarks on the unified model of elementary particles*, *Prog. Theor. Phys.* **28** (1962) 870.

[23] L. Wolfenstein, *Neutrino oscillations in matter*, *Phys. Rev. D* **17** (1978) 2369.

[24] L. Wolfenstein, *Neutrino Oscillations in Matter*, *Phys. Rev. D* **17** (1978) 2369.

[25] S. P. Mikheyev and A. Y. Smirnov, *Resonance Amplification of Oscillations in Matter and Spectroscopy of Solar Neutrinos*, *Sov. J. Nucl. Phys.* **42** (1985) 913.

[26] S. P. Mikheev and A. Y. Smirnov, *Resonance Oscillations of Neutrinos in Matter*, *Sov. Phys. Usp.* **30** (1987) 759.

[27] A. Y. Smirnov, *The MSW effect and solar neutrinos*, in *10th International Workshop on Neutrino Telescopes*, pp. 23–43, 5, 2003, hep-ph/0305106.

[28] S. P. Rosen, *Msw effect and solar neutrino experiments*, .

[29] G. L. Fogli, E. Lisi and D. Montanino, *Matter enhanced three flavor oscillations and the solar neutrino problem*, *Phys. Rev. D* **54** (1996) 2048 [hep-ph/9605273].

[30] A. S. Joshipura and P. I. Krastev, *Common origin for the solar and atmospheric neutrino deficits*, *Phys. Rev. D* **50** (1994) 3484 [hep-ph/9308348].

[31] M. Lindner, *The Physics Potential of Future Long-Baseline Neutrino Oscillation Experiments*, pp. 209–242. Springer Berlin Heidelberg, Berlin, Heidelberg, 2003. 10.1007/978-3-540-44901-0$_7$.

[32] M. Freund, M. Lindner, S. T. Petcov and A. Romanino, *Testing matter effects in very long baseline neutrino oscillation experiments*, *Nucl. Phys. B* **578** (2000) 27 [hep-ph/9912457].

[33] W. Winter, *Direct test of the msw effect by the solar appearance term in beam experiments*, *Physics Letters B* **613** (2005) 67.

[34] H. A. Bethe, *Supernova mechanisms*, *Rev. Mod. Phys.* **62** (1990) 801.

[35] A. Mirizzi, I. Tamborra, H.-T. Janka, N. Saviano, K. Scholberg, R. Bollig et al., *Supernova Neutrinos: Production, Oscillations and Detection*, *Riv. Nuovo Cim.* **39** (2016) 1 [1508.00785].

[36] "IAU Circular 4316 (1987)." http://www.cbat.eps.harvard.edu/iauc/04300/04316.html.

[37] C. Giunti and C. W. Kim, *Fundamentals of Neutrino Physics and Astrophysics*. 2007.

[38] E. K. Akhmedov, *Neutrino physics*, in *ICTP Summer School in Particle Physics*, pp. 103–164, 6, 1999, hep-ph/0001264.

[39] M. Escudero, T. Schwetz and J. Terol-Calvo, *A seesaw model for large neutrino masses in concordance with cosmology*, 2211.01729.

[40] KATRIN collaboration, *Improved Upper Limit on the Neutrino Mass from a Direct Kinematic Method by KATRIN*, *Phys. Rev. Lett.* **123** (2019) 221802 [1909.06048].

[41] Y. Farzan and S. Hannestad, *Neutrinos secretly converting to lighter particles to please both KATRIN and the cosmos*, *JCAP* **02** (2016) 058 [1510.02201].

[42] M. Steidl, *Experiments for the absolute neutrino mass measurement*, in *Heavy Quarks and Leptons 2008 (HQ&L08)*, 6, 2009, 0906.0454.

[43] S. Pascoli, S. T. Petcov and C. E. Yaguna, *Quasidegenerate neutrino mass spectrum, mu —> e + gamma decay and leptogenesis*, *Phys. Lett. B* **564** (2003) 241 [hep-ph/0301095].

[44] KATRIN collaboration, *Direct neutrino-mass measurement with sub-electronvolt sensitivity*, *Nature Phys.* **18** (2022) 160 [2105.08533].

[45] Planck collaboration, *Planck 2018 results. VI. Cosmological parameters*, *Astron. Astrophys.* **641** (2020) A6 [1807.06209].

[46] R. N. Mohapatra and P. B. Pal, *Massive neutrinos in physics and astrophysics*, vol. 41. 1991.

[47] SNO collaboration, *Measurement of the total active B-8 solar neutrino flux at the Sudbury Neutrino Observatory with enhanced neutral current sensitivity*, *Phys. Rev. Lett.* **92** (2004) 181301 [nucl-ex/0309004].

[48] Super-Kamiokande collaboration, *A Measurement of atmospheric neutrino oscillation parameters by SUPER-KAMIOKANDE I*, *Phys. Rev. D* **71** (2005) 112005 [hep-ex/0501064].

[49] Borexino collaboration, *First real time detection of Be-7 solar neutrinos by Borexino*, *Phys. Lett. B* **658** (2008) 101 [0708.2251].

[50] GALLEX collaboration, *GALLEX solar neutrino observations: Results for GALLEX IV*, *Phys. Lett. B* **447** (1999) 127.

[51] MINOS collaboration, *Measurement of Neutrino and Antineutrino Oscillations Using Beam and Atmospheric Data in MINOS*, *Phys. Rev. Lett.* **110** (2013) 251801 [1304.6335].

[52] I. Esteban, M. C. Gonzalez-Garcia, M. Maltoni, T. Schwetz and A. Zhou, *The fate of hints: updated global analysis of three-flavor neutrino oscillations*, *JHEP* **09** (2020) 178 [2007.14792].

[53] T2K collaboration, *Search for Electron Antineutrino Appearance in a Long-baseline*

Muon Antineutrino Beam, *Phys. Rev. Lett.* **124** (2020) 161802 [1911.07283].

[54] NOvA collaboration, *First Measurement of Neutrino Oscillation Parameters using Neutrinos and Antineutrinos by NOvA*, *Phys. Rev. Lett.* **123** (2019) 151803 [1906.04907].

[55] A. Morales and J. Morales, *The Neutrinoless double beta decay: The Case for germanium detectors*, *Nucl. Phys. B Proc. Suppl.* **114** (2003) 141 [hep-ph/0211332].

[56] S. Karmakar and M. K. Singh, *Current status of different detector technologies in the searches of $0\nu\beta\beta$ decay*, *Int. J. Mod. Phys. E* **30** (2021) 2130008.

[57] J. D. Vergados, H. Ejiri and F. Šimkovic, *Neutrinoless double beta decay and neutrino mass*, *Int. J. Mod. Phys. E* **25** (2016) 1630007 [1612.02924].

[58] F. Couchot, S. Henrot-Versillé, O. Perdereau, S. Plaszczynski, B. Rouillé d'Orfeuil, M. Spinelli et al., *Cosmological constraints on the neutrino mass including systematic uncertainties*, *Astron. Astrophys.* **606** (2017) A104 [1703.10829].

[59] A. Loureiro et al., *On The Upper Bound of Neutrino Masses from Combined Cosmological Observations and Particle Physics Experiments*, *Phys. Rev. Lett.* **123** (2019) 081301 [1811.02578].

[60] G. G. Raffelt, *Stars as laboratories for fundamental physics: The astrophysics of neutrinos, axions, and other weakly interacting particles*. 5, 1996.

[61] A. Mezzacappa, *Ascertaining the core collapse supernova mechanism: The state of the art and the road ahead*, *Annual Review of Nuclear and Particle Science* **55** (2005) 467 [https://doi.org/10.1146/annurev.nucl.55.090704.151608].

[62] K. Kotake, K. Sato and K. Takahashi, *Explosion mechanism, neutrino burst, and gravitational wave in core-collapse supernovae*, *Rept. Prog. Phys.* **69** (2006) 971 [astro-ph/0509456].

[63] S. Woosley and T. Janka, *The physics of core-collapse supernovae*, *Nature Phys.* **1** (2005) 147 [astro-ph/0601261].

[64] H.-T. Janka, K. Langanke, A. Marek, G. Martinez-Pinedo and B. Mueller, *Theory of Core-Collapse Supernovae*, *Phys. Rept.* **442** (2007) 38 [astro-ph/0612072].

[65] H.-T. Janka, *Explosion Mechanisms of Core-Collapse Supernovae*, *Ann. Rev. Nucl. Part. Sci.* **62** (2012) 407 [1206.2503].

[66] G. E. Brown, *The fate of massive stars - Collapse, bounce and shock formation*, in *Supernovae: A Survey of Current Research*, M. J. Rees and R. J. Stoneham, eds., vol. 90 of *NATO Advanced Study Institute (ASI) Series C*, pp. 13–33, Nov., 1982.

[67] W. Baade and F. Zwicky, *On super-novae*, *Proceedings of the National Academy of Sciences* **20** (1934) 254 [https://www.pnas.org/doi/pdf/10.1073/pnas.20.5.254].

[68] S. A. Colgate and R. H. White, *The Hydrodynamic Behavior of Supernovae Explosions*, *Astrophys. J.* **143** (1966) 626.

[69] H. A. Bethe and J. R. Wilson, *Revival of a stalled supernova shock by neutrino heating*, *Astrophys. J.* **295** (1985) 14.

[70] O. Just, R. Bollig, H.-T. Janka, M. Obergaulinger, R. Glas and S. Nagataki,

Core-collapse supernova simulations in one and two dimensions: comparison of codes and approximations, *Mon. Not. Roy. Astron. Soc.* **481** (2018) 4786 [1805.03953].

[71] B. Müller, *The Status of Multi-Dimensional Core-Collapse Supernova Models*, **33** (2016) e048 [1608.03274].

[72] J. R. Wilson and R. W. Mayle, *Convection in core collapse supernovae*, *Physics Reports* **163** (1988) 63.

[73] E. O'Connor and C. D. Ott, *THE PROGENITOR DEPENDENCE OF THE PRE-EXPLOSION NEUTRINO EMISSION IN CORE-COLLAPSE SUPERNOVAE*, *The Astrophysical Journal* **762** (2012) 126.

[74] E. P. O'Connor and S. M. Couch, *Two Dimensional Core-Collapse Supernova Explosions Aided by General Relativity with Multidimensional Neutrino Transport*, *Astrophys. J.* **854** (2018) 63 [1511.07443].

[75] T. Fischer, S. C. Whitehouse, A. Mezzacappa, F.-K. Thielemann and M. Liebendörfer, *Protoneutron star evolution and the neutrino-driven wind in general relativistic neutrino radiation hydrodynamics simulations*, *Astronomy and Astrophysics* **517** (2010) A80.

[76] A. Bandyopadhyay, P. Bhattacharjee, S. Chakraborty, K. Kar and S. Saha, *Detecting supernova neutrinos with iron and lead detectors*, *Phys. Rev. D* **95** (2017) 065022 [1607.05591].

[77] S. Chakraborty, T. Fischer, A. Mirizzi, N. Saviano and R. Tomas, *Analysis of matter suppression in collective neutrino oscillations during the supernova accretion phase*, *Phys. Rev. D* **84** (2011) 025002 [1105.1130].

[78] F. S. Kitaura, H.-T. Janka and W. Hillebrandt, *Explosions of O-Ne-Mg cores, the Crab supernova, and subluminous type II-P supernovae*, *Astron. Astrophys.* **450** (2006) 345 [astro-ph/0512065].

[79] L. Dessart, A. Burrows, C. Ott, E. Livne, S.-C. Yoon and N. Langer, *Multi-dimensional simulations of the accretion-induced collapse of white dwarfs to neutron stars*, *Astrophys. J.* **644** (2006) 1063 [astro-ph/0601603].

[80] T. Fischer, S. C. Whitehouse, A. Mezzacappa, F. K. Thielemann and M. Liebendorfer, *Protoneutron star evolution and the neutrino driven wind in general relativistic neutrino radiation hydrodynamics simulations*, *Astron. Astrophys.* **517** (2010) A80 [0908.1871].

[81] T. Melson, H.-T. Janka and A. Marek, *Neutrino-driven supernova of a low-mass iron-core progenitor boosted by three-dimensional turbulent convection*, *Astrophys. J. Lett.* **801** (2015) L24 [1501.01961].

[82] H. T. Janka, F. Hanke, L. Huedepohl, A. Marek, B. Mueller and M. Obergaulinger, *Core-collapse supernovae: Reflections and directions*, 2012. 10.48550/ARXIV.1211.1378.

[83] D. Vartanyan, A. Burrows, D. Radice, M. A. Skinner and J. Dolence, *Revival of the Fittest: Exploding Core-Collapse Supernovae from 12 to 25 $M_\odot$*, *Mon. Not. Roy. Astron. Soc.* **477** (2018) 3091 [1801.08148].

[84] I. Tamborra, F. Hanke, H.-T. Janka, B. Müller, G. G. Raffelt and A. Marek, *Self-sustained asymmetry of lepton-number emission: A new phenomenon during the*

supernova shock-accretion phase in three dimensions, *Astrophys. J.* **792** (2014) 96 [1402.5418].

[85] J. M. Blondin, A. Mezzacappa and C. DeMarino, *Stability of Standing Accretion Shocks, with an Eye toward Core-Collapse Supernovae*, **584** (2003) 971 [astro-ph/0210634].

[86] T. Foglizzo, R. Kazeroni, J. Guilet, F. Masset, M. González, B. Krueger et al., *The explosion mechanism of core-collapse supernovae: Progress in supernova theory and experiments*, *Publications of the Astronomical Society of Australia* **32** (2015) .

[87] R. Bollig, H. T. Janka, A. Lohs, G. Martinez-Pinedo, C. J. Horowitz and T. Melson, *Muon Creation in Supernova Matter Facilitates Neutrino-driven Explosions*, *Phys. Rev. Lett.* **119** (2017) 242702 [1706.04630].

[88] A. S. Dighe and A. Y. Smirnov, *Identifying the neutrino mass spectrum from the neutrino burst from a supernova*, *Phys. Rev. D* **62** (2000) 033007 [hep-ph/9907423].

[89] S. Horiuchi and J. P. Kneller, *What can be learned from a future supernova neutrino detection?*, *J. Phys. G* **45** (2018) 043002 [1709.01515].

[90] H. T. Janka and W. Hillebrandt, *Neutrino emission from type II supernovae : an analysis of the spectra.*, **224** (1989) 49.

[91] M. T. Keil, G. G. Raffelt and H.-T. Janka, *Monte Carlo study of supernova neutrino spectra formation*, *Astrophys. J.* **590** (2003) 971 [astro-ph/0208035].

[92] L. Stodolsky, *Treatment of neutrino oscillations in a thermal environment*, *Phys. Rev. D* **36** (1987) 2273.

[93] G. Sigl and G. Raffelt, *General kinetic description of relativistic mixed neutrinos*, *Nucl. Phys. B* **406** (1993) 423.

[94] T. K. Kuo and J. Pantaleone, *Nonadiabatic neutrino oscillations in matter*, *Phys. Rev. D* **39** (1989) 1930.

[95] T. K. Kuo and J. Pantaleone, *Supernova neutrinos and their oscillations*, *Phys. Rev. D* **37** (1988) 298.

[96] S. E. Woosley and T. A. Weaver, *The Evolution and explosion of massive stars. 2. Explosive hydrodynamics and nucleosynthesis*, *Astrophys. J. Suppl.* **101** (1995) 181.

[97] R. Tomas, M. Kachelriess, G. Raffelt, A. Dighe, H. T. Janka and L. Scheck, *Neutrino signatures of supernova shock and reverse shock propagation*, *JCAP* **09** (2004) 015 [astro-ph/0407132].

[98] T. Lund and J. P. Kneller, *Combining collective, msw, and turbulence effects in supernova neutrino flavor evolution*, *Phys. Rev. D* **88** (2013) 023008.

[99] F. N. Loreti, Y.-Z. Qian, G. M. Fuller and A. B. Balantekin, *Effects of random density fluctuations on matter-enhanced neutrino flavor transitions in supernovas and implications for supernova dynamics and nucleosynthesis*, *Phys. Rev. D* **52** (1995) 6664.

[100] S. Choubey, N. P. Harries and G. G. Ross, *Turbulent supernova shock waves and the sterile neutrino signature in megaton water detectors*, *Phys. Rev. D* **76** (2007) 073013.

[101] F. Benatti and R. Floreanini, *Dissipative neutrino oscillations in randomly fluctuating matter*, *Phys. Rev. D* **71** (2005) 013003.

[102] J. P. Kneller and A. W. Mauney, *Consequences of large θ_{13} for the turbulence signatures*

in supernova neutrinos, *Phys. Rev. D* **88** (2013) 025004.

[103] G. Fogli, E. Lisi, A. Mirizzi and D. Montanino, *Damping of supernova neutrino transitions in stochastic shock-wave density profiles*, *Journal of Cosmology and Astroparticle Physics* **2006** (2006) 012.

[104] J. Kneller and C. Volpe, *Turbulence effects on supernova neutrinos*, *Phys. Rev. D* **82** (2010) 123004.

[105] A. Friedland and A. Gruzinov, *Neutrino signatures of supernova turbulence*, astro-ph/0607244.

[106] V. A. Kostelecky and S. Samuel, *Selfmaintained coherent oscillations in dense neutrino gases*, *Phys. Rev. D* **52** (1995) 621 [hep-ph/9506262].

[107] S. Samuel, *Bimodal coherence in dense selfinteracting neutrino gases*, *Phys. Rev. D* **53** (1996) 5382 [hep-ph/9604341].

[108] H. Duan, G. M. Fuller and Y.-Z. Qian, *Collective neutrino flavor transformation in supernovae*, *Phys. Rev. D* **74** (2006) 123004 [astro-ph/0511275].

[109] H. Duan, G. M. Fuller, J. Carlson and Y.-Z. Qian, *Simulation of Coherent Non-Linear Neutrino Flavor Transformation in the Supernova Environment. 1. Correlated Neutrino Trajectories*, *Phys. Rev. D* **74** (2006) 105014 [astro-ph/0606616].

[110] H. Duan, G. M. Fuller, J. Carlson and Y.-Z. Qian, *Coherent Development of Neutrino Flavor in the Supernova Environment*, *Phys. Rev. Lett.* **97** (2006) 241101 [astro-ph/0608050].

[111] S. Hannestad, G. G. Raffelt, G. Sigl and Y. Y. Y. Wong, *Self-induced conversion in dense neutrino gases: Pendulum in flavour space*, *Phys. Rev.* **D74** (2006) 105010 [astro-ph/0608695].

[112] H. Duan, G. M. Fuller, J. Carlson and Y.-Z. Qian, *Analysis of Collective Neutrino Flavor Transformation in Supernovae*, *Phys. Rev. D* **75** (2007) 125005 [astro-ph/0703776].

[113] G. G. Raffelt, *n-mode coherence in collective neutrino oscillations*, *Phys. Rev. D* **83** (2011) 105022.

[114] G. Fogli, E. Lisi, A. Marrone and A. Mirizzi, *Collective neutrino flavor transitions in supernovae and the role of trajectory averaging*, *Journal of Cosmology and Astroparticle Physics* **2007** (2007) 010.

[115] L. Johns and G. M. Fuller, *Strange mechanics of the neutrino flavor pendulum*, *Phys. Rev. D* **97** (2018) 023020 [1709.00518].

[116] R. F. Sawyer, *Neutrino cloud instabilities just above the neutrino sphere of a supernova*, *Phys. Rev. Lett.* **116** (2016) 081101 [1509.03323].

[117] S. Chakraborty, R. S. Hansen, I. Izaguirre and G. G. Raffelt, *Self-induced neutrino flavor conversion without flavor mixing*, *JCAP* **1603** (2016) 042 [1602.00698].

[118] B. Dasgupta, A. Mirizzi and M. Sen, *Fast neutrino flavor conversions near the supernova core with realistic flavor-dependent angular distributions*, *JCAP* **1702** (2017) 019 [1609.00528].

[119] S. Airen, F. Capozzi, S. Chakraborty, B. Dasgupta, G. Raffelt and T. Stirner,

Normal-mode Analysis for Collective Neutrino Oscillations, *JCAP* **12** (2018) 019 [1809.09137].

[120] I. Izaguirre, G. G. Raffelt and I. Tamborra, *Fast Pairwise Conversion of Supernova Neutrinos: A Dispersion-Relation Approach*, *Phys. Rev. Lett.* **118** (2017) 021101 [1610.01612].

[121] X. Li and D. M. Siegel, *Neutrino Fast Flavor Conversions in Neutron-Star Postmerger Accretion Disks*, *Phys. Rev. Lett.* **126** (2021) 251101 [2103.02616].

[122] I. Padilla-Gay, I. Tamborra and G. G. Raffelt, *Neutrino Flavor Pendulum Reloaded: The Case of Fast Pairwise Conversion*, *Phys. Rev. Lett.* **128** (2022) 121102 [2109.14627].

[123] M.-R. Wu, M. George, C.-Y. Lin and Z. Xiong, *Collective fast neutrino flavor conversions in a 1D box: Initial conditions and long-term evolution*, *Phys. Rev. D* **104** (2021) 103003 [2108.09886].

[124] S. Richers, D. E. Willcox, N. M. Ford and A. Myers, *Particle-in-cell Simulation of the Neutrino Fast Flavor Instability*, *Phys. Rev. D* **103** (2021) 083013 [2101.02745].

[125] S. Richers, D. Willcox and N. Ford, *Neutrino fast flavor instability in three dimensions*, *Phys. Rev. D* **104** (2021) 103023 [2109.08631].

[126] J. D. Martin, C. Yi and H. Duan, *Dynamic fast flavor oscillation waves in dense neutrino gases*, *Phys. Lett. B* **800** (2020) 135088 [1909.05225].

[127] S. Abbar and M. C. Volpe, *On Fast Neutrino Flavor Conversion Modes in the Nonlinear Regime*, *Phys. Lett.* **B790** (2019) 545 [1811.04215].

[128] L. Johns, H. Nagakura, G. M. Fuller and A. Burrows, *Fast oscillations, collisionless relaxation, and spurious evolution of supernova neutrino flavor*, *Phys. Rev. D* **102** (2020) 103017 [2009.09024].

[129] G. Sigl, *Simulations of fast neutrino flavor conversions with interactions in inhomogeneous media*, *Phys. Rev. D* **105** (2022) 043005 [2109.00091].

[130] Z. Xiong and Y.-Z. Qian, *Stationary solutions for fast flavor oscillations of a homogeneous dense neutrino gas*, *Phys. Lett. B* **820** (2021) 136550 [2104.05618].

[131] S. Abbar and F. Capozzi, *Suppression of fast neutrino flavor conversions occurring at large distances in core-collapse supernovae*, *JCAP* **03** (2022) 051 [2111.14880].

[132] M. Delfan Azari, S. Yamada, T. Morinaga, H. Nagakura, S. Furusawa, A. Harada et al., *Fast collective neutrino oscillations inside the neutrino sphere in core-collapse supernovae*, *Phys. Rev. D* **101** (2020) 023018 [1910.06176].

[133] H. Nagakura, T. Morinaga, C. Kato and S. Yamada, *Fast-pairwise collective neutrino oscillations associated with asymmetric neutrino emissions in core-collapse supernova*, 1910.04288.

[134] H. Nagakura and L. Johns, *New method for detecting fast neutrino flavor conversions in core-collapse supernova models with two-moment neutrino transport*, *Phys. Rev. D* **104** (2021) 063014 [2106.02650].

[135] S. Abbar, *Searching for Fast Neutrino Flavor Conversion Modes in Core-collapse Supernova Simulations*, *JCAP* **05** (2020) 027 [2003.00969].

[136] H. Nagakura, L. Johns, A. Burrows and G. M. Fuller, *Where, when, and why: Occurrence of fast-pairwise collective neutrino oscillation in three-dimensional core-collapse supernova models*, *Phys. Rev. D* **104** (2021) 083025 [2108.07281].

[137] C. J. Stapleford, C. Fröhlich and J. P. Kneller, *Coupling Neutrino Oscillations and Simulations of Core-Collapse Supernovae*, *Phys. Rev. D* **102** (2020) 081301 [1910.04172].

[138] F. Capozzi, B. Dasgupta and A. Mirizzi, *Model-independent diagnostic of self-induced spectral equalization versus ordinary matter effects in supernova neutrinos*, *Phys. Rev. D* **98** (2018) 063013 [1807.00840].

[139] M.-R. Wu, I. Tamborra, O. Just and H.-T. Janka, *Imprints of neutrino-pair flavor conversions on nucleosynthesis in ejecta from neutron-star merger remnants*, *Phys. Rev. D* **96** (2017) 123015 [1711.00477].

[140] M. Zaizen, J. F. Cherry, T. Takiwaki, S. Horiuchi, K. Kotake, H. Umeda et al., *Neutrino halo effect on collective neutrino oscillation in iron core-collapse supernova model of a 9.6 $M_\odot$ star*, *JCAP* **06** (2020) 011 [1908.10594].

[141] G. G. Raffelt and G. Sigl, *Self-induced decoherence in dense neutrino gases*, *Phys. Rev. D* **75** (2007) 083002 [hep-ph/0701182].

[142] A. Esteban-Pretel, S. Pastor, R. Tomas, G. G. Raffelt and G. Sigl, *Decoherence in supernova neutrino transformations suppressed by deleptonization*, *Phys. Rev. D* **76** (2007) 125018 [0706.2498].

[143] I. Tamborra and S. Shalgar, *New Developments in Flavor Evolution of a Dense Neutrino Gas*, *Ann. Rev. Nucl. Part. Sci.* **71** (2021) 165 [2011.01948].

[144] F. Capozzi and N. Saviano, *Neutrino Flavor Conversions in High-Density Astrophysical and Cosmological Environments*, *Universe* **8** (2022) 94 [2202.02494].

[145] G. L. Fogli, E. Lisi, A. Marrone and A. Mirizzi, *Collective neutrino flavor transitions in supernovae and the role of trajectory averaging*, *JCAP* **12** (2007) 010 [0707.1998].

[146] G. G. Raffelt and A. Y. Smirnov, *Adiabaticity and spectral splits in collective neutrino transformations*, *Phys. Rev. D* **76** (2007) 125008 [0709.4641].

[147] G. L. Fogli, E. Lisi, A. Marrone, A. Mirizzi and I. Tamborra, *Low-energy spectral features of supernova (anti)neutrinos in inverted hierarchy*, *Phys. Rev. D* **78** (2008) 097301 [0808.0807].

[148] G. Fogli, E. Lisi, A. Marrone and I. Tamborra, *Supernova neutrinos and antineutrinos: Ternary luminosity diagram and spectral split patterns*, *JCAP* **10** (2009) 002 [0907.5115].

[149] S. Chakraborty, G. Raffelt, H.-T. Janka and B. Müller, *Supernova deleptonization asymmetry: Impact on self-induced flavor conversion*, *Phys. Rev. D* **92** (2015) 105002 [1412.0670].

[150] B. Dasgupta, A. Dighe, G. G. Raffelt and A. Y. Smirnov, *Multiple Spectral Splits of Supernova Neutrinos*, *Phys. Rev. Lett.* **103** (2009) 051105 [0904.3542].

[151] A. Mirizzi and R. Tomas, *Multi-angle effects in self-induced oscillations for different*

supernova neutrino fluxes, *Phys. Rev. D* **84** (2011) 033013 [1012.1339].

[152] J. F. Cherry, G. M. Fuller, J. Carlson, H. Duan and Y.-Z. Qian, *Multi-Angle Simulation of Flavor Evolution in the Neutrino Neutronization Burst From an O-Ne-Mg Core-Collapse Supernova*, *Phys. Rev. D* **82** (2010) 085025 [1006.2175].

[153] A. Mirizzi and P. D. Serpico, *Instability in the Dense Supernova Neutrino Gas with Flavor-Dependent Angular Distributions*, *Phys. Rev. Lett.* **108** (2012) 231102 [1110.0022].

[154] A. Mirizzi and P. D. Serpico, *Flavor Stability Analysis of Dense Supernova Neutrinos with Flavor-Dependent Angular Distributions*, *Phys. Rev. D* **86** (2012) 085010 [1208.0157].

[155] G. Raffelt, S. Sarikas and D. de Sousa Seixas, *Axial Symmetry Breaking in Self-Induced Flavor Conversion of Supernova Neutrino Fluxes*, *Phys. Rev. Lett.* **111** (2013) 091101 [1305.7140].

[156] G. Raffelt and D. de Sousa Seixas, *Neutrino flavor pendulum in both mass hierarchies*, *Phys. Rev. D* **88** (2013) 045031 [1307.7625].

[157] H. Duan, *Flavor Oscillation Modes In Dense Neutrino Media*, *Phys. Rev. D* **88** (2013) 125008 [1309.7377].

[158] A. Mirizzi, *Multi-azimuthal-angle effects in self-induced supernova neutrino flavor conversions without axial symmetry*, *Phys. Rev. D* **88** (2013) 073004 [1308.1402].

[159] S. Chakraborty and A. Mirizzi, *Multi-azimuthal-angle instability for different supernova neutrino fluxes*, *Phys. Rev. D* **90** (2014) 033004 [1308.5255].

[160] G. Mangano, A. Mirizzi and N. Saviano, *Damping the neutrino flavor pendulum by breaking homogeneity*, *Phys. Rev. D* **89** (2014) 073017 [1403.1892].

[161] H. Duan and S. Shalgar, *Flavor instabilities in the neutrino line model*, *Phys. Lett. B* **747** (2015) 139 [1412.7097].

[162] A. Mirizzi, G. Mangano and N. Saviano, *Self-induced flavor instabilities of a dense neutrino stream in a two-dimensional model*, *Phys. Rev. D* **92** (2015) 021702 [1503.03485].

[163] A. Mirizzi, *Breaking the symmetries in self-induced flavor conversions of neutrino beams from a ring*, *Phys. Rev. D* **92** (2015) 105020 [1506.06805].

[164] H. Duan, *Collective neutrino oscillations and spontaneous symmetry breaking*, *Int. J. Mod. Phys. E* **24** (2015) 1541008 [1506.08629].

[165] S. Abbar and H. Duan, *Neutrino flavor instabilities in a time-dependent supernova model*, *Phys. Lett. B* **751** (2015) 43 [1509.01538].

[166] S. Chakraborty, R. S. Hansen, I. Izaguirre and G. Raffelt, *Self-induced flavor conversion of supernova neutrinos on small scales*, *JCAP* **01** (2016) 028 [1507.07569].

[167] B. Dasgupta and A. Mirizzi, *Temporal Instability Enables Neutrino Flavor Conversions Deep Inside Supernovae*, *Phys. Rev. D* **92** (2015) 125030 [1509.03171].

[168] F. Capozzi, B. Dasgupta and A. Mirizzi, *Self-induced temporal instability from a neutrino antenna*, *JCAP* **04** (2016) 043 [1603.03288].

[169] B. Dasgupta, A. Mirizzi, I. Tamborra and R. Tomas, *Neutrino mass hierarchy and*

three-flavor spectral splits of supernova neutrinos, *Phys. Rev. D* **81** (2010) 093008 [1002.2943].

[170] R. F. Sawyer, *Speed-up of neutrino transformations in a supernova environment*, *Phys. Rev. D* **72** (2005) 045003 [hep-ph/0503013].

[171] R. F. Sawyer, *The multi-angle instability in dense neutrino systems*, *Phys. Rev. D* **79** (2009) 105003 [0803.4319].

[172] F. Capozzi, B. Dasgupta, E. Lisi, A. Marrone and A. Mirizzi, *Fast flavor conversions of supernova neutrinos: Classifying instabilities via dispersion relations*, *Phys. Rev.* **D96** (2017) 043016 [1706.03360].

[173] A. Dighe and M. Sen, *Nonstandard neutrino self-interactions in a supernova and fast flavor conversions*, *Phys. Rev.* **D97** (2018) 043011 [1709.06858].

[174] B. Dasgupta and M. Sen, *Fast Neutrino Flavor Conversion as Oscillations in a Quartic Potential*, *Phys. Rev.* **D97** (2018) 023017 [1709.08671].

[175] B. Dasgupta, A. Mirizzi and M. Sen, *Simple method of diagnosing fast flavor conversions of supernova neutrinos*, *Phys. Rev.* **D98** (2018) 103001 [1807.03322].

[176] S. Abbar, H. Duan, K. Sumiyoshi, T. Takiwaki and M. C. Volpe, *On the occurrence of fast neutrino flavor conversions in multidimensional supernova models*, 1812.06883.

[177] M. D. Azari, S. Yamada, T. Morinaga, W. Iwakami, H. Nagakura and K. Sumiyoshi, *Linear Analysis of Fast-Pairwise Collective Neutrino Oscillations in Core-Collapse Supernovae based on the Results of Boltzmann Simulations*, 1902.07467.

[178] L. Johns, H. Nagakura, G. M. Fuller and A. Burrows, *Neutrino oscillations in supernovae: angular moments and fast instabilities*, *Phys. Rev. D* **101** (2020) 043009 [1910.05682].

[179] R. Glas, H. T. Janka, F. Capozzi, M. Sen, B. Dasgupta, A. Mirizzi et al., *Fast Neutrino Flavor Instability in the Neutron-star Convection Layer of Three-dimensional Supernova Models*, *Phys. Rev. D* **101** (2020) 063001 [1912.00274].

[180] S. Shalgar, I. Padilla-Gay and I. Tamborra, *Neutrino propagation hinders fast pairwise flavor conversions*, 1911.09110.

[181] S. Bhattacharyya and B. Dasgupta, *Fast Neutrino Flavor Conversion at Late Time*, 2005.00459.

[182] S. Bhattacharyya and B. Dasgupta, *Fast Flavor Depolarization of Supernova Neutrinos*, *Phys. Rev. Lett.* **126** (2021) 061302 [2009.03337].

[183] S. Bhattacharyya and B. Dasgupta, *Fast flavor oscillations of astrophysical neutrinos with 1, 2, ..., ∞ crossings*, *JCAP* **07** (2021) 023 [2101.01226].

[184] T. Morinaga, *Fast neutrino flavor instability and neutrino flavor lepton number crossings*, 2103.15267.

[185] B. Dasgupta, *Collective Neutrino Flavor Instability Requires a Crossing*, *Phys. Rev. Lett.* **128** (2022) 081102 [2110.00192].

[186] S. Bhattacharyya and B. Dasgupta, *Elaborating the Ultimate Fate of Fast Collective Neutrino Flavor Oscillations*, 2205.05129.

[187] C. Yi, L. Ma, J. D. Martin and H. Duan, *Dispersion relation of the fast neutrino*

oscillation wave, *Phys. Rev. D* **99** (2019) 063005 [1901.01546].

[188] F. Capozzi, G. Raffelt and T. Stirner, *Fast Neutrino Flavor Conversion: Collective Motion vs. Decoherence*, *JCAP* **09** (2019) 002 [1906.08794].

[189] H. Nagakura and L. Johns, *Constructing angular distributions of neutrinos in core-collapse supernovae from zeroth and first moments calibrated by full boltzmann neutrino transport*, *Phys. Rev. D* **103** (2021) 123025.

[190] I. Tamborra, L. Huedepohl, G. Raffelt and H.-T. Janka, *Flavor-dependent neutrino angular distribution in core-collapse supernovae*, *Astrophys. J.* **839** (2017) 132 [1702.00060].

[191] M. Delfan Azari, S. Yamada, T. Morinaga, W. Iwakami, H. Okawa, H. Nagakura et al., *Linear Analysis of Fas t-Pairwise Collective Neutrino Oscillations in Core-Collapse Supernovae based on the Results of Boltzmann Simulations*, *Phys. Rev. D* **99** (2019) 103011 [1902.07467].

[192] E. P. O'Connor and S. M. Couch, *Exploring Fundamentally Three-dimensional Phenomena in High-fidelity Simulations of Core-collapse Supernovae*, *Astrophys. J.* **865** (2018) 81 [1807.07579].

[193] R. Glas, H. T. Janka, T. Melson, G. Stockinger and O. Just, *Effects of LESA in Three-Dimensional Supernova Simulations with Multi-Dimensional and Ray-by-Ray-plus Neutrino Transport*, 1809.10150.

[194] H. Nagakura, K. Sumiyoshi and S. Yamada, *Possible early linear acceleration of proto-neutron stars via asymmetric neutrino emission in core-collapse supernovae*, *Astrophys. J. Lett.* **880** (2019) L28 [1907.04863].

[195] T. Morinaga, H. Nagakura, C. Kato and S. Yamada, *Fast neutrino-flavor conversion in the preshock region of core-collapse supernovae*, *Phys. Rev. Res.* **2** (2020) 012046 [1909.13131].

[196] F. Capozzi, S. Abbar, R. Bollig and H. T. Janka, *Fast neutrino flavor conversions in one-dimensional core-collapse supernova models with and without muon creation*, *Phys. Rev. D* **103** (2021) 063013 [2012.08525].

[197] S. Abbar, F. Capozzi, R. Glas, H. T. Janka and I. Tamborra, *On the characteristics of fast neutrino flavor instabilities in three-dimensional core-collapse supernova models*, *Phys. Rev. D* **103** (2021) 063033 [2012.06594].

[198] S. Shalgar and I. Tamborra, *Dispelling a myth on dense neutrino media: fast pairwise conversions depend on energy*, *JCAP* **01** (2021) 014 [2007.07926].

[199] F. Capozzi, B. Dasgupta, A. Mirizzi, M. Sen and G. Sigl, *Collisional triggering of fast flavor conversions of supernova neutrinos*, *Phys. Rev. Lett.* **122** (2019) 091101 [1808.06618].

[200] M.-R. Wu and I. Tamborra, *Fast neutrino conversions: Ubiquitous in compact binary merger remnants*, *Phys. Rev. D* **95** (2017) 103007 [1701.06580].

[201] I. Padilla-Gay, S. Shalgar and I. Tamborra, *Multi-Dimensional Solution of Fast Neutrino Conversions in Binary Neutron Star Merger Remnants*, *JCAP* **01** (2021) 017

[2009.01843].

[202] Z. Xiong, A. Sieverding, M. Sen and Y.-Z. Qian, *Potential Impact of Fast Flavor Oscillations on Neutrino-driven Winds and Their Nucleosynthesis*, *Astrophys. J.* **900** (2020) 144 [2006.11414].

[203] A. Banerjee, A. Dighe and G. Raffelt, *Linearized flavor-stability analysis of dense neutrino streams*, *Phys. Rev. D* **84** (2011) 053013 [1107.2308].

[204] S. Chakraborty, R. Hansen, I. Izaguirre and G. Raffelt, *Collective neutrino flavor conversion: Recent developments*, *Nucl. Phys. B* **908** (2016) 366 [1602.02766].

[205] S. Sarikas, G. G. Raffelt, L. Hudepohl and H.-T. Janka, *Suppression of Self-Induced Flavor Conversion in the Supernova Accretion Phase*, *Phys. Rev. Lett.* **108** (2012) 061101 [1109.3601].

[206] N. Saviano, S. Chakraborty, T. Fischer and A. Mirizzi, *Stability analysis of collective neutrino oscillations in the supernova accretion phase with realistic energy and angle distributions*, *Phys. Rev. D* **85** (2012) 113002 [1203.1484].

[207] B. Dasgupta and A. Dighe, *Collective three-flavor oscillations of supernova neutrinos*, *Phys. Rev. D* **77** (2008) 113002 [0712.3798].

[208] A. Friedland, *Self-refraction of supernova neutrinos: mixed spectra and three-flavor instabilities*, *Phys. Rev. Lett.* **104** (2010) 191102 [1001.0996].

[209] A. Esteban-Pretel, S. Pastor, R. Tomas, G. G. Raffelt and G. Sigl, *Mu-tau neutrino refraction and collective three-flavor transformations in supernovae*, *Phys. Rev. D* **77** (2008) 065024 [0712.1137].

[210] A. Mirizzi, S. Pozzorini, G. G. Raffelt and P. D. Serpico, *Flavour-dependent radiative correction to neutrino-neutrino refraction*, *JHEP* **10** (2009) 020 [0907.3674].

[211] C. J. Horowitz, *Weak magnetism for antineutrinos in supernovae*, *Phys. Rev. D* **65** (2002) 043001.

[212] M. Chakraborty and S. Chakraborty, *Three flavor neutrino conversions in supernovae: slow \& fast instabilities*, *JCAP* **01** (2020) 005 [1909.10420].

[213] F. Capozzi, E. Lisi, A. Marrone and A. Palazzo, *Current unknowns in the three neutrino framework*, *Prog. Part. Nucl. Phys.* **102** (2018) 48 [1804.09678].

[214] S. Chakraborty, T. Fischer, A. Mirizzi, N. Saviano and R. Tomas, *No collective neutrino flavor conversions during the supernova accretion phase*, *Phys. Rev. Lett.* **107** (2011) 151101 [1104.4031].

[215] C. Döring, R. S. L. Hansen and M. Lindner, *Stability of three neutrino flavor conversion in supernovae*, *JCAP* **08** (2019) 003 [1905.03647].

[216] A. Vlasenko, G. M. Fuller and V. Cirigliano, *Neutrino Quantum Kinetics*, *Phys. Rev.* **D89** (2014) 105004 [1309.2628].

[217] C. Volpe, *Neutrino Quantum Kinetic Equations*, *Int. J. Mod. Phys. E* **24** (2015) 1541009 [1506.06222].

[218] S. A. Richers, G. C. McLaughlin, J. P. Kneller and A. Vlasenko, *Neutrino Quantum Kinetics in Compact Objects*, *Phys. Rev. D* **99** (2019) 123014 [1903.00022].

[219] F. Capozzi, M. Chakraborty, S. Chakraborty and M. Sen, *Fast flavor conversions in*

supernovae: the rise of mu-tau neutrinos, *Phys. Rev. Lett.* **125** (2020) 251801 [2005.14204].

[220] S. Shalgar and I. Tamborra, *Three flavor revolution in fast pairwise neutrino conversion*, *Phys. Rev. D* **104** (2021) 023011 [2103.12743].

[221] F. Capozzi, M. Chakraborty, S. Chakraborty and M. Sen, *Supernova Fast Flavor Conversions in 1+1 D : Influence of Mu-tau neutrinos*, 2205.06272.

[222] S. Abbar and H. Duan, *Fast neutrino flavor conversion: roles of dense matter and spectrum crossing*, 1712.07013v1.

[223] Private communication with Thomas Janka and Robert Bollig.

[224] S. Abbar, H. Duan, K. Sumiyoshi, T. Takiwaki and M. C. Volpe, *Fast Neutrino Flavor Conversion Modes in Multidimensional Core-collapse Supernova Models: the Role of the Asymmetric Neutrino Distributions*, *Phys. Rev. D* **101** (2020) 043016 [1911.01983].

[225] R. Diehl et al., *Radioactive Al-26 and massive stars in the galaxy*, *Nature* **439** (2006) 45 [astro-ph/0601015].

[226] R. M. Bionta, G. Blewitt, C. B. Bratton, D. Casper, A. Ciocio, R. Claus et al., *Observation of a neutrino burst in coincidence with supernova 1987a in the large magellanic cloud*, *Phys. Rev. Lett.* **58** (1987) 1494.

[227] K. Hirata, T. Kajita, M. Koshiba, M. Nakahata, Y. Oyama, N. Sato et al., *Observation of a neutrino burst from the supernova sn1987a*, *Phys. Rev. Lett.* **58** (1987) 1490.

[228] E. N. Alekseev, L. N. Alekseeva, V. I. Volchenko and I. V. Krivosheina, *Possible Detection of a Neutrino Signal on 23 February 1987 at the Baksan Underground Scintillation Telescope of the Institute of Nuclear Research*, *JETP Lett.* **45** (1987) 589.

[229] G. S. BISNOVATYI-KOGAN and Z. F. SEIDOV, *Supernovae, neutrino rest mass, and the middle-energy neutrino background in the universe*, *Annals of the New York Academy of Sciences* **422** (1984) 319 [https://nyaspubs.onlinelibrary.wiley.com/doi/pdf/10.1111/j.1749-6632.1984.tb23362.x].

[230] L. M. Krauss, S. L. Glashow and D. N. Schramm, *Antineutrino astronomy and geophysics*, **310** (1984) 191.

[231] S. E. Woosley, J. R. Wilson and R. Mayle, *Gravitational Collapse and the Cosmic Antineutrino Background*, **302** (1986) 19.

[232] C. Lunardini, *Diffuse supernova neutrinos at underground laboratories*, *Astropart. Phys.* **79** (2016) 49 [1007.3252].

[233] J. F. Beacom, *The Diffuse Supernova Neutrino Background*, *Ann. Rev. Nucl. Part. Sci.* **60** (2010) 439 [1004.3311].

[234] S. Chakraborty, S. Choubey, B. Dasgupta and K. Kar, *Effect of Collective Flavor Oscillations on the Diffuse Supernova Neutrino Background*, *JCAP* **09** (2008) 013 [0805.3131].

[235] C. Lunardini and I. Tamborra, *Diffuse supernova neutrinos: oscillation effects, stellar cooling and progenitor mass dependence*, *JCAP* **07** (2012) 012 [1205.6292].

[236] A. M. Hopkins and J. F. Beacom, *On the normalisation of the cosmic star formation*

history, *Astrophys. J.* **651** (2006) 142 [astro-ph/0601463].

[237] S. Horiuchi, J. F. Beacom and E. Dwek, *The Diffuse Supernova Neutrino Background is detectable in Super-Kamiokande*, *Phys. Rev. D* **79** (2009) 083013 [0812.3157].

[238] H. Yuksel, M. D. Kistler, J. F. Beacom and A. M. Hopkins, *Revealing the High-Redshift Star Formation Rate with Gamma-Ray Bursts*, *Astrophys. J. Lett.* **683** (2008) L5 [0804.4008].

[239] K. Nakazato, E. Mochida, Y. Niino and H. Suzuki, *Spectrum of the Supernova Relic Neutrino Background and Metallicity Evolution of Galaxies*, *Astrophys. J.* **804** (2015) 75 [1503.01236].

[240] S. Horiuchi, K. Sumiyoshi, K. Nakamura, T. Fischer, A. Summa, T. Takiwaki et al., *Diffuse supernova neutrino background from extensive core-collapse simulations of* 8-100$M_\odot$ *progenitors*, *Mon. Not. Roy. Astron. Soc.* **475** (2018) 1363 [1709.06567].

[241] L. E. Strigari, J. F. Beacom, T. P. Walker and P. Zhang, *The Concordance Cosmic Star Formation Rate: Implications from and for the supernova neutrino and gamma ray backgrounds*, *JCAP* **04** (2005) 017 [astro-ph/0502150].

[242] R. A. Malaney, *Evolution of the cosmic gas and the relic supernova neutrino background*, *Astropart. Phys.* **7** (1997) 125 [astro-ph/9612012].

[243] D. Hartmann and S. Woosley, *The cosmic supernova neutrino background*, *Astroparticle Physics* **7** (1997) 137.

[244] T. Totani, K. Sato and Y. Yoshii, *Spectrum of the supernova relic neutrino background and evolution of galaxies*, *Astrophys. J.* **460** (1996) 303 [astro-ph/9509130].

[245] M. Kaplinghat, G. Steigman and T. P. Walker, *The Supernova relic neutrino background*, *Phys. Rev. D* **62** (2000) 043001 [astro-ph/9912391].

[246] L. E. Strigari, M. Kaplinghat, G. Steigman and T. P. Walker, *The Supernova relic neutrino backgrounds at KamLAND and Super-Kamiokande*, *JCAP* **03** (2004) 007 [astro-ph/0312346].

[247] M. Fukugita and M. Kawasaki, *Constraints on the star formation rate from supernova relic neutrino observations*, *Mon. Not. Roy. Astron. Soc.* **340** (2003) L7 [astro-ph/0204376].

[248] M. Wurm, F. von Feilitzsch, M. Goeger-Neff, K. A. Hochmuth, T. M. Undagoitia, L. Oberauer et al., *Detection potential for the diffuse supernova neutrino background in the large liquid-scintillator detector LENA*, *Phys. Rev. D* **75** (2007) 023007 [astro-ph/0701305].

[249] S. Ando and K. Sato, *Relic neutrino background from cosmological supernovae*, *New J. Phys.* **6** (2004) 170 [astro-ph/0410061].

[250] E. Cappellaro, M. Turatto, D. Y. Tsvetkov, O. S. Bartunov, C. Pollas, R. Evans et al., *The Rate of supernovae from the combined sample of five searches*, *Astron. Astrophys.* **322** (1997) 431 [astro-ph/9611191].

[251] S. Ando, K. Sato and T. Totani, *Detectability of the supernova relic neutrinos and neutrino oscillation*, *Astropart. Phys.* **18** (2003) 307 [astro-ph/0202450].

[252] S. Ando and K. Sato, *Supernova relic neutrinos and observational implications for neutrino oscillation*, *Phys. Lett. B* **559** (2003) 113 [astro-ph/0210502].

[253] C. Lunardini, *The diffuse supernova neutrino flux, supernova rate and sn1987a*, *Astropart. Phys.* **26** (2006) 190 [astro-ph/0509233].

[254] S. Ando, *Cosmic star formation history and the future observation of supernova relic neutrinos*, *Astrophys. J.* **607** (2004) 20 [astro-ph/0401531].

[255] C. Volpe and J. Welzel, *Supernova Relic Electron Neutrinos and anti-Neutrinos in future Large-scale Observatories*, 0711.3237.

[256] C. Lunardini, *Diffuse neutrino flux from failed supernovae*, *Phys. Rev. Lett.* **102** (2009) 231101.

[257] J. F. Beacom, *The diffuse supernova neutrino background*, *Annual Review of Nuclear and Particle Science* **60** (2010) 439 [https://doi.org/10.1146/annurev.nucl.010909.083331].

[258] A. Lien, B. D. Fields and J. F. Beacom, *Synoptic sky surveys and the diffuse supernova neutrino background: Removing astrophysical uncertainties and revealing invisible supernovae*, *Phys. Rev. D* **81** (2010) 083001.

[259] G. J. Mathews, J. Hidaka, T. Kajino and J. Suzuki, *SUPERNOVA RELIC NEUTRINOS AND THE SUPERNOVA RATE PROBLEM: ANALYSIS OF UNCERTAINTIES AND DETECTABILITY OF ONeMg AND FAILED SUPERNOVAE*, *The Astrophysical Journal* **790** (2014) 115.

[260] K. Nakazato, K. Sumiyoshi, H. Suzuki and S. Yamada, *Oscillation and future detection of failed supernova neutrinos from a black-hole-forming collapse*, *Phys. Rev. D* **78** (2008) 083014.

[261] K. Nakazato, E. Mochida, Y. Niino and H. Suzuki, *SPECTRUM OF THE SUPERNOVA RELIC NEUTRINO BACKGROUND AND METALLICITY EVOLUTION OF GALAXIES*, *The Astrophysical Journal* **804** (2015) 75.

[262] A. Priya and C. Lunardini, *Diffuse neutrinos from luminous and dark supernovae: prospects for upcoming detectors at the O(10) kt scale*, *JCAP* **11** (2017) 031 [1705.02122].

[263] A. Das and M. Sen, *Boosted dark matter from diffuse supernova neutrinos*, *Phys. Rev. D* **104** (2021) 075029 [2104.00027].

[264] A. De Gouvêa, I. Martinez-Soler, Y. F. Perez-Gonzalez and M. Sen, *Fundamental physics with the diffuse supernova background neutrinos*, *Phys. Rev. D* **102** (2020) 123012 [2007.13748].

[265] A. de Gouvêa, I. Martinez-Soler, Y. F. Perez-Gonzalez and M. Sen, *The diffuse supernova neutrino background as a probe of late-time neutrino mass generation*, 2205.01102.

[266] R. Singh and V. Rentala, *Neutrinos from the cosmic noon: a probe of the cosmic star formation history*, *JCAP* **08** (2021) 019 [2007.02951].

[267] K. Møller, A. M. Suliga, I. Tamborra and P. B. Denton, *Measuring the supernova unknowns at the next-generation neutrino telescopes through the diffuse neutrino*

background, *JCAP* **05** (2018) 066 [1804.03157].

[268] D. Kresse, T. Ertl and H.-T. Janka, *Stellar Collapse Diversity and the Diffuse Supernova Neutrino Background*, *Astrophys. J.* **909** (2021) 169 [2010.04728].

[269] E. E. Salpeter, *The Luminosity Function and Stellar Evolution.*, **121** (1955) 161.

[270] A. M. Hopkins and J. F. Beacom, *On the Normalization of the Cosmic Star Formation History*, **651** (2006) 142 [astro-ph/0601463].

[271] Super-Kamiokande Collaboration collaboration, *Search for supernova relic neutrinos at super-kamiokande*, *Phys. Rev. Lett.* **90** (2003) 061101.

[272] Super-Kamiokande Collaboration collaboration, *Supernova relic neutrino search at super-kamiokande*, *Phys. Rev. D* **85** (2012) 052007.

[273] *Supernova relic neutrino search with neutron tagging at super-kamiokande-iv*, *Astroparticle Physics* **60** (2015) 41.

[274] K. Sumiyoshi, S. Yamada and H. Suzuki, *Dynamics and neutrino signal of black hole formation in non-rotating failed supernovae. 1. EOS dependence*, *Astrophys. J.* **667** (2007) 382 [0706.3762].

[275] T. Fischer, S. C. Whitehouse, A. Mezzacappa, F. K. Thielemann and M. Liebendorfer, *The neutrino signal from protoneutron star accretion and black hole formation*, *Astron. Astrophys.* **499** (2009) 1 [0809.5129].

[276] K. Sumiyoshi, S. Yamada and H. Suzuki, *Dynamics and neutrino signal of black hole formation in non-rotating failed supernovae. II. progenitor dependence*, *Astrophys. J.* **688** (2008) 1176 [0808.0384].

[277] K. Nakazato, K. Sumiyoshi, H. Suzuki and S. Yamada, *Oscillation and Future Detection of Failed Supernova Neutrinos from Black Hole Forming Collapse*, *Phys. Rev. D* **78** (2008) 083014 [0810.3734].

[278] K. i. Nakazato, K. Sumiyoshi and S. Yamada, *Neutrino Emission from Stellar Core Collapse and Black Hole Formation*, in *16th Workshop on General Relativity and Gravitation*, pp. 82–85, 2006.

[279] K. Sumiyoshi, H. Suzuki and S. Yamada, *Fate of core-collapse supernovae: formation of neutron star and black hole*, *AIP Conf. Proc.* **847** (2006) 473.

[280] "L. Hüdepohl. Ph.D. Thesis, Technische Universität München, available at." https://d-nb.info/1060194147/34.

[281] "H.-T. Janka. The Garching Core-Collapse Supernova Research.." https://wwwmpa.mpa-garching.mpg.de/ccsnarchive/.

[282] S. E. Woosley, A. Heger and T. A. Weaver, *The evolution and explosion of massive stars*, *Rev. Mod. Phys.* **74** (2002) 1015.

[283] J. M. Lattimer and F. Douglas Swesty, *A generalized equation of state for hot, dense matter*, *Nuclear Physics A* **535** (1991) 331.

[284] M. Ugliano, H.-T. Janka, A. Marek and A. Arcones, *PROGENITOR-EXPLOSION CONNECTION AND REMNANT BIRTH MASSES FOR NEUTRINO-DRIVEN SUPERNOVAE OF IRON-CORE PROGENITORS*, *The Astrophysical Journal* **757**

(2012) 69.

[285] O. Pejcha and T. A. Thompson, *THE LANDSCAPE OF THE NEUTRINO MECHANISM OF CORE-COLLAPSE SUPERNOVAE: NEUTRON STAR AND BLACK HOLE MASS FUNCTIONS, EXPLOSION ENERGIES, AND NICKEL YIELDS*, *The Astrophysical Journal* **801** (2015) 90.

[286] A. Esteban-Pretel, A. Mirizzi, S. Pastor, R. Tomas, G. G. Raffelt, P. D. Serpico et al., *Role of dense matter in collective supernova neutrino transformations*, *Phys. Rev. D* **78** (2008) 085012 [0807.0659].

[287] C. Lunardini and I. Tamborra, *Diffuse supernova neutrinos: oscillation effects, stellar cooling and progenitor mass dependence*, *Journal of Cosmology and Astroparticle Physics* **2012** (2012) 012.

[288] E. Borriello, S. Chakraborty, A. Mirizzi, P. D. Serpico and I. Tamborra, *(Down-to-)Earth matter effect in supernova neutrinos*, *Phys. Rev. D* **86** (2012) 083004 [1207.5049].

[289] K. Nakazato, K. Sumiyoshi, H. Suzuki, T. Totani, H. Umeda and S. Yamada, *Supernova Neutrino Light Curves and Spectra for Various Progenitor Stars: From Core Collapse to Proto-neutron Star Cooling*, *Astrophys. J. Suppl.* **205** (2013) 2 [1210.6841].

[290] K. Nakazato, K. Sumiyoshi and H. Togashi, *Numerical study of stellar core collapse and neutrino emission using the nuclear equation of state obtained by the variational method*, *Publ. Astron. Soc. Jap.* **73** (2021) 639 [2103.14386].

[291] H. Shen, H. Toki, K. Oyamatsu and K. Sumiyoshi, *Relativistic Equation of State of Nuclear Matter for Supernova Explosion*, *Progress of Theoretical Physics* **100** (1998) 1013 [https://academic.oup.com/ptp/article-pdf/100/5/1013/5281814/100-5-1013.pdf].

[292] H. Shen, H. Toki, K. Oyamatsu and K. Sumiyoshi, *RELATIVISTIC EQUATION OF STATE FOR CORE-COLLAPSE SUPERNOVA SIMULATIONS*, *The Astrophysical Journal Supplement Series* **197** (2011) 20.

[293] Super-Kamiokande collaboration, *Supernova Relic Neutrino Search with Neutron Tagging at Super-Kamiokande-IV*, *Astropart. Phys.* **60** (2015) 41 [1311.3738].

[294] C. Simpson, *Physics Potential of Super-K Gd*, *PoS* **ICHEP2018** (2019) 008.

[295] J. F. Beacom and M. R. Vagins, *GADZOOKS! Anti-neutrino spectroscopy with large water Cherenkov detectors*, *Phys. Rev. Lett.* **93** (2004) 171101 [hep-ph/0309300].

[296] Hyper-Kamiokande collaboration, *Hyper-Kamiokande Design Report*, 1805.04163.

[297] JUNO collaboration, *Neutrino Physics with JUNO*, *J. Phys. G* **43** (2016) 030401 [1507.05613].

[298] DUNE collaboration, *Deep Underground Neutrino Experiment (DUNE), Far Detector Technical Design Report, Volume II: DUNE Physics*, 2002.03005.

[299] Theia collaboration, *THEIA: an advanced optical neutrino detector*, *Eur. Phys. J. C* **80** (2020) 416 [1911.03501].

[300] I. Gil-Botella and A. Rubbia, *Decoupling supernova and neutrino oscillation physics with LAr TPC detectors*, *Journal of Cosmology and Astroparticle Physics* **2004** (2004) 001.

[301] LBNE collaboration, *The Long-Baseline Neutrino Experiment: Exploring Fundamental Symmetries of the Universe*, in *Snowmass 2013: Workshop on Energy Frontier*, 7, 2013, 1307.7335.

[302] MicroBooNE collaboration, *MicroBooNE: A New Liquid Argon Time Projection Chamber Experiment*, *AIP Conf. Proc.* **1189** (2009) 83 [0910.3497].

[303] "SNOwGLoBES." https://github.com/SNOwGLoBES/snowglobes.

[304] S. Choubey, B. Dasgupta, A. Dighe and A. Mirizzi, *Signatures of collective and matter effects on supernova neutrinos at large detectors*, 1008.0308.

[305] M. Kachelriess, R. Tomas, R. Buras, H. T. Janka, A. Marek and M. Rampp, *Exploiting the neutronization burst of a galactic supernova*, *Phys. Rev. D* **71** (2005) 063003 [astro-ph/0412082].

[306] S. Ando, *Appearance of neutronization peak and decaying supernova neutrinos*, *Phys. Rev. D* **70** (2004) 033004 [hep-ph/0405200].

[307] A. Esmaili, O. L. G. Peres and P. D. Serpico, *Impact of sterile neutrinos on the early time flux from a galactic supernova*, *Phys. Rev. D* **90** (2014) 033013 [1402.1453].

[308] S. Chakraborty, A. Mirizzi and G. Sigl, *Testing Lorentz invariance with neutrino bursts from supernova neutronization*, *Phys. Rev. D* **87** (2013) 017302 [1211.7069].

[309] E. K. Akhmedov and T. Fukuyama, *Supernova prompt neutronization neutrinos and neutrino magnetic moments*, *JCAP* **12** (2003) 007 [hep-ph/0310119].

[310] P. D. Serpico, S. Chakraborty, T. Fischer, L. Hudepohl, H.-T. Janka and A. Mirizzi, *Probing the neutrino mass hierarchy with the rise time of a supernova burst*, *Phys. Rev. D* **85** (2012) 085031 [1111.4483].

[311] C. Lunardini and A. Y. Smirnov, *Probing the neutrino mass hierarchy and the 13 mixing with supernovae*, *JCAP* **06** (2003) 009 [hep-ph/0302033].

[312] A. S. Dighe, M. T. Keil and G. G. Raffelt, *Detecting the neutrino mass hierarchy with a supernova at IceCube*, *JCAP* **06** (2003) 005 [hep-ph/0303210].

[313] V. Barger, P. Huber and D. Marfatia, *Supernova neutrinos can tell us the neutrino mass hierarchy independently of flux models*, *Phys. Lett. B* **617** (2005) 167 [hep-ph/0501184].

[314] V. Brdar and X.-J. Xu, *Timing and multi-channel: novel method for determining the neutrino mass ordering from supernovae*, *JCAP* **08** (2022) 067 [2204.13135].

[315] A. S. Dighe, M. T. Keil and G. G. Raffelt, *Identifying earth matter effects on supernova neutrinos at a single detector*, *JCAP* **06** (2003) 006 [hep-ph/0304150].

[316] A. S. Dighe, M. Kachelriess, G. G. Raffelt and R. Tomas, *Signatures of supernova neutrino oscillations in the earth mantle and core*, *JCAP* **01** (2004) 004 [hep-ph/0311172].

[317] R. C. Schirato and G. M. Fuller, *Connection between supernova shocks, flavor transformation, and the neutrino signal*, astro-ph/0205390.

[318] G. L. Fogli, E. Lisi, D. Montanino and A. Mirizzi, *Analysis of energy and time dependence of supernova shock effects on neutrino crossing probabilities*, *Phys. Rev. D* **68** (2003) 033005 [hep-ph/0304056].

[319] G. L. Fogli, E. Lisi, A. Mirizzi and D. Montanino, *Probing supernova shock waves and*

neutrino flavor transitions in next-generation water-Cerenkov detectors, *JCAP* **04** (2005) 002 [hep-ph/0412046].

[320] B. Dasgupta and A. Dighe, *Phase effects in neutrino conversions during a supernova shock wave*, *Phys. Rev. D* **75** (2007) 093002 [hep-ph/0510219].

[321] J. P. Kneller, G. C. McLaughlin and J. Brockman, *Oscillation Effects and Time Variation of the Supernova Neutrino Signal*, *Phys. Rev. D* **77** (2008) 045023 [0705.3835].

[322] E. Borriello, S. Chakraborty, H.-T. Janka, E. Lisi and A. Mirizzi, *Turbulence patterns and neutrino flavor transitions in high-resolution supernova models*, *JCAP* **11** (2014) 030 [1310.7488].

[323] Z. Xiong, M.-R. Wu and Y.-Z. Qian, *Active-sterile Neutrino Oscillations in Neutrino-driven Winds: Implications for Nucleosynthesis*, 1904.09371.

[324] E. Pllumbi, I. Tamborra, S. Wanajo, H.-T. Janka and L. Hüdepohl, *Impact of neutrino flavor oscillations on the neutrino-driven wind nucleosynthesis of an electron-capture supernova*, *Astrophys. J.* **808** (2015) 188 [1406.2596].

[325] M. L. Warren, M. Meixner, G. Mathews, J. Hidaka and T. Kajino, *Sterile neutrino oscillations in core-collapse supernovae*, *Phys. Rev. D* **90** (2014) 103007 [1405.6101].

[326] M.-R. Wu, T. Fischer, L. Huther, G. Martínez-Pinedo and Y.-Z. Qian, *Impact of active-sterile neutrino mixing on supernova explosion and nucleosynthesis*, *Phys. Rev. D* **89** (2014) 061303 [1305.2382].

[327] I. Tamborra, G. G. Raffelt, L. Hudepohl and H.-T. Janka, *Impact of eV-mass sterile neutrinos on neutrino-driven supernova outflows*, *JCAP* **01** (2012) 013 [1110.2104].

[328] Y. Farzan and S. Palomares-Ruiz, *Dips in the diffuse supernova neutrino background*, *Journal of Cosmology and Astroparticle Physics* **2014** (2014) 014.